Title
Crosstalk Between Type I Interferon and Cholesterol Homeostasis in Host Defense

Author
Zhou, Quan

Publication Date
2019

Peer reviewed|Thesis/dissertation

UNIVERSITY OF CALIFORNIA

Los Angeles

Crosstalk Between Type I Interferon and Cholesterol Homeostasis in Host Defense

A dissertation submitted in partial satisfaction of the

requirements for the degree Doctor of Philosophy

in Molecular and Medical Pharmacology

by

Quan Zhou

2019

ABSTRACT OF THE DISSERTATION

Crosstalk Between Type I Interferon and Cholesterol Homeostasis in Host Defense

by

Quan Zhou

Doctor of Philosophy in Molecular and Medical Pharmacology

University of California, Los Angeles, 2019

Professor Steven J. Bensinger, Chair

Lipid metabolism of immune cells can be rapidly reprogramed by inflammatory signals in a cell type and signal-specific manner. This reprogramming can have profound influence on host defense against pathogens, anti-cancer immunity, self-tolerance, and pathogenesis of autoimmune diseases. Despite its importance, the molecular mechanisms underlying the crosstalk between lipid metabolic reprogramming and host defense are still poorly understood. In this thesis, I focus on defining the crosstalk between cholesterol metabolic reprogramming and Type I IFN immune response in macrophages, a major immune cell type in the body. In macrophages, Type I IFN mediated anti-pathogen responses can be triggered through sensing of various Pathogen Associated Molecular Patterns (PAMPs). On the other hand, cholesterol is a key component of membranes, and its homeostasis is tightly controlled by balancing synthesis, uptake and efflux to ensure proper immune cell function. Recent studies

showed that Type I IFN signals modulates cholesterol biosynthetic activities in macrophages to regulate inflammation and to facilitate host defense. However, how this process is achieved at intracellular level remains unclear. The work presented in this thesis focuses on elucidating mechanisms in which Type I IFN regulates synthesis, modification and efflux programs in macrophages. In Chapter 2, I investigated how Type I IFN reprograms cholesterol metabolism at subcellular level to provide resistance to bacterial toxins. In Chapter 3, I investigated how cholesterol homeostasis can regulate the production of Type I IFN through an adaptor protein known as Stimulator of interferon genes (STING). It is our expectation that these studies will mechanistically advance our understanding of the crosstalk between lipid reprogramming and inflammation.

The dissertation for Quan Zhou is approved.

Alexander Hoffmann

Jing Huang

Ren Sun

Steven J. Bensinger, Committee Chair

University of California, Los Angeles

2019

DEDICATION

To my parents Xingcang and Caichun,

my husband Hao,

and my friend Yushen

TABLE OF CONTENTS

LIST OF FIGURES

ACKNOWLEDGEMENTS

Five years ago when I entered graduate school at UCLA, I was expecting this experience to totally reshape my way of thinking and looking at things. During the past five years, together with my excellent colleagues, I studied some world cutting edge problems in the field of immunometabolism, and made my humble contribution to the understanding of crosstalk between immune signal and lipid metabolism. These past five years not only helped me understand the field better, but also saw my gradual transformation from a medical student to a scientist with the ability of critical thinking. Many people helped me start this journey from the beginning. The people I want to thank here can be roughly divided into three categories: colleagues, family, and friends. But just like how different types of immune responses can overlap (they are arbitrarily defined after all), there're also overlaps between the categories mentioned above, where the largest overlap can be seen between these two: colleagues and friends.

I would like to thank my mentor, Dr. Steven J. Bensinger, for his support and guidance throughout the years. In American culture, mentors are considered colleagues, and we call them by their first names despite their title. Dr. Steven J. Bensinger truly views all graduate students as his colleagues, and he believes in my independence and provides freedom for me to explore science. Steve sees potential not only in people, but also in the field of immunometabolism. He picked immunometabolism as his field of interest several years ago, when its importance was not much appreciated as today. I've very much

enjoyed having conversations, science related or not, with Steve, and have learnt how to think critically, to make friends with excellent scientists, and to be a person with vision.

I would like to thank my committee members Dr. Alexander Hoffmann, Dr. Jing Huang and Dr. Ren Sun for their support and insightful discussions over the past three years on my projects.

Here I want to specially thank Dr. Ren Sun for the critical roles he plays in my career pursuing science. He is one of the two people who made me start to consider entering graduate school for PhD training in the first place.

The other person is my very dear friend Yushen, or Dr. Yushen Du. I've known Yushen since college, and have been continuously amazed how this age-matched peer to me can have such vision, insights, enthusiasm and courage for things. I would like to thank Yushen for her great influence on my life.

I would like to acknowledge these previous members of the Bensinger Lab, Dr. Kevin J. Williams, Dr. Joseph P. Argus, Dr. Autumn G. York, for laying the important foundation for my projects and making me to be the scientist I am today.

I would like to acknowledge these current members of the Bensinger Lab, Dr. Xun Chi, Dr. Wei Yuan Hsieh, Jonathan J. Mkrtchyan, Min Sub Lee and Margarita Calderon. You are the most amazing team I've ever been working with.

I would like to acknowledge my coauthors Viet L. Bui (UCLA), Eliza B. Kronenberger (UCLA), Dr. Alexandra Ferrari (UCLA), Dr. Xiao Xu (UCLA), Dr. Peter Tontonoz (UCLA), Dr. Cuiwen He (UCLA), Thomas Weston (UCLA), Rachel S. Jung (UCLA), Dr. Stephen G. Young (UCLA), Allison E. Daly (UCLA), Dr. Stephen Smale (UCLA), Dr. Elizabeth J. Tarling (UCLA), Dr. Marco Morselli (UCLA), Dr. Matteo Pellegrini (UCLA), Dr. Robert Damoiseaux (UCLA) for their help with my manuscript “Interferon-mediated reprogramming of membrane cholesterol to evade bacterial toxins”. I would like to acknowledge Dr. Philip Scumpia (UCLA), Dr. An-chieh Feng (UCLA), Dr. Anjie Zhen (UCLA), Dr. Melody Li (UCLA) and her lab member Emily Yang, for their help with follow-up studies.

I would like to acknowledge my colleagues and collaborators Ian Ford (UCLA), Dr. Keri Backus (UCLA) and her lab member Brie Hill-Payne, Dr. James Wohlschelgel and his lab member Dr. Vijaya Pandey, Dr. Genhong Cheng (UCLA) and his lab member Dr. Kislay Parvatiyar, Dr. Yousang Gwack (UCLA) and Dr. Sonal Srikanth (UCLA), Dr. Daniel Ory (Washinton University) and Dr. Douglas Covey (Washington Univerisity), Dr. Roberto Zoncu (UC Berkeley) and Dr. Martin Phillips (UCLA), for their help with my project presented in Chapter 3.

I would like to thank Dr. Xun Chi, Dr. Wei Yuan Hsieh, Min Sub Lee and Ian Ford for help with editing this thesis.

I would like to acknowledge Dr. Tingting Wu, Dr. Junhui Hu, Tianhao Zhang, Dr Shili Xu, Dr. Kevin Huynh, Dr. Xin Rong, Dr. Jaspreet Sandhu for insightful discussions and help on my projects.

Last but not least, I would like to thank my parents for their mental and intellectual support throughout the years. I've learnt extremely valuable life lessons and characters from them — integrity, bravery, self-management, as well as a good sense of humor. I would like to thank my husband Hao Jiang for being a husband, a friend as well as a researcher who I can discuss science and share excitement/disappointment with, and for his appreciation of my sense of humor mentioned earlier.

Chapter 2

Chapter 2 is a version of the following manuscript:

Zhou QD, Chi X, Hsieh WY, Mkrtchyan JJ, Bui VL, Kronenberger EB, Lee MS, Ferrrari A, Xiao Xu, Daly AE, Smale S, Willams KJ, Tontonoz P, Bensinger SJ. Interferon-mediated reprogramming of membrane cholesterol to evade bacterial toxins

VITA

EDUCATION:

B.S. in Mathematics and Applied Mathematics, Zhejiang University, China; 2011
Medical Student, Zhejiang University School of Medicine, China; 2011-2014

SELECTED PUBLICATIONS:

1. York AG, Williams KJ, Argus JP, **Zhou QD**, *et al.* Limiting Cholesterol Biosynthetic Flux Spontaneously Engages Type I IFN Signaling. *Cell* 163, 1–14 (2015).
2. Argus JP, Moses MQ, **Zhou QD**, *et al*. Development and Application of FASA, a Model for Quantifying Fatty Acid Metabolism Using Stable Isotope Labeling. *Cell Rep*. 25, 2919-2934.e8 (2018).

AWARDS & HONORS:

1. Abstract selected for a short talk. Immunometabolism: Fundamentals to Prospective New Therapies. Oral Presentation Title “Understanding the importance of Type I Interferon mediated changes to Cholesterol homeostasis in host defense” Jun 2019; Boston, US
2. Best Poster Award. UCLA Molecular and Medical Pharmacology Retreat. Nov 2018
3. Best Student Talk Award. UCLA Molecular and Medical Pharmacology Retreat. Nov 2017
4. Outstanding graduates of Zhejiang University. Jun 2011
5. Anzhong Scholarship for International Exchange. Jul 2009
6. Second Prize of Mathematical Modeling Competition of Zhejiang University. May 2009
7. Excellent student of Zhejiang University. 2007-2008 and 2008-2009
8. Scholarship for outstanding students of Zhejiang University. 2007-2008, 2008-2009

PRESENTATIONS:

1. Immunometabolism: Fundamentals to Prospective New Therapies. Oral Presentation Title “Understanding the importance of Type I Interferon mediated changes to Cholesterol homeostasis in host defense” Jun 2019; Boston, MA
2. UCLA Molecular and Medical Pharmacology Retreat. Poster Title: “Type I Interferon Mediated Reprogramming of Membrane Cholesterol in Macrophages”. Nov 2018. Huntington Beach, CA
3. UCLA Molecular and Medical Pharmacology Retreat. Oral Presentation. Title: “Reprogramming of Cholesterol Homeostasis by Type I Interferon in Host Defense”. Nov 2017. Huntington Beach, CA
4. 2017 DEUEL Conference on Lipids. Poster Title: “Profiling of Reprogrammed Subcellular Cholesterol Metabolism in Response to Type I Interferon Signaling” Mar 2017. Monterey, CA
5. UCLA Molecular and Medical Pharmacology Retreat. Poster Title: “Quantitative Profiling of Reprogrammed Cholesterol Homeostasis in Response to Type I Interferon Signaling”. Nov 2016. Huntington Beach, CA
6. 2016 DEUEL Conference on Lipids. Poster Title: “Identification of Novel Regulators of Cancer Cell Lipid Homeostasis Using High-throughput SiRNA Screening.” Mar 2016. Napa, CA
7. UCLA Immunology, Inflammation, Infection and Transplantation (I3T) seminar series. Talk title: “Type I IFN Mediated Reprogramming of Membrane Cholesterol in Macrophages” Dec 2018. Los Angeles, CA
8. UCLA Molecular and Medical Pharmacology Retreat. Poster Title: “Identification of Novel Regulators of Cancer Cell Lipid Homeostasis Using High-throughput Gene Silencing Coupled with Lipid Metabolic Flux Analysis”. Nov 2015. Huntington Beach, CA

CHAPTER 1:

An introduction to cellular lipid homeostasis

and

Immunometabolism

What are lipids and why are they important

Lipids are a major group of naturally occurring biological molecules with a unifying feature of hydrophobicity. Lipids make up 15-20 % dry weight of mammalian cells on average[1], and play key roles in a variety of biological processes, including supporting membrane structure, energy storage and signaling. Major classes of lipids include free fatty acids, glycerolipids, glycerophospholipids, sphingolipids, eicosanoids, prenols, and sterols like cholesterol[2]. Lipids are fundamental building blocks of all membrane structure in mammalian cells, where they house cellular components and isolate them from the environment, and segregate functionally linked molecules together in subcellular organelles such as endoplasmic reticulum (ER), mitochondria, and Golgi apparatus. Neutral lipids, also known as “fat”, are stored in lipid droplets as a long-term energy reservoir, since the human body is not capable of storing as much glycogen as lipids. Furthermore, lipids in the membrane can regulate membrane features such as fluidity and lipid packing, which in turn regulates membrane protein functions[3]. Covalent lipid modification of proteins with fatty acids, isoprenoids, or cholesterol can regulate protein function by altering protein conformation and its interaction with other membrane lipids[4]. Other than their structural and energy roles, lipids *per se* can serve as messengers in signaling pathways[5–7]. For example, phosphatidylinositol (PIn) in the membrane can be phosphorylated by Phosphoinositide 3-kinases (PI3Ks) to transduce growth and proliferation related signals. And lipids are increasingly being recognized as ligands for signaling receptors, such as sphingosine-1-phosphate (S1P) receptors, CD1α receptors,

and Toll-like receptors (TLRs). Homeostasis of lipids are maintained via multiple biochemical and physiology regulations. Failure to maintain such homeostasis can result in a wide spectrum of metabolic disorders, such as diabetes and obesity. More recently, the critical roles of lipids are drawing attention in the field of cancer and immunology studies[8,9].

Immunometabolism: A rapid growing field

Immunometabolism is an emerging field interfacing immunology and metabolism. In the past decade, this field has become one of the most exciting areas of research in both basic science and translational studies. The two main questions in this field are, 1) how does immune response alter metabolism at systematic and and cellular level? 2) what's the biological relevance of the alteration mentioned above.

Research in metabolism can be broadly categorized to these four branches: anabolic, energy-consuming, biosynthetic processes, and energy-generating catabolic processes[10]. The major metabolic pathways currently studied in the immune cells are glycolysis, TCA cycle, the pentose phosphate pathway, fatty acid oxidation, fatty acid synthesis and amino acid metabolism[11]. The focus of immunometabolism in the early years are to characterize how metabolism supports immunity with energy and biomass, for example, large amounts of lipids are required during the rapid CD8+ T cell expansion. Over the past years, there's a paradigm shift in the understanding of biological impact of metabolism reprogramming by immune signals. Apart from providing fuels and biomass, metabolism can be actively

involved in many immune signaling pathways give “instructions” to modulate the intensity, duration and the type of immune responses[12,13].

The importance of lipid metabolism in immunity has been appreciated from very early on, with a the major focus on fatty acid metabolism. However, the role of cholesterol is less understood. Earlier work from our lab showed that cholesterol synthesis is required for CD8+ T cell proliferation[14,15]. Apart from providing structural support for fast proliferating CD8+ T cells, cholesterol is also important for TCR clustering on the T membrane for optimal signal transduction[16]. In macrophages, modulation in cholesterol synthesis has been shown to participate Type I Interferon responses against pathogens[17–21]. In addition, cholesterol in the lysosome has been shown to activate mTORC1 mediated by cholesterol by direct binding to lysosomal membrane proteins SLC38A9 and Niemann-Pick C1[22]. Given the importance of mTORC1 in growth and proliferation in various cell types and the newly characterized roles in immunity[23], the role of cholesterol in shaping immune responses via mTORC1 is worth exploring.

Cholesterol homeostasis at cellular level

Cholesterol is an essential molecule in mammalian cells. Given its exceeding hydrophobicity, cholesterol can be present in a cell in two main forms: free cholesterol and esterified cholesterol. Free cholesterol molecules are unable to diffuse in the cytosol, thus they are exclusively associated with membrane lipids. Fatty acyl tail linked

cholesterol, also known as cholesterol esters, are stored in the lipid droplets together with triacyl glycerol (TAG).

Cholesterol homeostasis is maintained by balancing import, *de novo* synthesis, and efflux. Cholesterol can be synthesized in from acetyl-CoA through a series of enzymatic steps involving more than 30 enzyme. The final steps of this process occur in the ER. The rate limiting enzyme of cholesterol synthesis is 3-Hydroxy-3-Methylglutaryl-CoA Reductase (HMGCR) Regulation of HMGCR is achieved through various substrate mediated negative-feedback loop. In addition, HMGCR can be pharmacologically inhibited by statins, leading to reduction in circulating cholesterol levels. The master regulator of cholesterol synthesis is the transcription factor SREBP and its chaperone protein SCAP [24–26]. SCAP acts as a sensor for changes in ER cholesterol levels. When ER cholesterol level is reduced, SCAP mediates the translocation and cleavage of SREBP to the nucleus where SREBP transactivates cholesterol biosynthesis genes and other lipid metabolism related genes.

In addition to *de novo* synthesis, cholesterol imported from the environment via low density lipoprotein receptor (LDLR). Deficiencies or mutation in LDLR in humans lead to hypercholesterolemia, with increasing risk of developing cardiovascular diseases. LDLR can be degraded by Proprotein convertase subtilisin/kexin type 9 serine protease (PCSK9) in the lysosome, and anti-PCSK9 antibody has been shown to significantly lower cholesterol in clinical trials recently[27]. Unlike fatty acids, cholesterol cannot be degraded by cells, and the removal of cellular cholesterol relies on the efflux program. LXRs are

members of nuclear receptor superfamily of transcription factors. Upon activation by ligands including oxysterols, LXRs can turn on genes such as *Abcg1* and *Abca1*, whose protein product can effectively remove intracellular cholesterol. High-density lipoprotein (HDL) in the blood stream are the major acceptors of cholesterol from cells, they move cholesterol from peripheral tissue to the for reutilization and excretion in the form of bile acids[28] .

Cholesterol homeostasis at subcellular level

Cholesterol has been shown to distribute unevenly in the cell membranes, where the plasma membrane is estimated to contain about 60 – 80% of total cellular cholesterol. Cholesterol has a molar ratio of 30 – 40% among lipid molecules in the plasma membrane[28–31]. ER has the lowest cholesterol molar ratio in comparison to other organelles. Newly synthesized cholesterol, as well as excess cholesterol arriving at ER, can be shuttled away by esterification and deposit to the lipid droplets, converted to oxysterols, or moved away by multiple cholesterol transporters[30]. It has been shown that trafficking of cholesterol between subcellular membranes are mediated by two distinct mechanisms, namely vesicular transport and non-vesicular transport[28–30], and the relative importance of these two pathways still remain poorly understood.

<u>Vesicular transport of cholesterol</u>

Vesicular transport of cholesterol is mediated by vesicular and tubular intermediates, which ferry membrane components and luminal cargo between subcellular organelles[30].

For example, LDLR on the plasma membrane can bind to lipo-proteins from the environment, upon binding, LDLR together with lipo-protein can be internalized by endocytosis and enter the endolysosomal system. Esterified cholesterol in the endocytosed lipoprotein can be broken down to free cholesterol and free fatty acids. Cholesterol can be removed from the endolysosomal system by two crucial cholesterol transporters NPC1 and NPC2[32], and then be delivered to other membranes such as plasma membrane, ER, recycling endosomes and mitochondria[28–30].

Non-vesicular transport of cholesterol

Non-vesicular transport of cholesterol usually involves proteins with following features: 1) they can bind cholesterol, presumably with a “deep pocket” that can harbor cholesterol molecules away from the aqueous cytosolic environment, and 2) they have access to different membranes. Over the past few years, several proteins have been identified to facilitate non-vesicular transport of cholesterol. Some of these proteins are soluble and can shuttle cholesterol molecules between different membranes. Others are integral membrane proteins such as Aster proteins. Oxysterol-binding protein (OSBP) is an example of cytosolic protein that exchanges cholesterol between ER and Golgi[33,34]. Another example is the Aster protein family. Aster proteins contain an Aster domain that can bind to cholesterol, several transmembrane domains that localizes the proteins to ER, and a GRAM domain that binds to both phosphatidylserine (PS) and phosphatidic acid (PA) in the inner leaflet of plasma membrane[35]. When cholesterol molecules are loaded onto the plasma membrane, PM-ER junction can rapidly form via unknown mechanism, which allows cholesterol non-vesicular transport from PM to ER by Aster-B[35]. Cholesterol

is also the precursor for steroid synthesis, where the first step involves cleavage of the cholesterol side chain in the mitochondria. Steroidogenic acute regulatory proteins, such as STARD1, are required to move cholesterol from outer membrane to the inner membrane of mitochondria[36].

Subcellular cholesterol homeostasis in cells are critical to maintain organelle functions. Excessive cholesterol accumulation can lead to ER stress. In macrophages, cholesterol loading has been shown to deplete calcium storage in the ER and triggers unfolded protein response (UPR)[37–40]. Mitochondria membrane cholesterol homeostasis is also known to be critical. Accumulation of mitochondria cholesterol can lead to compromised membrane integrity and lead to mitochondrial DNA leakage, thus trigger AIM2-mediated inflammasome activation[17].

In addition to cholesterol homeostasis at the organelle level, recent studies by Radhakrishnan and colleagues have characterized different pools of cholesterol within the plasma membrane[41–47]. Cholesterol in the plasma membrane is not uniformly distributed and can be regulated by distinct biological processes. Using bacterial derived cholesterol binding probes that have different affinities to different pools of membrane cholesterol, Radhakrishnan and colleagues revealed that there are at least three distinct cholesterol pools cholesterol in the plasma membrane. These elegant studies added a new layer of complexity to cholesterol homeostasis, and shed light upon a variety of long-standing puzzles such as “how could ER sense plasma membrane cholesterol content

given the large difference of cholesterol content between the two membranes". The biological importance of this partition is investigated in Chapter 2.

Technical hurdles to study lipids

Despite their critical roles in various biological processes, lipids, including cholesterol, are not as well characterized or intensively studied compared to proteins[48]. The technical hurdles of studying lipids are as follows. First, lipids are hydrophobic, but most of our biochemical experimental procedures rely on solubility in aqueous buffer systems. When it comes to lipids, organic solvents have to be used, which requires a higher level of safety standards for both researchers and laboratory setup. Secondly, given the abundance of environmental lipids, experiments involving quantification of lipids require specific materials to reduce background contamination. Here, glass based containers, instead of plastic, have to be used, since plastics are known to be "sticky" for lipids, and special lining of caps such as PTFE has to be used, since organic solvents can dissolve plastic caps. Thirdly, while gene-editing techniques, such as the CRISPR-cas9 system, are powerful tools to manipulate gene and protein expression, the freedom of manipulating lipids levels, both locally and globally, remains low. A growing body of evidence shows the critical roles of lipids, and measurement of lipids at the resolution of intra membrane level can be extremely informative. To advance our understanding of lipid to the next level, it calls for more tools to measure, visualize and manipulate lipids in a more effective and precise way.

Current methods to detect lipids

Lipidomics, a branch of metabolomics, is an emerging discipline in bioscience[49–56]. Changes in lipid compositions can be detected using various methods, such as mass-spectrometry (mass-spec), imaging, and biochemistry. Advance in mass-spectrometry has largely accelerated the field of lipidomics. A typical work flow of MS-based lipid measurement with mass-spec is as follows: 1) Sample generation. For cellular lipids quantification, efficient ways to lyse cells for lipid extraction are required. For subcellular lipids quantification, purification of different organelles needs to be performed; 2) lipid extraction from samples; 3) separation of different lipids using Gas Chromatography (GC) or Liquid Chromatography (LC); Shotgun lipidomics utilizes a totally different technique than chromatography-based separation, where different groups of lipids are simultaneously directly injected and are selected for detection based on their differential dipole moments; 4) Ionization and detection based on mass to charge ratio and 5) data analysis.

Gas Chromatography-Mass Spectrometry (GC-MS)

GC-MS is a powerful tool to quantify lipids, as well as other organic compounds in complex mixtures. Most cellular complex lipids can be broken down to fatty acids and free cholesterol by acid-methanolysis to ensure their evaporation in the gas phase, fatty acids can be derivatized to be fatty acid methyl esters and cholesterol can be trimethylsilylated, and both followed by hexane salt extraction before being analyzed using GC-MS. Our lab has developed a high-throughput pipeline to measure fatty acids and cholesterol with GC-

MS followed by mathematically modeling and data analysis[18,57,58]. GC-MS based quantification is powerful to measure fatty acyl tail and cholesterol composition of complex lipids such as phosphatidylcholine (PC) and cholesterol esters, but it is not able to analyze these complex lipids in their intact form.

Lipid detection with spatial resolution

The accuracy of detection with mass-spec has made it the gold standard for lipid quantification. However, the mass-spec technique *per se* does not yield information such as lipid abundance in different cellular organelles. To solve this problem, several methods have been developed to obtain spatial information of lipids.

Subcellular organelle isolation

One way to measure subcellular organelle lipid content is to isolate the organelle of interest before mass-spec quantification. Differential centrifugation is a common technique used by biochemists to separate organelles based on their different sedimentation rate. Several protocols have been established to isolate organelles for protein quantification, while fewer are optimized for lipids[59–62]. Optimizing isolation protocols for lipids measurement is not trivial, and the protocols need to be optimized based on cell types and treatments, since both can affect sediment rate of organelles. After isolation, purity can be checked by organelle markers western blot or enzymatic assays.

Other than different sediment rate, organelle specific markers have also been taken advantage to isolate organelles of interest. For example, the well-known lysosomal marker LAMP1 can be immunoprecipitated to pull down lysosome[22]. Plasma membrane, given its easy access, can be biotinylated at 4 ˚C to disable endocytosis and then pulled down with streptavidin beads[16,42]. For plasma membrane cholesterol, cells can be fixed followed by plasma membrane cholesterol oxidization using cholesterol oxidase, then the remaining intracellular cholesterol as well as the total cholesterol without oxidation can be measured, and plasma membrane cholesterol content can be calculated by subtraction[16]. However, given that there are three distinct pools of cholesterol in the plasma membrane, whether cholesterol oxidase can oxidize all plasma membrane cholesterol needs to be further examined.

Lipid imaging with microbial products

There is a list of commercially available lipid binding probes that can be visualized with fluorescent microscopy. Filipin III, a toxin bacterial product from *Streptomyces filipinensis* has been used to stain unesterified cholesterol for decades. Cholesterol dependent cytolysins (CDCs), is a family of secreted toxins from mainly Gram+ bacteria that can bind to the metabolically active cholesterol pool in the plasma membrane. Ostreolysin A (OlyA), a fungi product, has recently been characterized to bind cholesterol-sphingomyelin complex on the membrane[17]. Cholera toxin B (CTB), a major virulence factor from *V. cholerae* which causes cholera, can bind to the signature lipid raft GM1[63–65]. Interestingly, most of these lipid probes available on market are products from microorganisms, which

are all exclusively toxins. Given how important these lipids components are to the host, it is not surprising to see them being targeted by microorganisms through evolution.

One caveat of the probes mentioned above is their cytotoxicity, which makes live imaging not suitable. For example, filipin III can disrupt lipid bilayer, and CDCs can form pores on the plasma membrane and cause cell death. DHE and Bodipy-cholesterol are useful tools for live imaging biological processes related to cholesterol[66,67]. However, bodipy is a big fluorophore and DHE is structurally distinct from cholesterol, using these probes will bring artifact to the system and data needs to be examined with caution.

Nanoscale Secondary Ion Mass-spectrometry (NanoSIMS):

NanoSIMS is a mass-spec based imaging system with a spatial resolution of 50 nm or better. This technology has been used for research in material science and geology, and has just recently been utilized in biological studies[68]. NanoSIMS uses a cesium beam to bombard the sample pixel by pixel. The secondary ions released from the sample are then collected and analyzed with mass-spec. This technology allows for elemental and isotopic detection with spatial information, and researchers can use stable isotopes to trace the molecules of interest and obtain quantitative information. For example, ^{13}C-cholesterol fed to macrophages can be traced by NanoSIMS, in addition, ^{15}N labeled CDCs can also be incubated with cells and allow for specific plasma membrane cholesterol pool detection[69,70]. Furthermore, the process of sample preparation for NanoSIMS is compatible with traditional Electron Microscopy (EM), which can be used to correlate chemical information to morphology.

References for Chapter 1:

1. CHAFFEY, N. Alberts, B., Johnson, A., Lewis, J., Raff, M., Roberts, K. and Walter, P. Molecular biology of the cell. 4th edn. *Ann. Bot.* **91**, 401–401 (2003).
2. Vance, J. E. & Vance, D. E. *Biochemistry Of Lipids, Lipoproteins And Membranes*. *Biochemistry of Lipids, Lipoproteins and Membranes* (2008). doi:10.1016/B978-0-444-53219-0.X5001-6
3. Van Meer, G., Voelker, D. R. & Feigenson, G. W. Membrane lipids: Where they are and how they behave. *Nature Reviews Molecular Cell Biology* **9**, 112–124 (2008).
4. Resh, M. D. Covalent lipid modifications of proteins. *Current Biology* **23**, R431-5 (2013).
5. Fernandis, A. Z. & Wenk, M. R. Membrane lipids as signaling molecules. *Current Opinion in Lipidology* **18**, 121–128 (2007).
6. Eyster, K. M. The membrane and lipids as integral participants in signal transduction: lipid signal transduction for the non-lipid biochemist. *Adv. Physiol. Educ.* **31**, 5–16 (2007).
7. Hilgemann, D. W. *et al.* Lipid signaling to membrane proteins: From second messengers to membrane domains and adapter-free endocytosis. *J. Gen. Physiol.* **150**, 211–224 (2018).
8. Currie, E., Schulze, A., Zechner, R., Walther, T. C. & Farese, R. V. Cellular Fatty Acid Metabolism and Cancer. *Cell Metab.* **18**, 153–161 (2013).
9. Peck, B. & Schulze, A. Cholesteryl esters: fueling the fury of prostate cancer. *Cell Metab.* **19**, 350–2 (2014).

10. Wang, A., Luan, H. H. & Medzhitov, R. An evolutionary perspective on immunometabolism. *Science (80-.).* **363**, (2019).
11. O'Neill, L. A. J., Kishton, R. J. & Rathmell, J. A guide to immunometabolism for immunologists. *Nature Reviews Immunology* **16**, 553–565 (2016).
12. Ganeshan, K. & Chawla, A. Metabolic regulation of immune responses. *Annu. Rev. Immunol.* **32**, 609–34 (2014).
13. Buck, M. D., Sowell, R. T., Kaech, S. M. & Pearce, E. L. Metabolic Instruction of Immunity. *Cell* **169**, 570–586 (2017).
14. Kidani, Y. *et al.* Sterol regulatory element-binding proteins are essential for the metabolic programming of effector T cells and adaptive immunity. *Nat. Immunol.* **14**, 489–99 (2013).
15. Bensinger, S. J. *et al.* LXR Signaling Couples Sterol Metabolism to Proliferation in the Acquired Immune Response. *Cell* **134**, 97–111 (2008).
16. Yang, W. *et al.* Potentiating the antitumour response of CD8+ T cells by modulating cholesterol metabolism. *Nature* **531**, 651–655 (2016).
17. Dang, E. V., McDonald, J. G., Russell, D. W. & Cyster, J. G. Oxysterol Restraint of Cholesterol Synthesis Prevents AIM2 Inflammasome Activation. *Cell* 1–15 (2017). doi:10.1016/j.cell.2017.09.029
18. York, A. G. *et al.* Limiting Cholesterol Biosynthetic Flux Spontaneously Engages Type I IFN Signaling. *Cell* **163**, 1–14 (2015).
19. Reboldi, A. *et al.* Inflammation. 25-Hydroxycholesterol suppresses interleukin-1-driven inflammation downstream of type I interferon. *Science* **345**, 679–84 (2014).
20. Araldi, E. *et al.* Lanosterol Modulates TLR4-Mediated Innate Immune Responses

in Macrophages. *Cell Rep.* **19**, 2743–2755 (2017).

21. Blanc, M. *et al.* The Transcription Factor STAT-1 Couples Macrophage Synthesis of 25-Hydroxycholesterol to the Interferon Antiviral Response. *Immunity* **38**, 106–118 (2013).
22. Castellano, B. M. *et al.* Lysosomal cholesterol activates mTORC1 via an SLC38A9–Niemann-Pick C1 signaling complex. *Science (80-.).* **355**, 1306–1311 (2017).
23. Jones, R. G. & Pearce, E. J. MenTORing Immunity: mTOR Signaling in the Development and Function of Tissue-Resident Immune Cells. *Immunity* **46**, 730–742 (2017).
24. Ye, J., DeBose-Boyd, R. A. & Ye, J. Regulation of Cholesterol and Fatty Acid Synthesis. *Cold Spring Harb. Perspect. Biol.* **3**, 1–14 (2011).
25. Horton, J. D. J. J. D. *et al.* SREBPs: activators of the complete program of cholesterol and fatty acid synthesis in the liver. *J. Clin. Invest.* **109**, 1125–31 (2002).
26. Goldstein, J. L., DeBose-Boyd, R. A. & Brown, M. S. Protein sensors for membrane sterols. *Cell* **124**, 35–36 (2006).
27. Dadu, R. T. & Ballantyne, C. M. Lipid lowering with PCSK9 inhibitors. *Nat. Rev. Cardiol.* **11**, 563–575 (2014).
28. Chang, T.-Y., Chang, C. C. Y., Ohgami, N. & Yamauchi, Y. Cholesterol sensing, trafficking, and esterification. *Annu. Rev. Cell Dev. Biol.* **22**, 129–157 (2006).
29. Wüstner, D. Intracellular cholesterol transport. in *Cellular Lipid Metabolism* **110**, 157–190 (American Society for Clinical Investigation, 2009).
30. Ikonen, E. Cellular cholesterol trafficking and compartmentalization. *Nat. Rev. Mol. Cell Biol.* **9**, 125–138 (2008).

31. Soccio, R. E. & Breslow, J. L. Intracellular Cholesterol Transport. *Arterioscler. Thromb. Vasc. Biol.* **24**, (2004).

32. Subramanian, K. & Balch, W. E. NPC1/NPC2 function as a tag team duo to mobilize cholesterol. *Proc. Natl. Acad. Sci.* **105**, 15223–15224 (2008).

33. Mesmin, B. *et al.* A Four-Step Cycle Driven by PI(4)P Hydrolysis Directs Sterol/PI(4)P Exchange by the ER-Golgi Tether OSBP. *Cell* **155**, 830–843 (2013).

34. Im, Y. J., Raychaudhuri, S., Prinz, W. A. & Hurley, J. H. Structural mechanism for sterol sensing and transport by OSBP-related proteins. *Nature* **437**, 154–158 (2005).

35. Sandhu, J. *et al.* Aster Proteins Facilitate Nonvesicular Plasma Membrane to ER Cholesterol Transport in Mammalian Cells. *Cell* **175**, 514-529.e20 (2018).

36. Miller, W. L. Steroidogenic acute regulatory protein (StAR), a novel mitochondrial cholesterol transporter. *Biochimica et Biophysica Acta - Molecular and Cell Biology of Lipids* **1771**, 663–676 (2007).

37. Sozen, E. & Ozer, N. K. Impact of high cholesterol and endoplasmic reticulum stress on metabolic diseases: An updated mini-review. *Redox Biology* **12**, 456–461 (2017).

38. Röhrl, C. *et al.* Endoplasmic reticulum stress impairs cholesterol efflux and synthesis in hepatic cells. *J. Lipid Res.* **55**, 94–103 (2014).

39. Widenmaier, S. B. *et al.* NRF1 Is an ER Membrane Sensor that Is Central to Cholesterol Homeostasis. *Cell* **171**, 1094-1109.e15 (2017).

40. Feng, B. *et al.* The endoplasmic reticulum is the site of cholesterol-induced cytotoxicity in macrophages. *Nat. Cell Biol.* **5**, 781–792 (2003).

41. Das, A., Brown, M. S., Anderson, D. D., Goldstein, J. L. & Radhakrishnan, A. Three pools of plasma membrane cholesterol and their relation to cholesterol homeostasis. *Elife* **3**, (2014).

42. Das, A., Goldstein, J. L., Anderson, D. D., Brown, M. S. & Radhakrishnan, A. Use of mutant 125I-Perfringolysin O to probe transport and organization of cholesterol in membranes of animal cells. *Proc. Natl. Acad. Sci.* **110**, 10580–10585 (2013).

43. Endapally, S., Infante, R. E. & Radhakrishnan, A. Monitoring and modulating intracellular cholesterol trafficking using ALOD4, a cholesterol-binding protein. in *Methods in Molecular Biology* **1949**, 153–163 (Humana Press, New York, NY, 2019).

44. Chakrabarti, R. S. *et al.* Variability of cholesterol accessibility in human red blood cells measured using a bacterial cholesterol-binding toxin. *Elife* **6**, 1–27 (2017).

45. Infante, R. E. & Radhakrishnan, A. Continuous transport of a small fraction of plasma membrane cholesterol to endoplasmic reticulum regulates total cellular cholesterol. *Elife* **6**, 1–23 (2017).

46. Endapally, S. *et al.* Molecular Discrimination between Two Conformations of Sphingomyelin in Plasma Membranes. *Cell* **176**, 1040-1053.e17 (2019).

47. Gay, A., Rye, D. & Radhakrishnan, A. Switch-like responses of two cholesterol sensors do not require protein oligomerization in membranes. *Biophys. J.* **108**, 1459–1469 (2015).

48. Muro, E., Ekin Atilla-Gokcumen, G. & Eggert, U. S. Lipids in cell biology: How can we understand them better? *Molecular Biology of the Cell* **25**, 1819–1823 (2014).

49. Hsu, F.-F. Mass spectrometry-based shotgun lipidomics – a critical review from the

technical point of view. *Anal. Bioanal. Chem.* **410**, 6387–6409 (2018).

50. Wang, M., Wang, C., Han, R. H. & Han, X. Novel advances in shotgun lipidomics for biology and medicine. *Prog. Lipid Res.* **61**, 83–108 (2016).
51. Vaz, F. M., Pras-Raves, M., Bootsma, A. H. & van Kampen, A. H. C. Principles and practice of lipidomics. *J. Inherit. Metab. Dis.* **38**, 41–52 (2015).
52. Brügger, B. Lipidomics: Analysis of the Lipid Composition of Cells and Subcellular Organelles by Electrospray Ionization Mass Spectrometry. *Annu. Rev. Biochem.* **83**, 79–98 (2014).
53. Blanksby, S. J. & Mitchell, T. W. Advances in Mass Spectrometry for Lipidomics. *Annu. Rev. Anal. Chem.* **3**, 433–465 (2010).
54. Rolim, A. E. H., Henrique-Araújo, R., Ferraz, E. G., de Araújo Alves Dultra, F. K. & Fernandez, L. G. Lipidomics in the study of lipid metabolism: Current perspectives in the omic sciences. *Gene* **554**, 131–139 (2015).
55. Yang, L. *et al.* Recent advances in lipidomics for disease research. *J. Sep. Sci.* **39**, 38–50 (2016).
56. Yang, K. & Han, X. Lipidomics: Techniques, Applications, and Outcomes Related to Biomedical Sciences. *Trends Biochem. Sci.* **41**, 954–969 (2016).
57. Williams, K. J. *et al.* An essential requirement for the SCAP/SREBP signaling axis to protect cancer cells from lipotoxicity. *Cancer Res.* **73**, 2850–2862 (2013).
58. Argus, J. P. *et al.* Development and Application of FASA, a Model for Quantifying Fatty Acid Metabolism Using Stable Isotope Labeling. *Cell Rep.* **25**, 2919-2934.e8 (2018).
59. Andreyev, A. Y. *et al.* Application of proteomic marker ensembles to subcellular

organelle identification. *Mol. Cell. Proteomics* **9**, 388–402 (2010).

60. Andreyev, A. Y. *et al.* Subcellular organelle lipidomics in TLR-4-activated macrophages. *J. Lipid Res.* **51**, 2785–2797 (2010).

61. Croze, E. M. & Morré, D. J. Isolation of plasma membrane, golgi apparatus, and endoplasmic reticulum fractions from single homogenates of mouse liver. *J. Cell. Physiol.* **119**, 46–57 (1984).

62. Radhakrishnan, A., Goldstein, J. L., Mcdonald, J. G. & Brown, M. S. Switch-like Control of SREBP-2 Transport Triggered by Small Changes in ER Cholesterol: A Delicate Balance. *Cell Metab.* **8**, 512–521 (2008).

63. Fessler, M. B. & Parks, J. S. Inflammatory Cell Signaling Microdomains as Organizing Principles in Intracellular Lipid Flux and Membrane. doi:10.4049/jimmunol.1100253

64. Simons, K. & Toomre, D. Lipid rafts and signal transduction. *Nat. Rev. Mol. Cell Biol.* **1**, 31–39 (2000).

65. Lingwood, D. & Simons, K. Lipid rafts as a membrane-organizing principle. *Science* **327**, 46–50 (2010).

66. Maekawa, M. Domain 4 (D4) of Perfringolysin O to Visualize Cholesterol in Cellular Membranes-The Update. *Sensors (Basel).* **17**, (2017).

67. Maxfield, F. R. & Wüstner, D. Analysis of cholesterol trafficking with fluorescent probes. *Methods Cell Biol.* **108**, 367 (2012).

68. Nuñez, J., Renslow, R., Cliff, J. B. & Anderton, C. R. NanoSIMS for biological applications: Current practices and analyses. *Biointerphases* **13**, 03B301 (2018).

69. He, C. *et al.* Macrophages release plasma membrane-derived particles rich in

accessible cholesterol. *Proc. Natl. Acad. Sci.* **115**, E8499–E8508 (2018).

70. He, C. *et al.* High-resolution imaging and quantification of plasma membrane cholesterol by NanoSIMS. *Proc. Natl. Acad. Sci.* **114**, 2000–2005 (2017).

CHAPTER 2:

Interferon-mediated reprogramming of membrane cholesterol to evade bacterial toxins

Title: Interferon-mediated reprogramming of membrane cholesterol to evade bacterial toxins

Authors: Quan D. Zhou[1,2], Xun Chi[3], Wei Yuan Hsieh[3], Jonathan J. Mkrtchyan[3], Viet L. Bui[3], Eliza B. Kronenberger[3], Min Sub Lee[1], Alessandra Ferrari[5], Xu Xiao[5], Allison E. Daly[3], Stephen T. Smale[3], Kevin J. Williams[4], Peter Tontonoz[5], Steven J. Bensinger[1,3]

Affiliations:

[1]Department of Molecular and Medical Pharmacology, University of California, Los Angeles, CA 90095

[2]Department of Surgical Oncology, The First Affiliated Hospital, School of Medicine, Zhejiang University, Hangzhou, Zhejiang 310003, P.R. China

[3]Department of Microbiology, Immunology and Molecular Genetics, University of California, Los Angeles, CA 90095

[4]Department of Biological Chemistry, University of California, Los Angeles, CA 90095

[5]Department of Pathology and Laboratory Medicine, University of California, Los Angeles, CA 90095

Correspondence: Steven J. Bensinger (sbensinger@mednet.ucla.edu)

Introduction

Cholesterol is an essential molecule in the mammalian cell membrane. As a highly hydrophobic molecule, cholesterol can be incorporated in the membrane lipid bilayer and can regulate membrane integrity, fluidity as well as membrane protein functions via clustering or direct binding[1–3]. Given the critical role of cholesterol, it is not surprising that a variety of micro-organisms and viruses can target host cell cholesterol to facilitate their pathogenesis[4–7]. In the context of viral infection, some envelope viruses require host membrane cholesterol for entry and egress[4–7]. However, the role of host membrane cholesterol in the context of bacterial infection is less well characterized. The best known cholesterol targeting component from bacteria is called cholesterol dependent cytolysins (CDCs). It is a family of structurally similar pore-forming proteins secreted by more than 30 different bacterial species, mostly Gram-positive bacteria. Examples of CDCs include: streptolysin O (SLO) from *Streptococcus pyogenes*, perfringolysin O (PFO) from *Clostridium perfringens*, anthrolysin O (ALO) from *Bacillus anthracis* and listeriolysin O (LLO) from *Listeria monocytogenes*[8,9]. While bacteria *per se* don't contain cholesterol, the CDC monomer they secret can recognize and bind to membrane cholesterol of mammalian cells, followed by oligomerization and pore formation. The size of pores can be as large as 250 Å, which can disrupt the membrane integrity of the target cells, leading to cell dysfunction or even cell death[10,11]. Therefore CDC secreting bacteria can escape immune surveillance by evading phagolysosomal-dependent destruction, and weaken immune response by damaging immune cells[10–12].

On the other hand, host immune cells like macrophages can sense different components from different pathogens, termed pathogen-associated molecular patterns(PAMPs), via numerous Pattern recognition receptors (PRRs), such as Toll-like receptors (TLRs)[13,14]. Upon PAMP sensing, PRRs can trigger a variety of immune responses, such as Type I Interferon and NF-κB mediated response. These immune responses can help eliminate pathogens and protect the host. It has been shown by many groups, including us, that TLR3 or Type I IFN activation in macrophages can fundamentally alter their lipid composition and metabolism[15–18]. In particular, macrophages reduce cholesterol synthesis in response to these stimuli, which result in a positive feedback for more IFNβ production, as well as restraining NF-κB mediated inflammation[19–22].

Cholesterol homeostasis is maintained in a host cell in a very delicate way, including regulations of synthesis, uptake, export and continuous trafficking between different subcellular compartments[1,23]. How Type I IFN signaling would alter different aspects of cholesterol metabolism, and their potential biological impact is unclear. In this study, we found that Type I IFN signal leads to sequestration of plasma membrane cholesterol, which confers macrophages resistance to CDC-induced damage. Remarkably, this IFN-induced alteration in the plasma membrane pool is specific to the more dynamic and metabolically active pool, also known as the "accessible cholesterol"[24], whereas the sphingomyelin-associated cholesterol pool, critical to membrane microdomain referred to many as the "lipid rafts", is largely unchanged[25].

Type I Interferon signaling mediates resistance to cholesterol-dependent cytolysins

Macrophages have a variety of TLRs to sense different PAMPs. Given that Type I IFN downstream of TLR3 activation can lead to decrease of cholesterol synthesis[19,22,26], we asked whether other TLR activation would lead to the same change. To test this, C57BL/6 bone marrow derived macrophages (BMDMs) were stimulated with TLR1/2, TLR3, TLR4, TLR7 or TLR9 agonists (Pam3CSK4, Poly(I:C), LPS, CL307 and ODN1668, respectively), and cellular synthesized cholesterol were measured by GC-MS coupled with ^{13}C-glucose labeling. TLR3 activation led to decreased cholesterol synthesis (Fig 1A), consistent with previous findings. However, TLR1/2, TLR7 and TLR9 activation largely increase cholesterol synthesis, whereas TLR4 activation with LPS led to a dose-dependent, intermediate phenotype (Fig 1A). TLR3 activation triggers Type I IFN response and TLR1/2, TLR7 and TLR9 activation trigger MyD88-NF_KB mediated response, whereas TLR4 triggers both sides[13], which can help explain the intermediate phenotype of TLR4 activation.

Given that activation of different TLRs lead to differential alteration in cholesterol metabolism, we next asked whether activation of different TLRs can lead to different susceptibility to bacterial CDC challenge. Perfringolysin O (PFO) from *Clostridium perfringens* is one of the best characterized CDCs in the literature[27]. We first pre-treated BMDMs with or without TLR agonists, followed by a PFO challenge in the presence of propidium iodide (PI), a cell impermeable dye that only stains permeabilized cells. Within

20min, around 50% of BMDMs showed PI positive signal after 1 nM PFO challenge (Fig 1B). Remarkably,TLR3 pre-activation for 24h allowed BMDMs to become more resistant to PFO challenge, whereas TLR1/2, TLR7 and TLR9 pre-activation showed higher susceptibility. Consequently, TLR4 pre-treatment showed a dose-dependent, intermediate impact on BMDMs' susceptibility to PFO (Fig S1A).

It has been shown that these pore-forming toxins can damage macrophage function, such as phagocytosis[10,11]. We then tested whether TLR3 activation can maintain BMDM phagocytic capacity upon PFO challenge. To test this, we pre-activated BMDMs with TLR3 agonist, and then challenge cells with 1 nM PFO for 15 min so that only <20% cells are DAPI positive. Then we incubated the PFO-challenged BMDMs with either apoptotic thymocytes or pH-sensitive dead *S. aureus* particles, respectively. We gated on DAPI negative populations and assessed the percentage of macrophages that have phagocytosed *S. aureus* (Fig 1C) or apoptotic thymocytes (Fig 1D). Indeed PFO challenge can result in impaired phagocytosis, which can be largely rescued by pre-activation of TLR3 before PFO challenge(Fig 1C and D).

Next, we focused on TLR3 mediated effect due to its protective role against CDC challenge. It is interesting that TLR3, which senses viral dsRNA, can have a large impact on BMDMs susceptibility to a bacterial product. Given that the major consequence of TLR3 activation is Type I IFN response[13,28,29], we wonder if Type I IFN-IFNAR axis is mediating the protective effect of TLR3. Therefore, we challenged IFNAR KO BMDMs with PFO, followed by quantification of PI-positive cells. The susceptibility profile is

comparable to WT BMDMs at quiescent state, however, the protective effect by TLR3 pre-activation is abolished in the IFNAR KO BMDM (Fig 1E). Furthermore, pre-activation of BMDMs with IFNβ, a Type I IFN, can also protect against PFO challenge, which is abolished in the IFNAR KO BMDM (Fig 1E).

Type I IFN response has been better characterized in anti-viral response[29,30]. But more and more evidence shows Type I IFN also plays an important role in bacterial infection[31]. Bacterial products can be sensed by a variety of TLR receptors that trigger MyD88 response. Once bacterial products (e.g. nucleotides) reach the cytosol, cytosolic PRRs, such as STING and RIG-I, will sense these bacterial PAMPs to produce robust Type I IFN response[32]. Therefore, we activated RIG-I with 5'ppp dsRNA and STING using both its exogenous and endogenous ligand (c-di-GMP and 2'3'-cGAMP, respectively), and found both pathways are protective against PFO challenge to some level yet not significant in the current experimental setup (Fig S1B). We also tested the impact on susceptibility from other cytokines. IL-1β is one of the main cytokines secreted by BMDMs upon bacterial sensing, but it showed increased susceptibility to PFO challenge (Fig S1C), which further highlights the protective role of Type I IFN in this particular setting. IL-4 and IL-10 are critical cytokines involved in anti-inflammatory responses[33,34], and interestingly, both cytokines promoted protective effects against PFO challenge (Fig S1D and S1E). The mechanism of this phenotype needs further investigation.

Together, the data above showed activation of different TLRs led to different cholesterol metabolism reprogramming, as well as different susceptibility to CDC challenge.

Particularly, activation of TLR3-IFNβ axis led to decreased susceptibility to CDC challenge and is protective for BMDMs function.

Type I Interferon signal decreases CDC binding to plasma membrane

Next we investigated the molecular mechanisms underlying the protective effect by Type I IFN against CDC challenge. CDCs like PFO, SLO and ALO all have a common structure, where their domain 4 recognizes cholesterol in the plasma membrane of target mammalian cells. Upon cholesterol binding, these CDCs undergo conformational change to allow CDC monomers to polymerize into membrane pores that disrupt the integrity of the host cell membrane[8,9,35]. We therefore asked whether the protection from Type I IFN is due to decreased CDC binding to the plasma membrane. To test this, we used ALO-D4, an elegantly engineered tool developed by Radhakrishnan and colleagues, which only contains domain 4 of ALO that still binds to membrane cholesterol but loses its pore forming ability [36–39]. ALO-D4 was also engineered to have a single cysteine, which enables easy fluorescence labeling and can be visualized and quantified with fluorescence microscopy. The fluorescent ALO-D4 was incubated with BMDMs at 4˚C to disable internalization and endocytosis[40,41], followed by fixation and fluorescence microscope analysis. Binding of ALO-D4 to BMDMs plasma membrane is indeed decreased by TLR3 or IFNβ pre-activation, which is again IFNAR dependent (Fig 2A). Furthermore, TLR1/2 activation led to slightly increased ALO-D4 binding, and TLR4 activation again had an intermediated phenotype (Fig 2B).

The ALO-D4 binding data correlated with susceptibility data, indicating the protection from TLR3 or IFNβ is very likely due to decreased CDC binding. To test whether Type I IFN behaves similarly in human macrophages, we took human peripheral blood monocytes-derived macrophages, and found both IFNα and IFNβ can decrease their plasma membrane ALO-D4 binding (Fig 2C), suggesting that the decreased ALO-D4 binding by Type I IFN is a general phenomenon across species.

IFN signals selectively deplete "accessible" cholesterol from the plasma membrane

Given that TLR3-IFN axis activation led to decreased cholesterol synthesis, as well as decreased plasma membrane binding to cholesterol targeting CDC, we asked whether TLR3-IFN activation is causing the BMDMs to lose total cholesterol content. To our surprise, activation of all TLRs, including TLR3, led to increased total cholesterol content, and the increase by TLR3 activation is also IFNAR dependent (Fig 3A). Therefore we ask whether plasma membrane is losing cholesterol content upon TLR stimulation. To test this, we used Filipin III[42], a dye that stains free cholesterol but not cholesterol esters. Plasma membrane Filipin III intensity assessed by flow cytometry largely remains unchanged after TLR3 activation (Fig 3B).

This is somewhat puzzling to us since plasma membrane CDC binding is largely decreased by TLR3 and IFNβ signal, indicated by ALO-D4 staining. It has been shown that there are different cholesterol pools in the plasma membrane, of which only a relative

small portion is accessible to CDCs like ALO or PFO. This cholesterol pool is more dynamically regulated under different metabolic conditions, such as cholesterol starving and loading, therefore referred to as metabolically active pool[24,37,43]. Apart from the CDC-accessible cholesterol pool, a significant amounts of plasma cholesterol is associated with sphingomyelin or other membrane lipids, which make cholesterol inaccessible to CDCs and also less dynamically changed. Given that the total plasma membrane cholesterol pool is largely unchanged, we wondered if the sphingomyelin sequestered cholesterol pool is maintained by TLR3-IFN activation. To test this, we used a fungi derived protein, ostreolysin A (OlyA), which specifically binds to sphingomyelin-cholesterol complex but not CDC-accessible cholesterol[25]. Indeed the OlyA binding signal was largely unchanged despite IFNβ treatment (Fig 3C), indicating that this "inaccessible pool" is largely maintained, and the change of cholesterol composition is specific to the "accessible pool" of plasma membrane cholesterol.

To further validate the change of both ALO-D4 and OlyA binding, we took a high-resolution approach termed Nanoscale Secondary Ion Mass-spectrometry (NanoSIMS)[40,41]. This technique utilizes a cesium beam to bombard the sample pixel by pixel. Secondary ions released from the sample are collected and analyzed with a mass spectrometer. This assay allows us to 1) quantitatively access the membrane cholesterol pool change with much higher spatial resolution and 2) rule out the possibility that IFN signal is changing fluorescence stability. NanoSIMS images showed that Type IFN changes cell morphology, and the change of ALO-D4 and OlyA signal after Type I IFN stimulation is consistent with the previous fluorescent data (Fig 3D). To further investigate

the sphingomyelin sequestered cholesterol pool, we used sphingomyelinase (SMase), an enzyme that can digest sphingomyelin and force the sequestered cholesterol to be accessible to CDC[41]. As expected, even after TLR3 activation, there is still significant amount of cholesterol in the plasma membrane that are now accessible to ALO-D4 due to SMase treatment (Fig 3E).

Sphingomyelin has a more rigid biochemical feature compared to other lipids in the membrane, and cholesterol is critical to facilitate the ordered packing of sphingomyeline. The sphingomyelin-cholesterol complex can further associate with other lipid like monosialotetrahexosylganglioside (GM1) and proteins to form functional microdomains on the membrane, referred to by many as “lipid rafts”[44–48]. A variety of immune receptors are shown to be localized in these microdomains, and one can imagine disrupting cholesterol in these microdomains might disrupt proper lipid packing and therefore certain receptor functions. From the data above, we hypothesize that TLR3-IFN signaling specifically decreases the CDC-accessible cholesterol pool, without decreasing the function of lipids rafts. Cholera Toxin B (CTB) has been used by many groups to assess GM1 content on membranes[42], and the CTB intensity was actually increased by TLR3 activation (Fig 3F). In addition, the sphingomyelin signal, assessed by lysenin, a sphingomyelin binding toxin from earthworm *Eisenia fetida*, is largely maintained in the macrophage plasma membrane (Fig 3G). MHC II is a macrophage receptor critical for antigen presentation, and it’s shown to be associated with “lipid rafts”[49–51]. TLR3-IFN activation led to increased MHC II on the membrane (Fig 3H). In addition, TLR3 activation didn’t decrease the ability of macrophage to phagocytose, as shown earlier (Fig 1C and

D). Interestingly, transferrin receptor, as a representative of non-lipid raft associated protein[52–54], is decreased after IFN activation (Fig 3I).

Together, these data showed that TLR3-IFN activation specifically reprograms the CDC-accessible cholesterol pool for resistance against CDC challenge, while largely maintain the integrity of "lipid rafts", its associated receptor and the ability of macrophages to phagocytose.

IFN signal reprograms macrophage cholesterol metabolism to facilitate rapid depletion of "accessible" plasma membrane cholesterol and intracellular storage

Next we investigated the molecular mechanisms underlying the redistribution of plasma membrane cholesterol in response to TLR3-IFN signal. We first assessed the time kinetic of IFN mediated change of ALO-D4 binding. The decrease of ALO-D4 binding occurs as early as 2 h by IFNβ stimulation in a JAK/TYK-dependent manner (Fig 4A and B). IFNβ can still downregulate ALO-D4 in the presence of protein translation inhibitor, cycloheximide (Fig 4B), suggesting that this rapid decrease is mediated by IFN-JAK/TYK signaling pathway[29] which doesn't require *de novo* protein synthesis. Whereas the rapid decrease of ALO-D4 biding by TLR3 activation was largely abolished by CHX (Fig S4A), suggesting the requirement for synthesis of the cytokine IFN. After TLR3-IFN activation, the ALO-D4 signal remained at low level at later time points (24 h, Fig 2A, 48 h, data not shown).

We then investigated the possible cholesterol related biological processes downstream of IFNAR-JAK/TYK activation. To systematically assess this question, we performed RNA-seq analysis on BMDMs in response to IFNβ and TLR3 activation. As expected, in response to TLR3-IFN activation, cholesterol synthesis genes (e.g. *Hmgcr, Sqle*) were down-regulated. To our surprise, many genes involved in cholesterol redistribution were changed (e.g. *Abca1, Abcg1, Gramd1b, Npc2, Stard3, Osbp2, Soat2*) in an IFNAR-dependent manner (Fig 4C). These changes are more unique to TLR3 but not TLR1/2 or TLR4 (Fig S4B). And interestingly, these changes can also occur in response to Type II IFN stimulation, yet still largely dependent on IFNAR (Fig S4C), suggesting a cross-activation of IFNAR by IFNγ. In the panel of cholesterol trafficking genes reprogrammed by TLR3-IFNβ activation, *Msr1* is one of membrane receptor responsible to uptake lipids. Increased cholesterol uptake may lead to downregulation of cholesterol synthesis as well as other changes[55–57]. Therefore, we disabled cholesterol uptake by incubating BMDMs in lipoprotein-depleted serum (LPDS). In the absence of cholesterol in the media, we still see downregulation of cholesterol synthesis (Fig S4D), consistent with a previous study[21]. Other cholesterol trafficking genes were still reprogrammed similarly in both LPDS and normal serum media, (Fig S4D), suggesting that the transcriptional reprogramming of cholesterol distribution is an IFN stimulated effect but not a secondary change due to increased cholesterol uptake.

Membrane cholesterol trafficking are mediated by various processes, which can be categorized as 1) non-vesicular, and 2) vesicular transport[1,23,58–61]. Our RNA-seq data showed that genes in both categories are being reprogrammed. Therefore, we took a

genetic approach to disrupt both processes and assessed ALO-D4 binding in response to TLR3-IFN stimulation. NPC1 is a lysosomal/endosomal membrane protein that plays an important role in intracellular vesicular transport of cholesterol[62], NPC1 KO BMDMs showed significantly lower ALO-D4 signal at quiescent state, which disabled further investigation at this point (Fig S4E). Then we tested whether non-vesicular transport is involved. Aster-B, the protein product of gene *Gramd1b*, is a newly characterized transporter moving cholesterol from plasma membrane to endoplasmic reticulum (ER)[63]. In Aster-B KO BMDMs, ALO-D4 signal maintains high after 2h even with TLR3 of IFNβ activation (Fig 4D), suggesting that this non-vesicular cholesterol transporter Aster-B is mediating the rapid decrease of CDC-accessible cholesterol pool. Excess cholesterol arriving at the ER can be esterified to cholesterol esters by ACAT1 and ACAT2 in the ER[1,64]. To test whether IFN signal redistributed cholesterol to the ER, we measured cholesterol esters after TLR3-IFN activation. Cholesterol esters were indeed increased after TLR3-IFN activation, in an IFNAR-dependent manner (Fig 4E). In addition, TLR3 activation still led to cholesterol ester accumulation in cholesterol-free media (Fig S4F), indicating the excess cholesterol comes from an intracellular source, which is very likely plasma membrane since it has the largest cholesterol pool in the cell[2,65,66].

To conclude, these data showed that Type I IFN fundamentally reprograms cholesterol metabolism at transcription level, and can rapidly decrease CDC-accessible cholesterol in a non-vesicular, more specifically Aster-B dependent manner. However, at 24 h post TLR3 activation, Aster-B KO BMDMs also have decreased ALO-D4 binding (Fig S4G), suggesting the involvement of additional pathways.

Production of 25-hydroxycholesterol is required to maintain changes in plasma membrane cholesterol and mediates resistance to CDCs

Cholesterol 25-hydroxylase (CH25H) is a well-defined interferon-stimulated ER enzyme that converts cholesterol to 25-hydroxycholesterol (25-HC) [26,67]. Interestingly, 25-HC can also be incorporated into plasma membrane and does not bind CDCs [68,69]. To test the potential impact of CH25H, we took CH25H KO macrophages and activated their TLR3. TLR3 activation can still decrease ALO-D4 signal in CH25H KO BMDMs at 4 h (Fig 5A). However, 16 h after TLR3 activation, CH25H KO BMDMs showed high ALO-D4 signal, and to our surprise, the signal is even higher than quiescent cells (Fig 5A). Then we asked whether CH25H has a role in Type I IFN-mediated protection against CDC challenge. CH25H KO BMDMs were more susceptible to PFO challenge at quiescent state, and unable to be protected by either TLR3 or IFNβ (Fig 5B). Likewise, CH25H KO BMDMs that have been pre-activated with TLR3 fail to phagocytose after PFO challenge (Fig 5C). These data suggested a potential role of 25-HC, the enzymatic product of CH25H, in protection against CDC challenge. Indeed, exogenous 25-HC can largely protect both WT and CH25H KO macrophages from PFO challenge (Fig 5C and D) and 25-HC incubation can significantly decrease ALO-D4 binding, which phenocopies that of TLR3-IFN activation (Fig 5E). Next, we ask how 25-HC leads to decreased ALO-D4 signal. A well-known role of 25-HC is to inhibit cellular cholesterol synthesis[26,67,70]. And we found that acute inhibition cholesterol biosynthesis *per se* with simvastatin is also able to decrease ALO-D4 binding (Fig 5F). This suggests that the inhibition of cholesterol synthesis maybe one of the mechanisms by which 25-HC protects BMDMs from CDCs.

It has been shown that IFNγ can also upregulate CH25H expression and trigger 25-HC production[26,67]. We asked whether IFNγ can also protect macrophages against CDC challenge as TLR3-Type I IFN does. Indeed, IFNγ stimulation also leads to both decreased ALO-D4 binding (Fig 5G), and decreased susceptibility to PFO challenge (Fig 5H), which are both dependent on CH25H.

The fact that TLR1/2 activation leads to increased susceptibility to CDCs is puzzling to us. CDCs are mainly from Gram+ bacteria species that can activate TLR1/2 in macrophages. We ask how macrophages could possibly protect themselves in the context of Gram+ bacteria challenge. It has been shown that host IFN response can also be triggered by Gram+ bacteria via sensing their DNA/RNA as PAMPs[32,71]. Thus it is possible that the protective role of IFN can override the susceptibility effect by TLR1/2 activation. Consequently, we tested the effect of TLR1/2 activation in combination with IFNγ or IFNβ. Interestingly, the combination can decrease ALO-D4 binding even more than IFNγ or IFNβ alone (Fig 5I), and the protective effect of IFNβ overrides TLR1/2, which is still dependent on CH25H (Fig 5J).

Discussion

In this study, we found that Type I IFN can deplete a specific pool of plasma membrane cholesterol that is accessible to CDC, therefore providing protection to the host against

CDC challenge. This depletion is dependent on the IFNAR-CH25H axis, where exogenous metabolite 25-HC alone can recapitulate the protective role of IFN. For the underlying mechanism of decreased CDC binding and susceptibility conferred by IFN, here we propose a two-step model (Fig 6): At quiescent state, a macrophage has sufficient cholesterol levels in the plasma membrane accessible pool, and therefore these cholesterols can be targeted by bacterial-derived cholesterol dependent cytolysin (CDCs), leading to macrophage permeabilization and dysfunction**.** Upon IFN activation, at early stage (1-4h), cholesterol can be removed rapidly from plasma membrane accessible pool by non-vesicular transport to the ER mediated by cholesterol transporter, Aster-B, via unknown mechanisms. And at later stage (16 h - 48 h), excess cholesterol arriving at the ER can be converted to 1) cholesterol esters by ACAT, and 2) 25-HC by interferon-dependent CH25H. The removal of accessible cholesterol from the plasma membrane confers BMDMs resistance to CDC challenge.

As to how 25-HC leads to decreased CDC binding and resistance to CDC challenge downstream of Type I IFN still remains elusive at the moment. Based on our observation and previous studies, here we propose the following potential mechanisms: 1) 25-HC can inhibit cholesterol synthesis, and synthesis inhibition *per se* can decrease ALO-D4 binding (Fig 5F). How cholesterol synthesis regulates PM accessible cholesterol still remains unclear to the field. 2) 25-HC can promote esterification[72,73], which could further accelerate the sequestration of cholesterol. 3) 25-HC can be inserted into plasma membrane. And despite the high resemblance of structure to cholesterol, 25-HC doesn't bind to CDC[68,69]. Therefore, it is possible that IFN-activated macrophages replaced

plasma membrane accessible cholesterol with 25-HC, or simply diluting the pre-existing cholesterol under the threshold of CDC binding. 4) 25-HC in the plasma membrane can make cholesterol more "active"[69]. While this can lead to more PFO binding to cholesterol in the liposome, we think in a cell, this could also make cholesterol more accessible to cellular transporters to move cholesterol away from plasma membrane. In addition, 25-HC is also an LXR agonist which triggers efflux via cholesterol transporter Abcg1 and Abca1[74–77]. We do see Abcg1 RNA expression level is induced by IFN signal in an IFNAR-dependent manner, but we don't think these transporters are playing a critical role here since ABCG1 and ABCA1 KO BMDMs still have decreased ALO-D4 after IFNβ and TLR3 activation at 24 h (data not shown).

Plasma membrane cholesterol pool is our focus for this study. Given that IFN signal can transcriptionally reprogram a variety of cholesterol trafficking processes, it will be of great interest to see how it affects other membrane cholesterol pool such as endosome, phagosome, lysosome, mitochondria, etc. Listeriolysin O (LLO) from Listeria monocytogenes has been shown to escape phagosome and reach cytosol to escape immune surveillance[78–80]. Other CDC containing bacteria, such as GAS, can also survive in the macrophage cytoplasm[12]. For lysosome, previous studies have shown blocking lysosomal cholesterol export with small molecule U18666A can block Ebola viral infection[81]. For mitochondria, it has been shown that 25-HC triggered by LPS can inhibit mitochondria membrane cholesterol built up and prevent further AIM2 mediated immune response[20].

The fact that CDCs are only targeting a small pool of dynamically changing cholesterol pool is confusing to us. CDC has the same cholesterol binding kinetic as host cholesterol metabolism regulators such as SCAP. We think they may have the same evolutionary origin, but diverged later in evolution to either regulate cholesterol metabolism in the mammalian cells or were used by bacteria to target mammalian cell cholesterol, respectively. In addition, many bacteria actually produce SMase which can digest sphingomyelin, and make the sequestered cholesterol now accessible for CDCs, which can help the pathogens to target a bigger pool of host cholesterol. In fact, *Arcanobacterium haemolyticum* has both PLD (with SMase activity) and ALN (a type of CDC), and the SMase activity of PLD has been shown to be critical for ALN's hemolysis function[82]. Also, SMase can be produced by a common bacteria species *S. aureus,* and one could imagine that during skin infection, SMase secreted by *S. aureus* and SLO secreted by *S. pyogenes* can work synergistically to attack their host.

In this research we focused on investigating the role of Type I IFN signaling in macrophages when challenged by bacterial cytolysins. The role of cholesterol reprogramming by Type I IFN in an actual CDC-secreting bacterial infection setting needs to be further investigated. Based on our current finding, we think during an actual infection of CDC secreting bacteria, TLR1/2 and TLR4 on the host cell surface can first sense PAMPs from Gram + and Gram – bacteria, respectively, and both will trigger NF-κB response. Then the other bacterial PAMPs can later trigger robust IFN response when their DNA and RNA reaches the host cell cytosol and encounters PRRs like RIG-I and STING[31,32]. While TLR1/2 and Type I IFN activation have opposing effects on

susceptibility to CDC challenge, the protective effect confers by IFN is dominating when in combination with TLR1/2. It's interesting that TLR1/2 in combination with IFNβ can decrease ALO-D4 binding even more then IFNβ alone. We think this might be due to the crosstalk between MyD88 and IFN signal[83–85], and when both are triggered, as in the classic pro-inflammation model or "M1" polarization with LPS+IFNγ, these two pathways work synergistically. In addition, the kinetics of IFN and TLR stimulus may be important as well. Although different TLRs have different impact on cholesterol synthesis at a later point (24 – 48 h), they actually all decrease cholesterol synthesis gene expression at early time point (4 – 8 h, data not shown), where IFN signal maintains lower synthesis and MyD88 pathway can elevate cholesterol synthesis compared to quiescent state. It is possible that IFN can override this rebound to keep the synthesis low.

The role of Type I IFN in bacterial infection is a host, pathogen and context specific matter, which needs to be carefully examined on a case-by-case manner[31,32]. Robust IFN response can be triggered by the SLO secreting bacteria *S. pyogenes*, a CDC secreting bacteria, when their DNA reaches cytosol and encounters STING-IRF3 pathway[12,71]. IFN response in this setting turned out to be protective for the host[86]. The STING-IRF3 is conserved in many cell types such as macrophage, dendritic cells, fibroblasts and endothelial cells. One could imagine that the IFNβ produced within the primary infection site can enter circulation to trigger 25-HC production in macrophages. Moreover, 25-HC itself metabolite can re-enter the circulation and possibly exert its protective effect for different cell types against CDC challenge systematically.

In clinic, the SLO secreting bacteria *S. pyogenes*, or group A *Streptococcus* (GAS) is a leading human pathogen[12,71,86], which can cause disease conditions spanning a wide spectrum. On the mild end, patients can get pharyngitis and impetigo, and on the severe end, patients can get necrotizing fasciitis and even toxic-shock syndrome which could lead to death. Researchers have been investigating strategies to combat GAS infection, and SLO has been of great interest as a therapeutic target for many, due to its strong virulence. Recently, a group has engineered nanoparticles coated with red blood cell membrane, which is abundant of accessible cholesterol, as a decoy to sequester SLO in the circulation during GAS infection[87]. Also as mentioned earlier, Type I IFN provides protection in mice model GAS infection[71,86], where the proposed mechanism is that Type I IFN can restrict systematically exacerbated levels of the proinflammatory cytokine IL-1β. Here we provide another mechanism to explain IFN's protective effect, where Type I IFN can lead to less SLO binding to the host via IFNAR-CH25H axis. It is very likely that 25-HC administration alone might provide protection against GAS infection. It's been shown that systematic administration of 25-HC is beneficial against Zika and EBOV virus infection in multiple *in vivo* models[26,67,88]. But another previous study showed that loss of CH25H and 25-HC is protective during *Listeria* infection, since without 25-HC, mitochondria becomes "leaky" and mitochondrial DNA can trigger cytosolic AIM2 mediated inflammation, which can more efficiently restrict *Listeria*[20]. Given the complexity of different immune responses that the actual CDC secreting bacterial infection can trigger, the roles of CH25H and 25-HC need to be carefully examined.

In conclusion, the studies presented herein provide mechanistic insights as to how Type I IFN reprograms macrophage cholesterol metabolism at sub-cellular level, and extended our understanding of crosstalk between lipid metabolism and immune responses.

Experimental Procedures for Chapter 2

***Mouse strains**:* All WT and knockout mice were purchased from The Jackson Laboratory: WT C57BL/6 (JAX 000664). B6;129S6-*Ch25h*^{tm1Rus}/J (*Ch25h*$^{-/-}$, JAX 016263). B6.129-Npc1tm1Dso/J (*Npc1*$^{-/-}$, JAX 027704). Aster-B (GRAMD1B, *Gramd1b*$^{-/-}$) global knockout mice were a kind gift from Dr. Peter Tontonoz (UCLA), they were generated as previously described[63].

Peripheral blood mononuclear cells (PBMCs) derived macrophages: Human monocyte-derived monocytes were isolated from leukopacks using standard ficoll procedures and plastic adherence. Isolation of monocytes was conducted by UCLA The CFAR Virology Core. Monocytes were differentiated into macrophage with 50 ng/mL human GM-CSF (Peprotech, 300-03) in IMDM (Hyclone) media with 10% FBS and 1% v/v pen/strep for 7 days prior to experimental use.

***Mouse cells**:* Bone marrow was differentiated into macrophages in DMEM containing 10% v/v FBS (HyClone, GE SH3007103), 5% v/v M-CSF conditioned media, 1% v/v pen/strep, 1% v/v glutamine (Invitrogen) 0.5% v/v sodium pyruvate (Invitrogen) for 7-9 days prior to experimental use. Cells were changed to media with 5% FBS at the time of stimulation.

Reagents: PRR ligands: LPS (Invivogen, tlrl-smlps), Poly(I:C) (Invivogen tlrl-pic (HMW)), Pam3CSK4 (Invivogen, tlrl-pms), CL307 (Invivogen, tlrl-c307), ODN1668 (invivogen tlrl-1668), 2'3'-cGAMP (Invivogen tlrl-nacga23), c-di-GMP (Invivogen tlrl-cdg), 5'ppp-dsRNA (Invivogen tlrl-3prn). Cytokines: recombinant Murine IL-4 (Peprotech 214-14), Recombinant Murine IL-1β (211-11B), recombinant Murine IFN-γ (315-05), recombinant

Mouse IFN-β1 (carrier-free, Biolegend 581302), recombinant human IFN-β (Peprotech 300-02BC), IFN-α is a kind gift from Modlin lab (UCLA). Hyclone IMDM media (16750-088) and FBS (SH3007103) were purchased from VWR. PFO is a kind gift from Ajit S. Divakaruni lab[89] (Agilent 102504-100). Streptolysin O from Streptococcus pyogenes (gamma irradiated, Sigma S0149-25KU).

Lipidomics Analysis: Macrophages were cultured in 6 well dishes (Fisher, 08-772-1B) and stimulated with TLR ligands as described above. 48 h post-stimulation, cells were imaged for cell count as previously described[22], scraped and spun down in PBS, and snap-frozen as cell pellets. A modified Bligh and Dyer extraction[90] was carried out on samples. Prior to biphasic extraction, a 13-lipid class Lipidyzer Internal Standard Mix is added to each sample (AB Sciex, 5040156). Following two successive extractions, pooled organic layers were dried down in a Genevac EZ-2 Elite. Lipid samples were resuspended in 1:1 methanol/dichloromethane with 10 mM Ammonium Acetate and transferred to robovials (ThermoFisher, 10800107) for analysis. Samples were analyzed on the Sciex Lipidyzer Platform for targeted quantitative measurement of 1100 lipid species across 13 classes. Differential Mobility Device on Lipidyzer was tuned with SelexION tuning kit (Sciex, 5040141). Instrument settings, tuning settings, and MRM list available upon request. Data analysis performed on Lipidyzer software. Quantitative values were normalized to cell counts.

***Isotope Enrichment Experiments*:** Day 8 differentiated BMDMs were transferred to complete media containing 50% [13C]glucose (Cambridge Isotope Laboratories, CLM-1396-MPT-PK) with or without TLR stimulation for 48 h before collection. Analysis of

labeled fatty acids and cholesterol was performed as described previously[22,91,92]. The relative contributions of synthesis to the total cholesterol pool over the 48 h-labeling period were determined by fitting the isotopologue distributions for cholesterol in a model similar to Isotopomer Spectral Analysis (ISA) as described previously[22,91,92].

Gene expression analysis: RNA was extracted from all cells with Trizol (ThermoFisher, 15596-018) using manufacturer's protocols. cDNA was synthesized with high-capacity cDNA reverse transcription kit (Applied Biosystems, 4368814) as per manufacturer's instructions (700 ng/μL RNA per cDNA synthesis reaction). Quantitative PCR (qPCR) was conducted on the Roche LightCycler 480 using SYBR Green Master Mix (Kapa Biosciences) or PowerUp™ SYBR™ Green Master Mix (Thermofisher, A25778) and 0.5 μmol/L primers. Relative expression values are normalized to control gene (*36b4*) and expressed in terms of linear relative mRNA values.

PFO Permeabilization Live Imaging: BMDMs were seeded 30 k/well on 96 well plates (E&K Scientific, EK-25090, Greiner). Cells were left for 2 days before stimulation. Cells were pretreated with TLR ligands for 2-24 h depending on the experiment. For live imaging, culture media were replaced by 37 ˚C PBS with 0.05% BSA, 1 μg/mL propidium iodide (PI) (VWR, 80057-368) and 5μg/mL Hoechst 33342 (Thermofisher, H3570). Then cells were challenged by spiking recombinant PFO (final concentration 1 nM), and plates were imaged every 5-10 min on a Molecular Devices ImageXpress XL using a 20x Objective (Nikon Plan Fluor, 0.3 NA). Total (Hoechst 33342-positive) and permeabilized (PI-positive) cell number were assessed using MetaXpress Software with Powercore using the Multi-wavelength cell scoring module.

Macrophage phagocytosis assay: BMDMs were seeded 150 k/well on 24 well plates. Cells were left for 1-3 days before stimulation. Cells were pretreated with TLR ligands for 4-24 h depending on the experiment. PFO were spiked in with a final concentration of 10 nM, and cells were left to incubate for 1 h at 37˚C, then cells were washed with room temp PBS twice, and replaced with fresh BMDM media with 5% FBS. Apoptotic thymocytes (1 million/well), pHrodo™ Red *S. aureus* Bioparticles™ Conjugate (1 mg/mL) (ThermoFisher, A10010), pHrodo™ Red E. coli BioParticles™ Conjugate (1 mg/mL) (ThermoFisher, P35361), or pHrodo™ Red Zymosan Bioparticles™ Conjugate (0.5 mg/mL) (ThermoFisher, P35364) were added on top of the macrophages and incubated for 1 h at 37 ˚C. To remove the un-phagocytosed apoptotic thymocytes or pHrodo™ Red Bioparticles™ Conjugate, cells were washed twice with room temp PBS and then subject to flow cytometry analysis.

Preparation of apoptotic thymocytes: Thymus from WT C57BL/6J were dissected, grinded, and filtered into single cell suspension. Contaminations from red blood cells were removed by incubating the cell pellet with Red Blood Cell Lysis Buffer (Sigma-Aldrich, R7757). Thymocytes were then counted and resuspended at 5 million/mL. Apoptosis was induced by treating thymocytes with 1 μM dexamethasone (Sigma-Aldrich, D4902) at 37 °C for 3-18 h depending on the experiment. After apoptosis induction, thymocytes were labeled with 5 μM CellTrace CFSE (ThermoFisher, C34554). The reaction was quenched by adding 5 volumes of IMDM + 10% FBS. Labeled thymocytes were resuspended at 1 million/50 μL in blank DMEM.

***Flow cytometry analysis*:** BMDMs were lifted off the plates by scraping with the plunger of a 1 mL syringe and transferred to a 96-well round bottom plate. After pelleting, cells were first incubated with TruStain FcX™ (anti-mouse CD16/32) Antibody (BioLegend, 101319, 1:500) in FACS buffer (PBS with 2% FBS, 1 mM EDTA) for 10 min on ice. Cells were then stained with antibodies for surface markers CD11b (BioLegend, 101207, 1:400) or F4/80 (BioLegend, 123115, 1:200) for 20 min on ice. After one wash with FACS buffer, cells were resuspended in FACS buffer with 1 μg/mL DAPI (ThermoFisher, D1306) and analyzed with Attune NxT Flow Cytometer. Data were analyzed by FlowJo V10.

Cholera Toxin subunit B (CTB), MHC II and Transferrin Receptor staining: CTB-Alexa 594 (V34405) (ThermoFisher, C34777); PE/Cy7 anti-mouse CD71 antibody (Biolegend 113812); PE anti-mouse MHC Class II antibody (ebioscience 12-5321-82) 100 μL of 1X PBS was added to each vial to make a 1 mg/ml stock solution. BMDMs were scraped and transferred to 96-well plates. After pelleting, cells were gently resuspended in chilled, complete growth media with 1 μg/mL CTB-Alexa 594 and incubated on ice for 10 min. After incubation, cells were washed once, resuspended in 300 μL FACS buffer and analyzed by Attune NxT Flow Cytometer.

Filipin III staining: BMDMs were seeded at 150 k/well on 24-well plates. Cells were left for 2-3 days before stimulation. Cells were pretreated with TLR ligands for 4-24 h depending on the experiment. Filipin III was purchased from Sigma-Aldrich (F4767) and resuspended in ethanol to 2 mg/mL. BMDMs were washed once with room temp PBS and fixed with 3% paraformaldehyde for 15 min at room temp. Cells were then washed

twice and stained with 100 μg/mL filipin III for 30 min at room temp covered in dark. After staining, excess filipin was removed by pelleting cells. Cells were then resuspended in FACS buffer and analyzed by Attune NxT Flow Cytometer.

Preparation of [^{15}N] or [^{13}C] His-Tagged ALO-D4: A plasmid for ALO-D4 (ALO amino acids 404–512 with C472A and S404C substitutions) was originally obtained from Arun Radhakrishnan[38] (University of Texas Southwestern Medical Center, Dallas), and [^{15}N]-labeled ALO-D4 was prepared as described before[41]. Briefly, ALO-D4 was expressed in BL21 (DE3) pLysS Escherichia coli (Invitrogen) and induced with 1 mM isopropyl β-d-1-thiogalactopyranoside (IPTG) in 1 L of minimal medium containing 20.2 mM NH_4Cl and 2 g of Glucose at 18 °C for 16 h. [^{15}N] NH_4Cl or [^{13}C]Glucose were used for [^{15}N] or [^{13}C]ALO-D4, respectively. Cells were pelleted and lysed by sonication, and the lysate was centrifuged at 4 °C. The supernatant was mixed with 4 mL of HisPur Cobalt resin (50% bed volume; ThermoFisher Scientific). The mixture was loaded into a column and allowed to flow through by gravity. The column was washed, and [^{15}N] ALO-D4 was eluted with a buffer containing 300 mM imidazole. The eluates were pooled and concentrated to 1 mL with an Amicon 10 kDa cut off concentrator (Millipore). The purified [^{15}N] ALO-D4 was stored at 4 °C.

Preparation of His-Tagged ostreolysin A (OlyA) and His-mCherry-Tagged Lysenin: A plasmid for OlyA (with C62S C94S S151C substitution) was kindly provided by Arun Radhakrishnan[25] (University of Texas Southwestern Medical Center, Dallas). A plasmid for lysenin amino acids 161–297 were cloned into the vector pBADmCherry (Addgene).

Both OlyA and Lysenin were expressed and purified same way as ALO-D4. Lysenin was a kind gift from Stephen Young (UCLA).

Preparation of Fluorescent ALO-D4, OlyA: Purified protein was conjugated as described previously with slight modifications[39]. Briefly, cysteine-substituted ALO-D4 or OlyA were incubated with Alexa-488 or Alexa-594 (Life Technologies) at 4˚C overnight in 50 mM Tris-HCl (pH 7.5) and 150 mM NaCl (1x TBS) containing 1 mM TCEP. Free dye was separated by extensive buffer exchange with 1x TBS in Amicon 10 kDa cut off concentrator (Millipore), and stored at 4˚C.

Binding of ALO-D4, Lysenin and OlyA to Cells: Cells were seeded 150 k/well on PDL-coated coverslips (Neuvitro, fisher NC0672873) on a 24-well plate. After stimulation, cells were incubated with ALO-D4, lysenin or OlyA as described before[40]. Briefly, macrophages were washed three times for 10 min in PBS/Ca/Mg containing 0.2% (wt/vol) BSA. Cells were then incubated with ALO-D4, lysenin or OlyA (all 20 µg/mL) in PBS/Ca/Mg containing 0.2% (wt/vol) BSA for 2 h at 4°C. Unbound proteins were removed by washing with PBS/Ca/Mg three times for 2 min each.

Confocal Microscopy Analysis: After lysenin-mCherry or fluorescently labeld ALO-D4, or OlyA binding, cells were fixed with 3% paraformaldehyde for 15 min and stained with 5 µg/mL DAPI, then washed twice with PBS/Ca/Mg for imaging. Images were taken with an Axiovert 200M microscope and processed with Zen 2010 software (Zeiss).

Quantification of Fluorescence Intensity: For signal quantification, cell were plated on 24well plates (Cellvis, P24-0-N), treated, stained as above, and fixed cells in PBS/Ca/Mg were imaged within 2 hours. Images were taken at UCLA Molecular Screening Shared

Resource core facility on a Molecular Device ImageXpress Confocal using a 20x Objective (Nikon Plan Fluor, 0.3 NA). on a Molecular Devices ImageXpress XL. Maximum projected cellular fluorescence intensity was assessed by MetaXpress Software with Powercore using the Multi-wavelength cell scoring module. Integrated fluorescent intensity profile were exported and analyzed by R with ggplot2 package[93]. Differences were assessed by Student's *t* test with Welch's correction.

NanoSIMS Sample Preparation: As described before[40], after ALO-D4, lysenin or OlyA binding, cells were fixed with 4% paraformaldehyde (Electron Microscopy Sciences) and 2.5% glutaraldehyde (Electron Microscopy Sciences) in 0.1 M phosphate buffer (1.14 g NaH_2PO_4, 1.69 g Na_2HPO_4 in a 100 mL final volume of ddH_2O, pH 7.4) for 20 min at 4 °C followed by 1 h at room temperature. The samples were washed three times for 7 min each in 0.1 M phosphate buffer, postfixed with 1% osmium tetroxide (Electron Microscopy Sciences) in 0.1 M phosphate buffer for 45 min, and washed three times for 7 min each in ice-cold ddH_2O. Then cells were air-dried.

NanoSIMS Analyses: As described before[40,94], platinum-coated (5-nm) cells were analyzed with a nanoSIMS 50L instrument (CAMECA) with some modifications. Briefly, samples were bombarded with a focused $^{133}Cs+$ primary beam, and secondary ions (e.g., $^{12}C-$, $^{13}C-$, $^{16}O-$, $^{12}C^{14}N-$, $^{12}C^{15}N-$) and secondary electrons were collected. Before imaging, a high $^{133}Cs+$ primary beam (1-nA beam current; primary aperture D1 = 1) was used to presputter an area of 50 × 50 μm for 25 s to remove the platinum coating and implant $1^{33}Cs+$. In the same region, low-magnification images (~40 × 40 μm) were obtained with an ~2.5-pA beam current (primary aperture D1 = 2), a dwell time of 2.5 ms

per pixel, and scans of 512 × 512 pixels. High-magnification images (~10 × 10 μm) were obtained with an ~0.8-pA beam current (primary aperture D1 = 3), a dwell time of ~10 ms per pixel, and scans of 512 × 512 pixels.

NanoSIMS Quantification To quantify $^{13}C/^{12}C$ and $^{15}N/^{14}N$ ratios in cells, we identified particles by SEM and/or $^{12}C^-$, $^{12}C^{14}N^-$, $^{16}O^-$, or secondary electron nanoSIMS images, and regions of interest in the middle of the particles were defined with the OpenMIMS plugin in ImageJ (NIH). For each image, the mean $^{15}N/^{14}N$ and $^{13}C/^{12}C$ ratios of the regions of interest were measured by ImageJ and processed by Prism 7.0. Differences were assessed by a Student's t test with Welch's correction.

RNA-Seq: WT and IFNAR KO BMDMs were treated with IFNβ (20 ng/mL), Poly(I:C) (1 μg/mL) and RNA was was purified using QIAGEN RNeasy Kit. RNA-Seq library was prepared with KAPA mRNA HyperPrep Kit (KK8580) and multiplexing barcodes were also added. Samples were submitted to the UCLA Clinical Microarray Core for RNA-seq analysis. Sequencing was performed on Illumina Hiseq 3000 SBS PEx150. Data quality check was done on Illumina SAV. Demultiplexing was performed with Illumina CASAVA 1.8.2 and fastq files were generated.

RNA-Seq Data Analysis: Hisat2 was used to build the reference genome index from the mouse (NCBI37/mm9) reference genome available from UCSC[95]. Reads were aligned using the paired-end mode of Hisat2 to the mouse reference index[95]. The first distinct alignment for each read was used for further analysis. FPKM values were calculated by diving mapped reads within exonic regions by the length of the spliced product and then

by the total reads per million for each sample. Heatmap of FPKPM values was generated using guidelines described[96].

Chapter 2: Figure 1

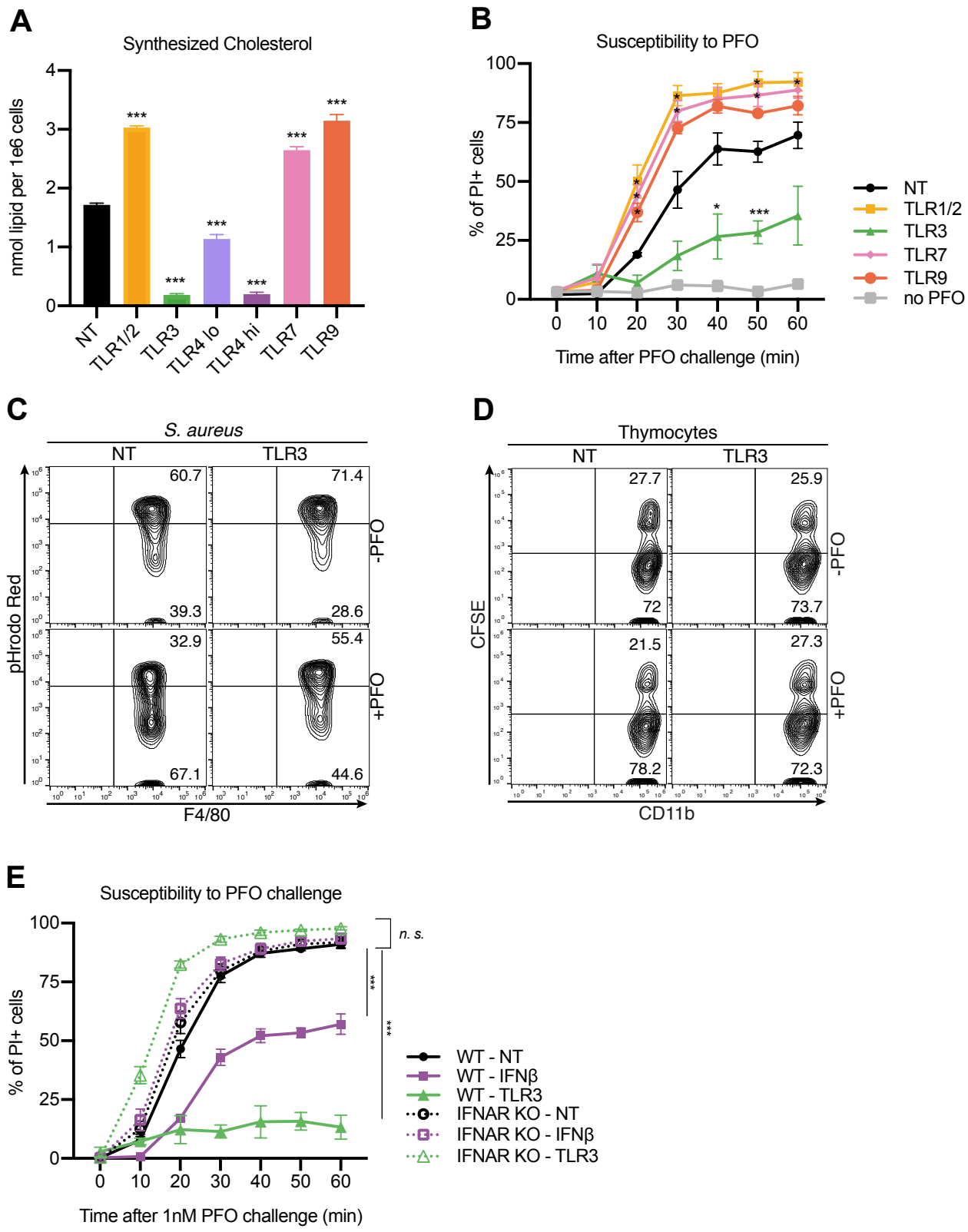

Chapter 2: Figure 1. Type I Interferon signaling mediates resistance to cholesterol-dependent cytolysin.

A. Net synthesized cholesterol (nmol/10^6 cells) from C57BL/6 bone marrow–derived macrophages (BMDMs) stimulated with TLR1/2 agonist (Pam3CSK4; 50 ng/mL), TLR3 agonist (Poly(I:C); 1 μg/mL), TLR4 agonist (LPS; lo = 10 ng/mL and hi = 50 ng/mL), TLR7 agonist (CL307; 100 nM), TLR9 (ODN1668; 100 nM), or unstimulated (NT) for 48 h. Synthesized cholesterol was determined by GC-MS and isotopomer spectral analysis modeling.

B. Percentage of propidium iodide (PI)–positive BMDMs treated with the indicated TLR agonist for 24 h and then challenged with perfringolysin O (PFO) for up to 60 min in the presence of propidium iodide (PI). Cells were imaged every 10 min to assess changes in PI incorporation.

C. Flow cytometry plots of *S. aureus* phagocytosed by control or TLR3-stimulated BMDMs. Macrophage cultures were stimulated with TLR3 agonist. After 24 h, BMDMs were washed and then incubated with PFO for 1 h. PFO containing media was then replaced with fresh media containing pHrodo-red-labeled *S. aureus*. Percentage of macrophages that phagocytosed labeled *S. aureus* are indicated in upper corner.

D. Flow cytometry plots of thymocytes phagocytosed by control or TLR3-stimulated BMDMs. Macrophage cultures were stimulated with TLR3 agonist. After 24 h, BMDMs were incubated with PFO for 1 h, and then media was replaced with fresh media containing CFSE-labeled apoptotic thymocytes. Percentage of macrophages that are positive for CFSE are indicated in upper corner of plot.

E. Percentage of propidium iodide (PI)–positive WT and IFNAR KO macrophages treated with a TLR3 agonist for 24 h and then challenged with PFO for up to 60 min in the presence of PI. Cell cultures were imaged every 10 min to assess changes in PI incorporation.

Data in **A, B and E** are mean ± s.e.m. (n=3) and representative of three independent experiments. Data were analyzed with Student's *t* test (A) or two-way ANOVA (B and H). *p<0.05; **p<0.01; ***p<0.001.

Chapter 2: Figure 2

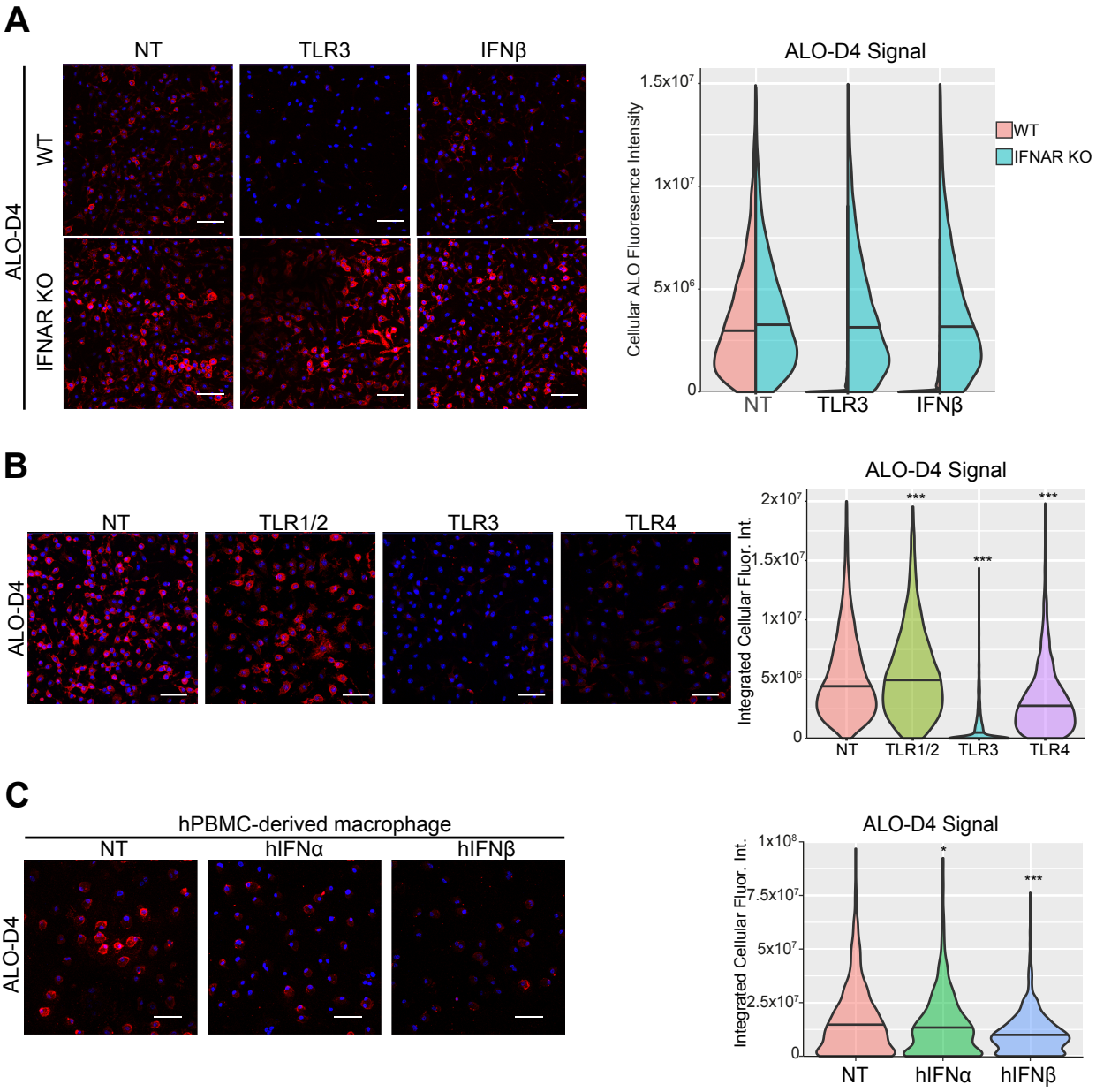

Chapter 2: Figure 2. Type I Interferon signal decreases CDC binding to plasma membrane

A. Confocal images of WT or type I interferon receptor-deficient (IFNAR KO) BMDMs cultures stimulated with TLR3 agonist (Poly(I:C); 1 μg/mL) or IFNβ (100 ng/mL) for 24 h, and then stained with fluorescent ALO-D4 and DAPI.

B. Confocal images of macrophage cultures stimulated with the indicated TLR agonists for 12 h and then stained with fluorescent ALO-D4 and DAPI.

C. Confocal images of human peripheral blood monocyte (PBMC)–derived macrophages stimulated with human IFNα or IFNβ = 10 ng/mL) for 24 h and then stained with fluorescent ALO-D4 and DAPI.

A-C right panel: Cellular fluorescent intensity distribution of ALO-D4 binding generated from confocal images of macrophages. Data of n=1700-2700 (A and B) or n=1000-1300 (C)**.** All data is shown as violin plots of cellular fluorescent intensity (smoothened probability density of all data) with bars set at median. Data are representative of three independent experiments. Statistical significance determined data was analyzed with Student's *t*-test with Welch's correction. *p<0.05; **p<0.01; ***p<0.001.

Chapter 2: Figure 3

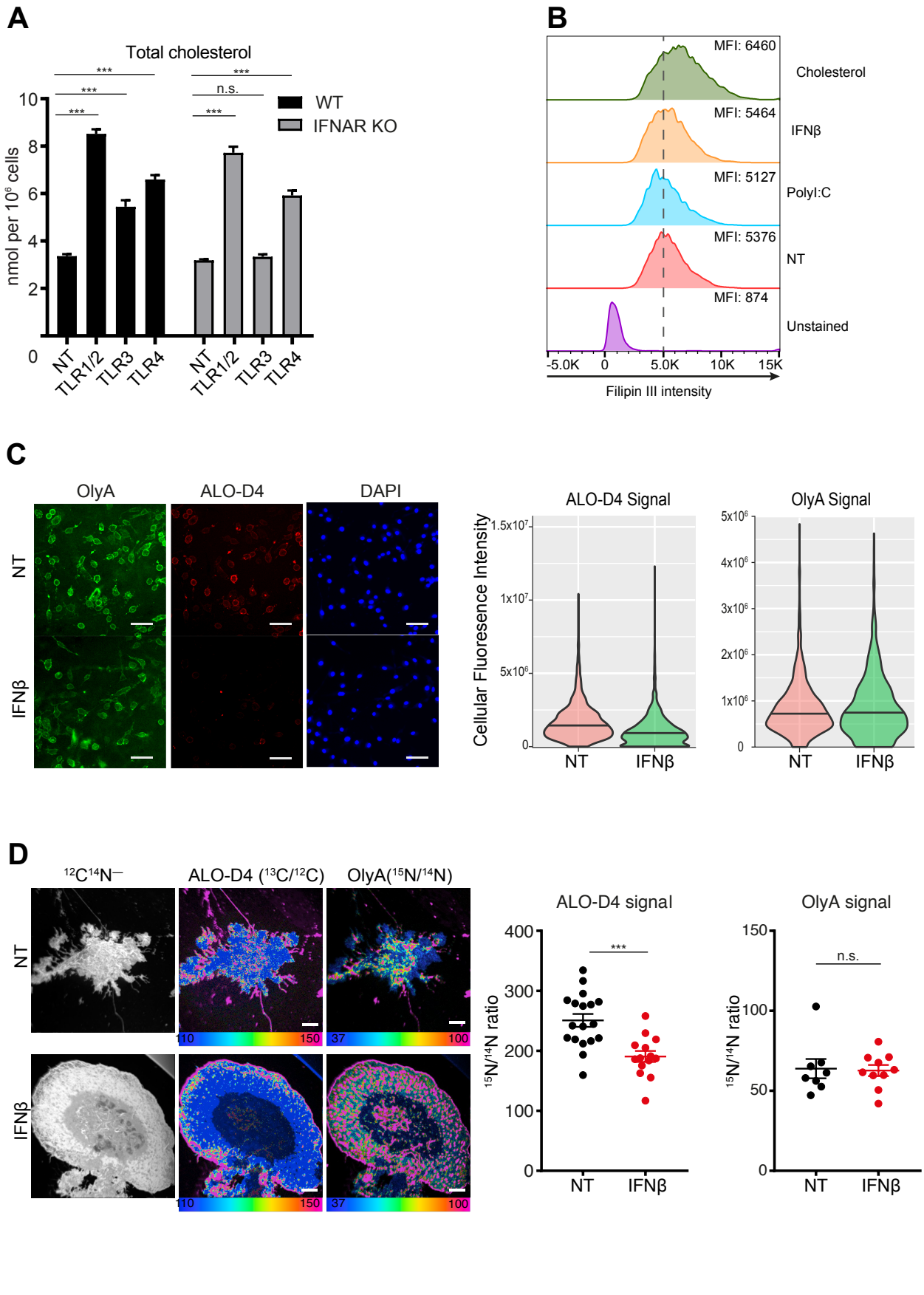

Chapter 2: Figure 3 (continued)

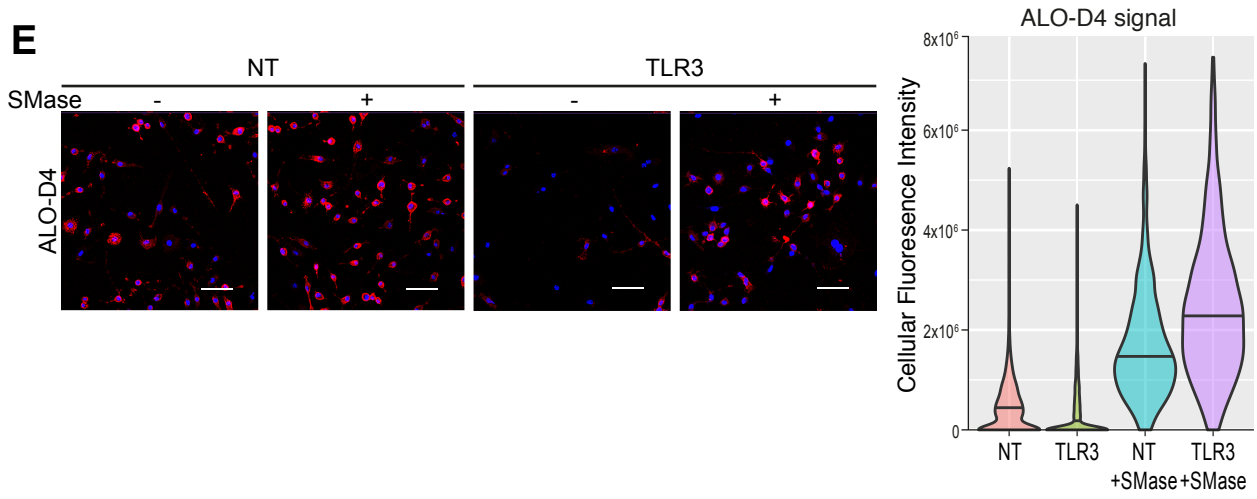

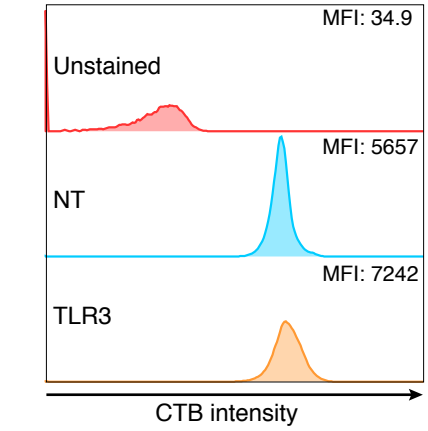

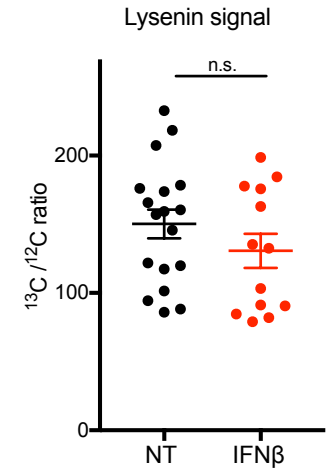

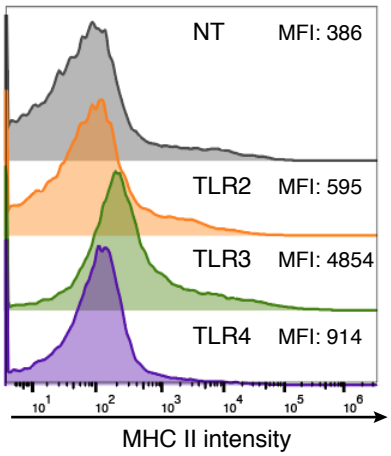

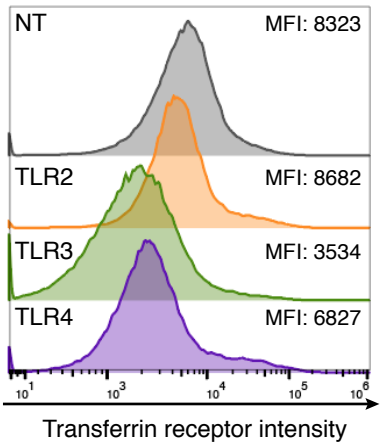

Chapter 2: Figure 3. IFN signals selectively deplete "accessible" cholesterol from the plasma membrane

A. Total amount of cholesterol (nmol/10^6 cells) in WT or type I interferon receptor–deficient (IFNAR KO) bone marrow derived macrophages (BMDMs) stimulated with TLR1/2 agonist (Pam3CSK4; 50 ng/mL), TLR3 agonist (Poly(I:C); 1 μg/mL), TLR4 agonist (LPS; 50 ng/mL) or unstimulated (NT) for 48 h. Total cholesterol was determined by GC-MS. Data are mean ± s.e.m (n=3) and analyzed with Student's *t* test.

B. Flow cytometry plots of BMDMs incubated with water-soluble cholesterol, or stimulated by TLR3 agonist or IFNβ (100 ng/mL) for 24 h. After treatment, macrophages were stained with Filipin III. Median fluorescence intensity (MFI) are indicated in upper corner of plot.

C. Confocal images of BMDM cultures stimulated with IFNβ (100 ng/mL) for 24 h then stained with fluorescent ALO-D4, OlyA and DAPI. (Scale bar, 50 μm).

D. Left: Nano-SIMS imaging of [^{13}C]ALO-D4 or [^{15}N]OlyA binding on untreated or IFNβ (100 ng/mL, 24 h)-stimulated BMDMs. NanoSIMS images were generated based on secondary electrons ($^{12}C^{14}N^-$), or the $^{13}C/^{12}C$ or $^{15}N/^{14}N$ ratio. (Scale bar, 5 μm.) The color scale shows the range of $^{13}C/^{12}C$ or $^{15}N/^{14}N$ ratios. Right: Quantification of [^{15}N]ALO-D4 or [^{15}N]OlyA binding on untreated or IFNβ (100 ng/mL, 24 h)-stimulated BMDMs determined by NanoSIMS. Quantification based on average $^{15}N/^{14}N$ ratio by cell. Data are mean ± s.e.m (n=18 vs 14 for ALO and n=8 vs 10 for OlyA). Data were analyzed by Student's *t* test with Welch's correction.

E. Confocal images of BMDM cultures stimulated with TLR3 agonist for 24 h. Indicated cultures were then treated with sphingomyelinase (SMase; 100 mU/mL) for 30 min followed by staining with fluorescent ALO-D4 and DAPI. (Scale bar, 50 μm.)

F. Flow cytometry plots of BMDMs stimulated by TLR3 agonist or Unstimulated (NT) for 24 h. After treatment, macrophages were stained with Cholera Toxin B (CTB). Median fluorescence intensity (MFI) are indicated in upper corner of plot.

G. Quantification of [^{13}C]Lysenin binding on untreated or IFNβ (100 ng/mL, 24 h)stimulated BMDMs determined by NanoSIMS. Quantification based on average ^{13}N/^{12}N ratio by cell. Data are mean ± s.e.m (n=18 vs13). Data were analyzed by Student's *t* test with Welch's correction.

H. Flow cytometry plots of BMDMs stimulated by TLR3 agonist or Unstimulated (NT) for 24 h. After treatment, macrophages were stained with anti MHC II antibody. Median fluorescence intensity (MFI) are indicated in upper corner of plot.

I. Flow cytometry plots of BMDMs stimulated by TLR3 agonist or Unstimulated (NT) for 24 h. After treatment, macrophages were stained with anti-Transferrin receptor antibody. Median fluorescence intensity (MFI) are indicated in upper corner of plot.

C and E right panel: Distribution of cellular fluorescent intensity (n=2000 cells) shown as violin plots (smoothened probability density of all data) with bars set at median. Statistical significance determined with Student's *t*-test with Welch's correction. (*p<0.05; **p<0.01; ***p<0.001)

Chapter 2: Figure 4

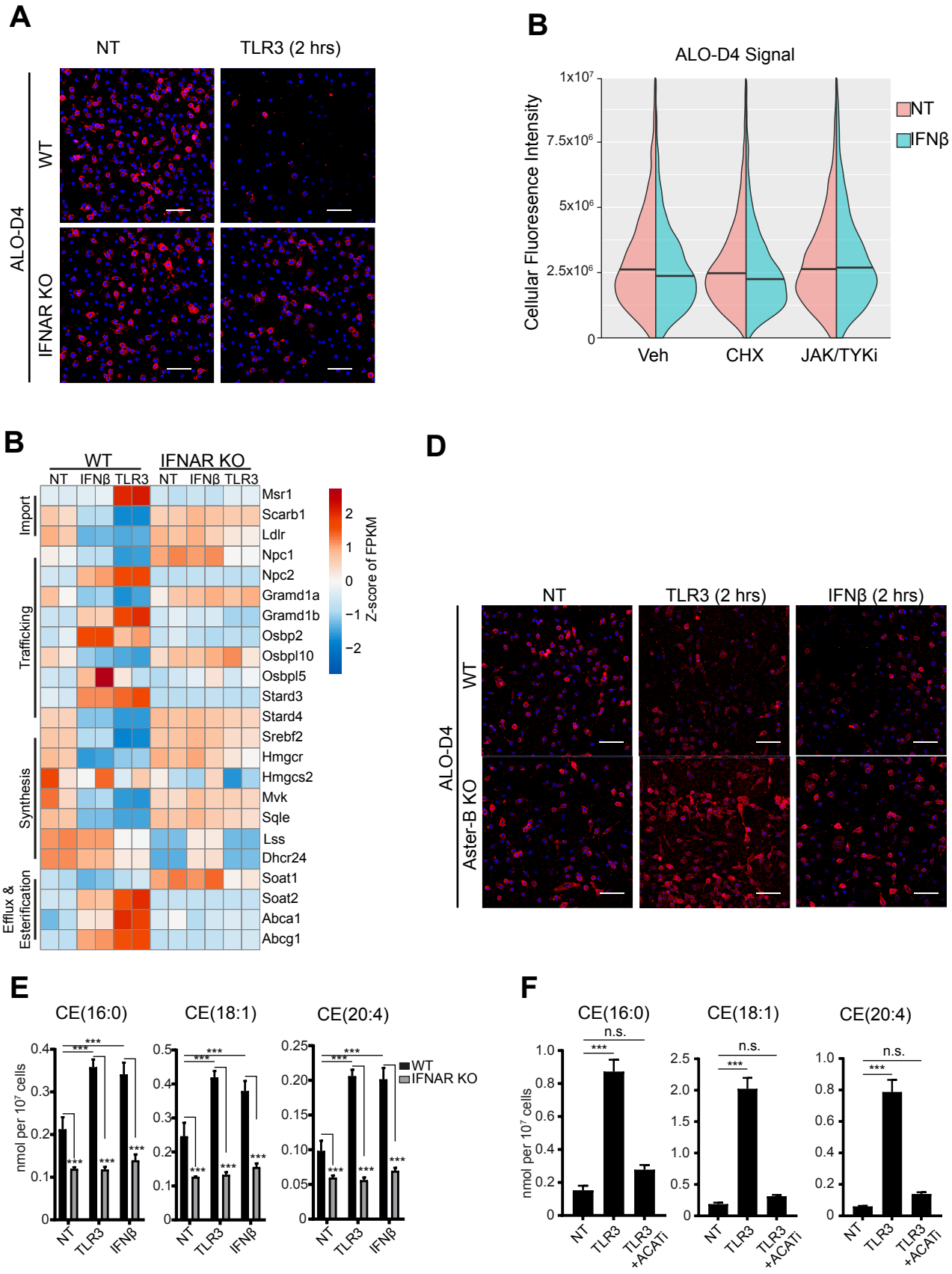

Chapter 2: Figure 4. IFN signaling reprograms macrophage cholesterol metabolism to facilitate rapid depletion of "accessible" plasma membrane cholesterol and intracellular storage

A. Confocal images of WT or IFNAR KO BMDM cultures stimulated with TLR3 agonist for 2 h, and then stained with fluorescent ALO-D4 and DAPI.

B. Distribution of cellular fluorescent intensity of ALO-D4 binding generated from confocal images of WT BMDM cultures pre-treated with cyclohexamide (CHX; 100 ng/mL) or TYK/JAK signaling inhibitor (PF-06700841; 2 μM) for 30 min, and then stimulated with IFNβ for 1 h, followed by staining with fluorescent labeled ALO-D4 and DAPI. Distribution of cellular fluorescent intensity shown (n=1700-2700 cells) as violin plots (smoothened probability density of all data) with bars set at median.

C. RNA-Seq analysis for expression heat map of indicated cholesterol metabolism genes from WT or type I interferon receptor-deficient (IFNAR KO) bone marrow derived macrophages (BMDMs) stimulated with IFNβ (20 ng/mL) or TLR3 agonist (Poly(I:C); 1 μg/mL) for 24 h. Expression levels are row-centered unit variance scaled (Z-score) from FPKM value.

D. Confocal images of WT or Aster-B KO (*Gramd1b* $^{-/-}$) BMDM cultures stimulated with TLR3 agonist or IFNβ for 2 h, and then stained with fluorescent ALO-D4 and DAPI.

E. Quantification (nmol/10^7 cells) of cholesterol ester species (16:0, 18:1, 20:4) in WT and IFNAR KO BMDMs stimulated with TLR3 agonist or IFNβ for 48 h. CE species pool sizes were determined by direct infusion mass spectrometry.

F. Quantification (nmol/10^7 cells) of cholesterol ester species (16:0, 18:1, 20:4) in BMDMs concomitantly activated TLR3 agonist in the presence of the ACAT inhibitor (Sandoz 58-035; 0.5 μg/mL) for 48 h. CE species pool sizes were determined by direct infusion MS.

Data in A, B, D and E are representative of three independent experiments. Data in E and F are analyzed with Student's *t* test. *p<0.05; **p<0.01; ***p<0.001. Scale bar, 50 μm.

Chapter 2: Figure 5

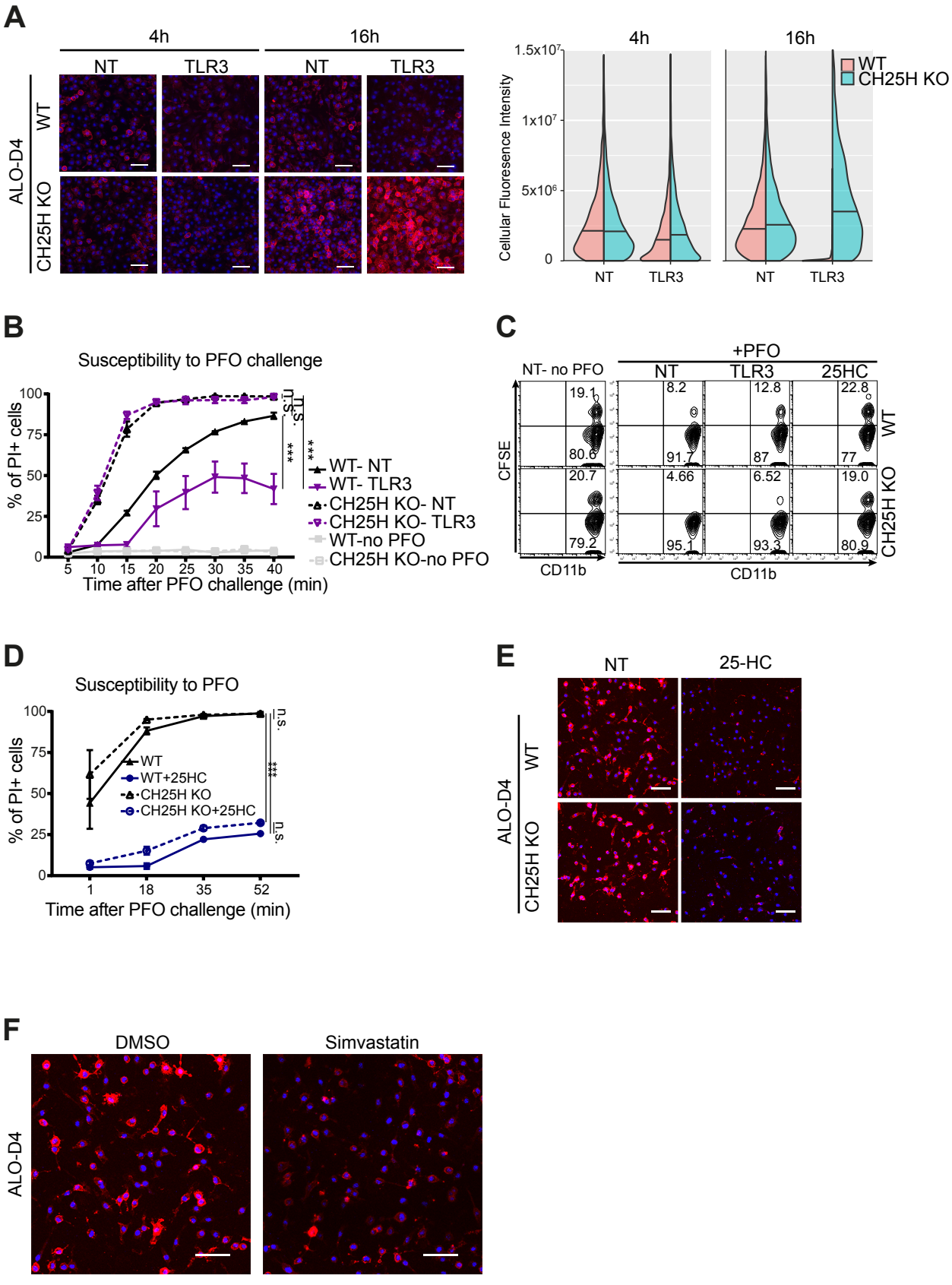

Chapter 2: Figure 5 continued

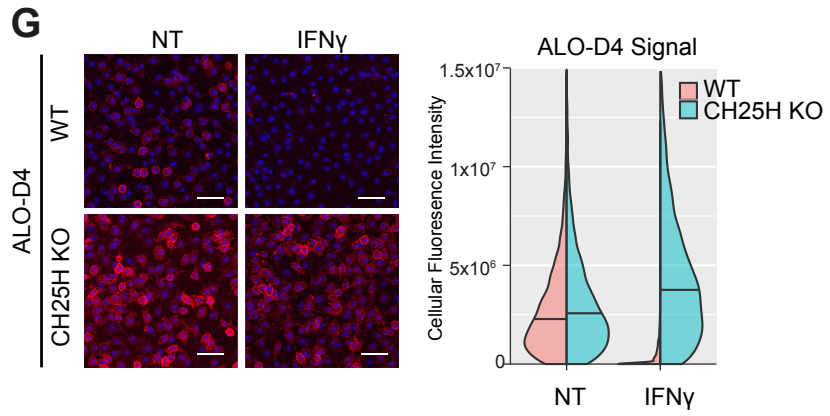

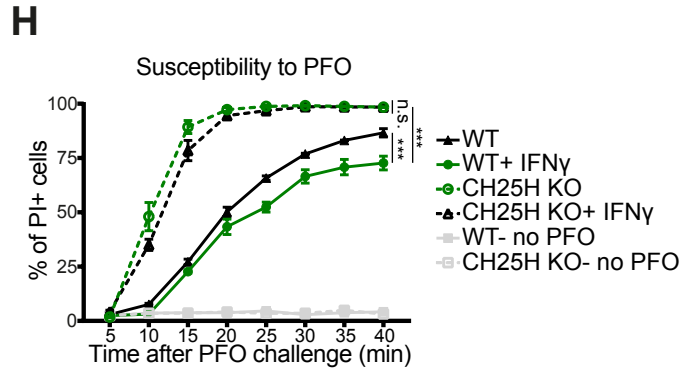

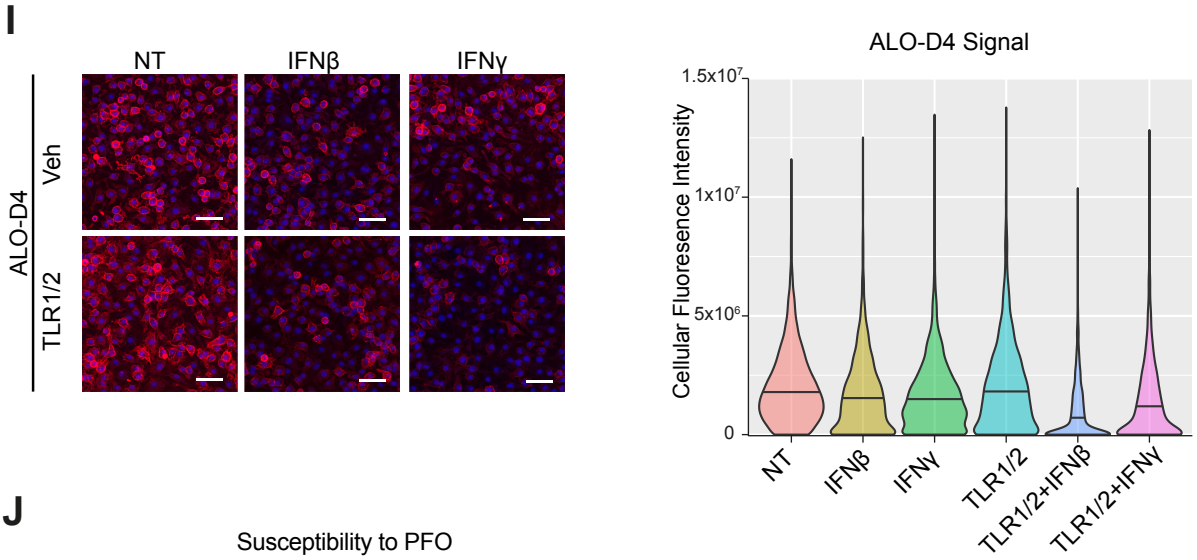

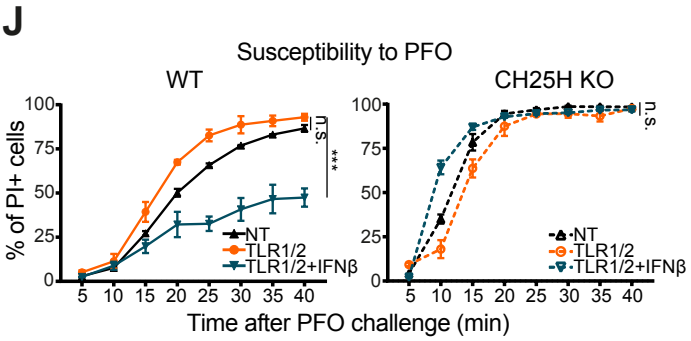

Chapter 2: Figure 5. Production of 25-hydroxycholesterol is required to maintain changes in plasma membrane cholesterol and mediates resistance to CDCs

A. Confocal images of WT or cholesterol 25-hydroxylase-deficient (CH25H KO) BMDMs cultures stimulated with TLR3 agonist (Poly(I:C); 1 μg/mL) for 4 h or 16 h, and then stained with fluorescent ALO-D4 and DAPI. Right: distribution of cellular fluorescent intensity (n=2000 cells) shown as violin plots (smoothened probability density of all data) with bars set at median.

B. Percentage of propidium iodide (PI) positive WT or CH25H KO BMDMs treated with TLR3 agonist for 16 h, and then challenged with PFO for up to 40 minutes in the presence of PI. Cell cultures were imaged every 5 minutes to assess changes in PI incorporation.

C. Flow cytometry plots of thymocytes phagocytosed by WT or CH25H KO BMDMs. Macrophages were activated by TLR3 agonist or treated with 25HC (3 μM). After 4 h, BMDMs were incubated with PFO for 1 h, and then media was replaced with fresh media containing CFSE-labeled apoptotic thymocytes for 1 h. Percentage of macrophages that are positive for CFSE are indicated in upper corner of plot.

D. Percentage of propidium iodide (PI) positive WT or CH25H KO BMDMs treated with TLR3 agonist for 24 h. WT or CH25H KO BMDM cultures were treated with 25HC (3 μM) for 2 h, and then challenged with PFO for up to 60 minutes. Cell cultures were imaged every 17 minutes to assess changes in PI incorporation.

E. Confocal images of WT or CH25H KO BMDMs cultures incubated with 25-HC (3 μM) over night, and then stained with fluorescently labeled ALO-D4 and DAPI.

F. Confocal images of WT BMDMs cultures incubated with vehicle (DMSO) or Simvastatin (5 μM) for 4 h, and then stained with fluorescently labeled ALO-D4 and DAPI.

G. Confocal images of WT BMDMs cultures stimulated with IFNγ (20 ng/ml) for 24 h, and then stained with fluorescently labeled ALO-D4 and DAPI.

H. Percentage of propidium iodide (PI) positive WT or CH25H KO BMDMs treated with IFNγ (20 ng/ml) for 24 h, and then challenged with PFO for up to 40 minutes in the presence of PI. Cell cultures were imaged every 5 minutes to assess changes in PI incorporation.

I. Confocal images of WT or CH25H KO BMDMs cultures stimulated with TLR1/2 agonist (Pam3CysK; 50 ng/mL), IFNβ (20 ng/mL) or IFNγ (20 ng/mL) alone, or in combination for 24 h, and then stained with fluorescent ALO-D4 and DAPI.

J. Percentage of propidium iodide (PI) positive WT or CH25H KO BMDMs treated with TLR1/2 agonist and IFNβ for 24 h, and then challenged with PFO for up to 40 minutes in the presence of PI. Cell cultures were imaged every 5 minutes to assess changes in PI incorporation.

Data in B, D, H and J are mean ± s.e.m.(n=3) and representative of three independent experiments and analyzed with two-way ANOVA. *$p<0.05$; **$p<0.01$; ***$p<0.001$. Scale bar, 50 μm.

Chapter 2: Figure 6

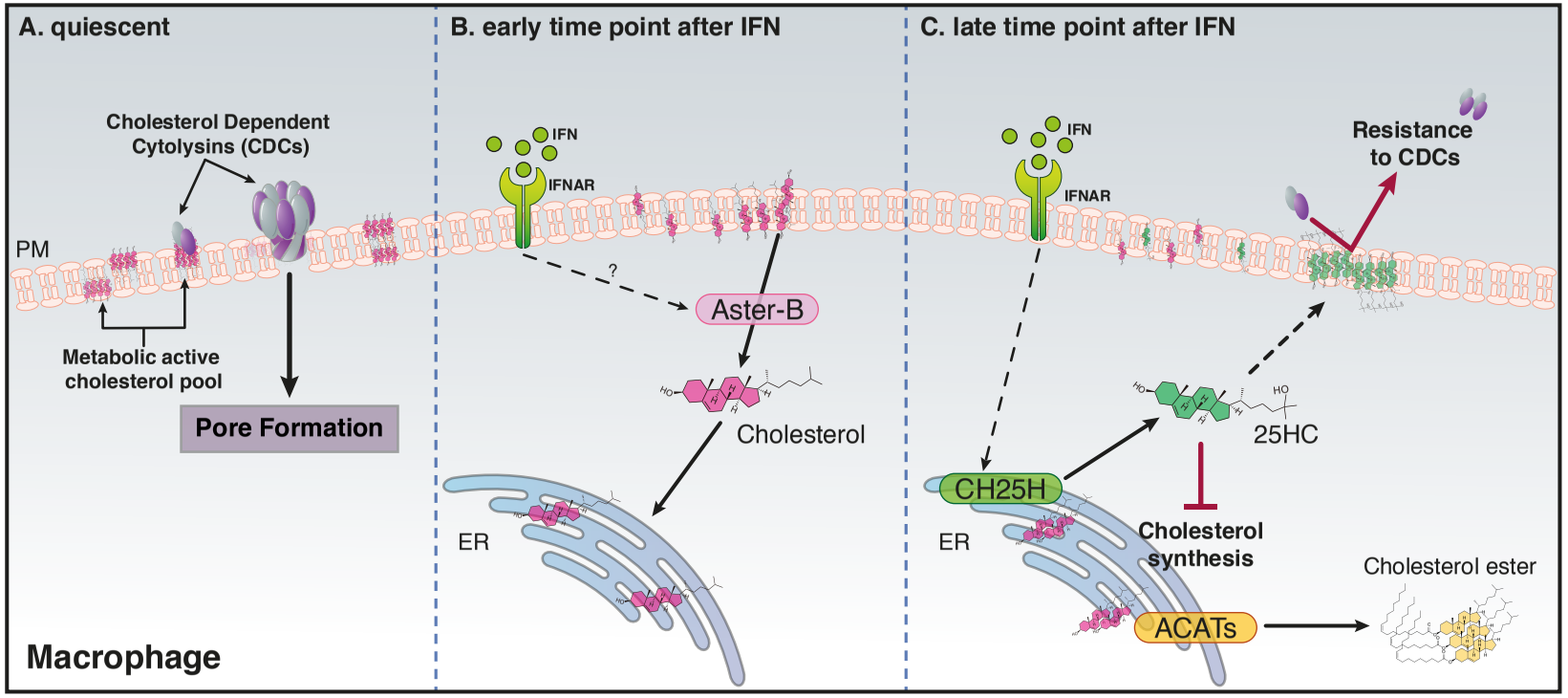

Chapter 2: Figure 6. Proposed model for interferon-induced resistance to CDCs in macrophages.

A. Quiescent state Quiescent macrophages have sufficient cholesterol in the plasma membrane “accessible pool” and can be targeted by bacterial-derived cholesterol dependent cytolysins (CDCs), leading to loss of membrane integrity and dysfunction**.**

B. Early time point after IFN Interferon (IFN) stimulation rapidly (within 1-2 hours) initiates movement of cholesterol from the “accessible pool” within the plasma membrane by Aster-B and perhaps other cholesterol transport proteins to the endoplasmic reticulum (ER).

C. Late time point after IFN Excess cholesterol in the ER is converted to cholesterol esters by ACAT enzymes in response to IFN signaling. 25HC is also produced in an interferon-dependent manner. Accumulation of 25HC in the ER inhibits cholesterol synthesis, thereby maintaining low cholesterol in the plasma membrane. Also, accumulation of 25HC in the plasma membrane decreases CDC binding. The combination of these actions ensures that cholesterol is maintained in a low level within the “accessible pool”, and confers resistance of macrophage to CDC challenge.

Chapter 2: Supplemental Figure 1

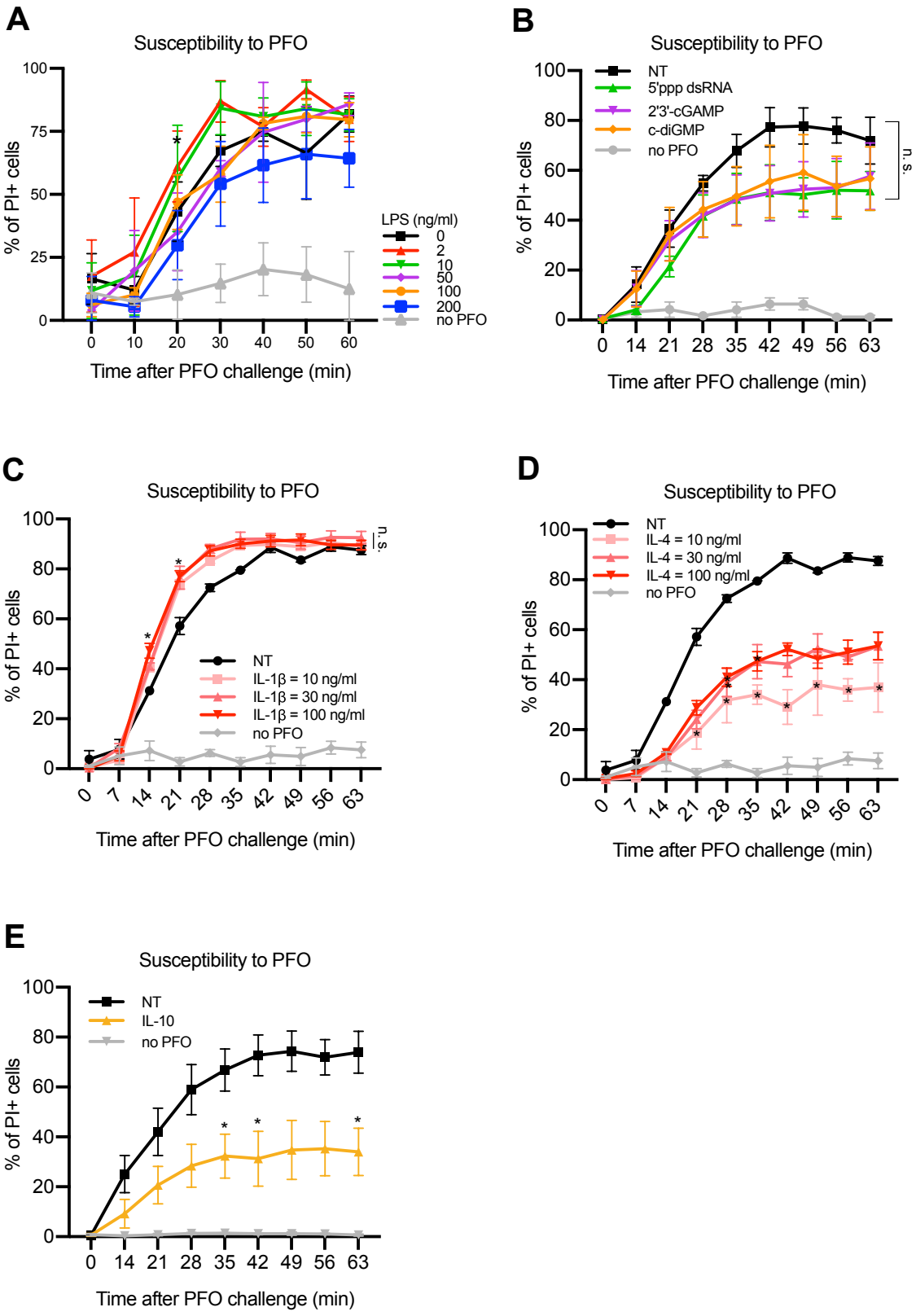

Supplemental Figure 1. Type I Interferon signaling mediates resistance to cholesterol-dependent cytolysin

(A-E) Percentage of propidium iodide (PI)–positive BMDMs treated with the indicated ligands or cytokines for 24 h and then challenged with perfringolysin O (PFO) for up to 60 min in the presence of propidium iodide (PI). Cells were imaged every 7 min to assess changes in PI incorporation.

Data are mean ± s.e.m. (n=3). Data were analyzed with two-way ANOVA. *p<0.05; **p<0.01; ***p<0.001.

Chapter 2: Supplemental Figure 4

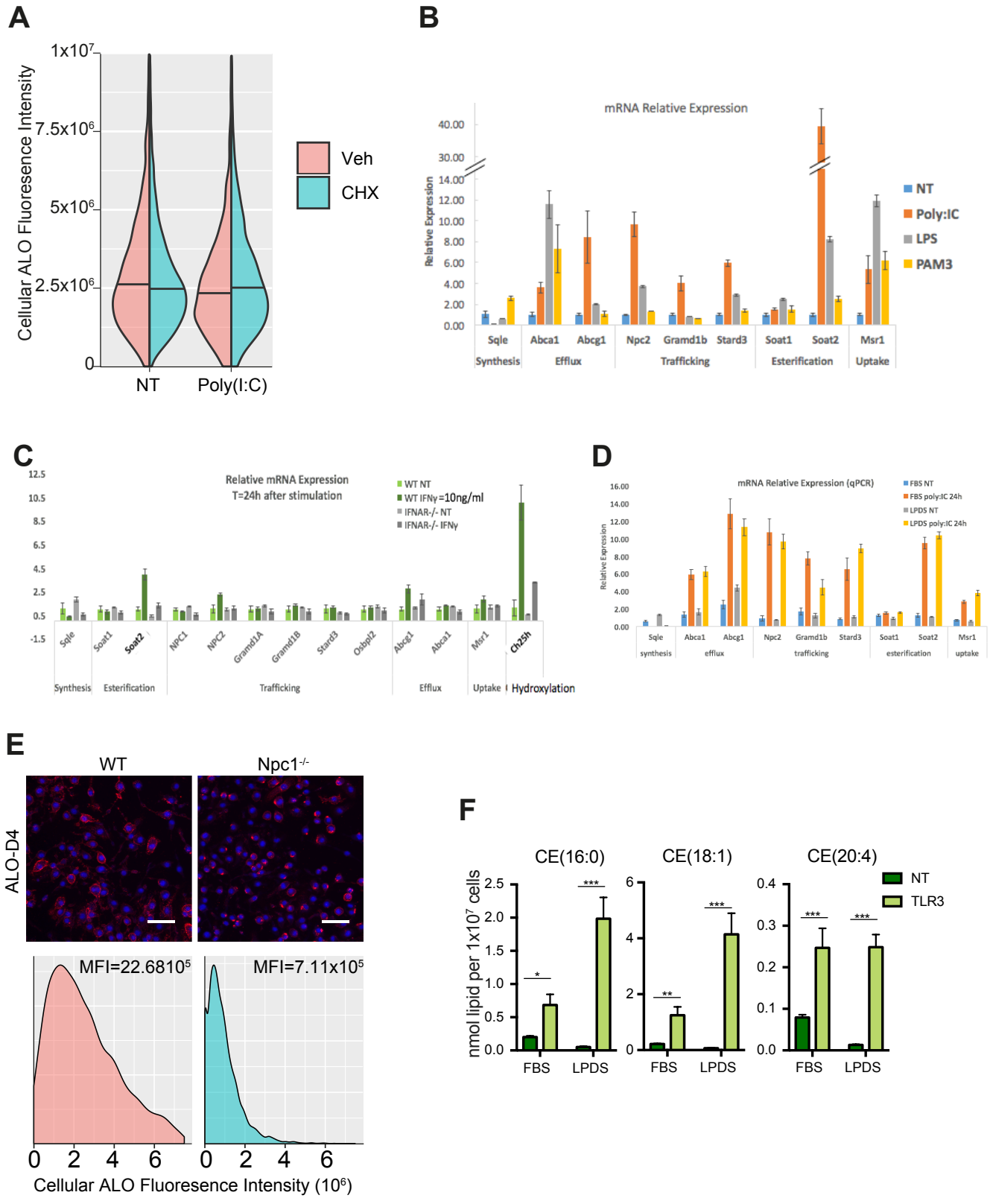

Chapter 2: Supplemental Figure 4

G

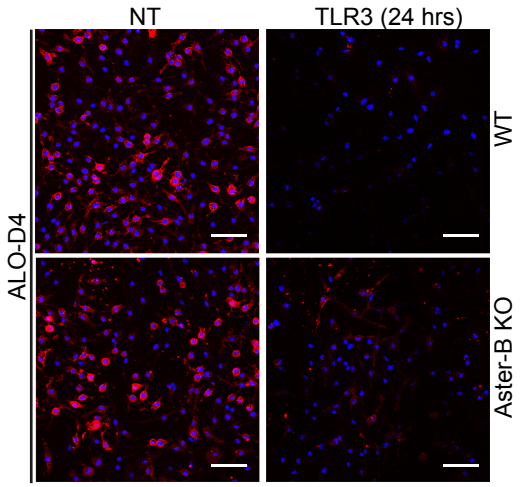

Supplemental Figure 4. Type I Interferon signaling mediates resistance to cholesterol-dependent cytolysin

A. Distribution of cellular fluorescent intensity (violin plot) of ALO-D4 binding generated from confocal images of WT BMDM cultures pre-treated with cyclohexamide (CHX; 100 ng/mL) for 30 min, and then stimulated with TLR3 agonist (Poly(I:C); 1 μg/mL) for 1 h. n=1700-2700 cells imaged with bars set at median.

B. qPCR analysis of representative cholesterol metabolism genes in WT BMDMs stimulated with TLR1/2 agonist (Pam3CSK4; 50 ng/mL), TLR3 agonist (Poly(I:C); 1 μg/mL), TLR4 agonist (LPS; 50 ng/mL), or unstimulated (NT) for 24 h.

C. qPCR analysis of representative cholesterol metabolism genes in WT or IFNAR KO BMDMs stimulated with IFNγ (10 ng/ml) or unstimulated (NT) for 24 h.

D. qPCR analysis of representative cholesterol metabolism genes in WT BMDM stimulated with TLR3 agonist (Poly(I:C); 1 μg/mL) for 24 h in media containing either 5% FBS (FBS) or lipo-protein depleted serum (LPDS).

E. Confocal images of quiescent (unstimulated) WT or *Npc1*$^{-/-}$ BMDM stained with fluorescent ALO-D4 and DAPI. Right: Cellular fluorescent intensity distribution of ALO-D4 binding generated from confocal images of macrophages, Median fluorescence intensity (MFI) is indicated at the upper corner.

F. Quantification (nmol/10^7 cells) of cholesterol ester species (16:0, 18:1, 20:4) in WT BMDMs stimulated with TLR3 agonist in FBS or lipoprotein-depleted serum (LPDS) for 48 h. CE species pool sizes were determined by direct infusion MS.

G. Confocal images of WT or Aster-B KO (*Gramd1* $^{-/-}$) BMDM cultures stimulated with TLR3 agonist (Poly(I:C); 1 μg/mL) for 24 h, and then stained with fluorescent ALO-D4 and DAPI.

(B, C, D and F) Statistical significance determined with Student's *t*-test. (*p<0.05; **p<0.01; ***p<0.001). Scale bar, 50 μm.

References for Chapter 2:

1. Ikonen, E. Cellular cholesterol trafficking and compartmentalization. *Nat. Rev. Mol. Cell Biol.* **9**, 125–138 (2008).
2. Van Meer, G., Voelker, D. R. & Feigenson, G. W. Membrane lipids: Where they are and how they behave. *Nature Reviews Molecular Cell Biology* **9**, 112–124 (2008).
3. Reboldi, A. & Dang, E. Cholesterol metabolism in innate and adaptive response. *F1000Research* **7**, 1647 (2018).
4. Viard, M. *et al.* Role of Cholesterol in Human Immunodeficiency Virus Type 1 Envelope Protein-Mediated Fusion with Host Cells. *J. Virol.* **76**, 11584–11595 (2002).
5. Goluszko, P. & Nowicki, B. Membrane Cholesterol: a Crucial Molecule Affecting Interactions of Microbial Pathogens with Mammalian Cells. *Infect. Immun.* **73**, 7791–7796 (2005).
6. Rawat, S. S. *et al.* Modulation of entry of enveloped viruses by cholesterol and sphingolipids. *Molecular Membrane Biology* **20**, 243–254 (2003).
7. Mazzon, M. & Mercer, J. Lipid interactions during virus entry and infection. *Cell. Microbiol.* **16**, 1493–1502 (2014).
8. Heuck, A. P., Moe, P. C. & Johnson, B. B. The cholesterol-dependent cytolysin family of gram-positive bacterial toxins. *Subcell. Biochem.* **51**, 551–577 (2010).
9. Tweten, R. K. Cholesterol-dependent cytolysins, a family of versatile pore-forming toxins. *Infect. Immun.* **73**, 6199–209 (2005).
10. Timmer, A. M. *et al.* Streptolysin O Promotes Group A Streptococcus Immune

Evasion by Accelerated Macrophage Apoptosis *. **284**, 862–871 (2009).

11. Bhattacharjee, P. & Keyel, P. A. Cholesterol-dependent cytolysins impair pro-inflammatory macrophage responses. *Sci. Rep.* 1–15 (2018). doi:10.1038/s41598-018-24955-2
12. Nizet, V. Group A Streptococcus encounters with host macrophages. (2017).
13. Barton, G. M. & Medzhitov, R. Toll-like receptor signaling pathways. *Science (80-.).* **300**, 1524–1525 (2003).
14. Könner, A. C. & Brüning, J. C. Toll-like receptors: linking inflammation to metabolism. *Trends Endocrinol. Metab.* **22**, 16–23 (2011).
15. Langston, P. K., Shibata, M. & Horng, T. Metabolism Supports Macrophage Activation. *Front. Immunol.* **8**, (2017).
16. American Association of Immunologists., B., Bohannon, J., Guo, Y. & Sherwood, E. *The journal of immunology : official journal of the American Association of Immunologists. The Journal of Immunology* **196**, (Williams & Wilkins, 1950).
17. Huang, L., Xu, H. & Peng, G. TLR-mediated metabolic reprogramming in the tumor microenvironment: potential novel strategies for cancer immunotherapy. *Cell. Mol. Immunol.* **15**, 428–437 (2018).
18. Diskin, C. & Pålsson-McDermott, E. M. Metabolic Modulation in Macrophage Effector Function. *Front. Immunol.* **9**, 270 (2018).
19. Reboldi, A. *et al.* Inflammation. 25-Hydroxycholesterol suppresses interleukin-1-driven inflammation downstream of type I interferon. *Science* **345**, 679–84 (2014).
20. Dang, E. V., McDonald, J. G., Russell, D. W. & Cyster, J. G. Oxysterol Restraint of Cholesterol Synthesis Prevents AIM2 Inflammasome Activation. *Cell* 1–15

(2017). doi:10.1016/j.cell.2017.09.029

21. Araldi, E. *et al.* Lanosterol Modulates TLR4-Mediated Innate Immune Responses in Macrophages. *Cell Rep.* **19**, 2743–2755 (2017).
22. York, A. G. *et al.* Limiting Cholesterol Biosynthetic Flux Spontaneously Engages Type I IFN Signaling. *Cell* **163**, 1–14 (2015).
23. Soccio, R. E. & Breslow, J. L. Intracellular Cholesterol Transport. *Arterioscler. Thromb. Vasc. Biol.* **24**, (2004).
24. Das, A., Brown, M. S., Anderson, D. D., Goldstein, J. L. & Radhakrishnan, A. Three pools of plasma membrane cholesterol and their relation to cholesterol homeostasis. *Elife* **3**, (2014).
25. Endapally, S. *et al.* Molecular Discrimination between Two Conformations of Sphingomyelin in Plasma Membranes. *Cell* **176**, 1040-1053.e17 (2019).
26. Blanc, M. *et al.* The Transcription Factor STAT-1 Couples Macrophage Synthesis of 25-Hydroxycholesterol to the Interferon Antiviral Response. *Immunity* **38**, 106–118 (2013).
27. Verherstraeten, S. *et al.* Perfringolysin O: The Underrated Clostridium perfringens Toxin? *Toxins (Basel).* **7**, 1702–21 (2015).
28. Stetson, D. B. & Medzhitov, R. Type I Interferons in Host Defense. *Immunity* **25**, 373–381 (2006).
29. McNab, F., Mayer-Barber, K., Sher, A., Wack, A. & O'Garra, A. Type I interferons in infectious disease. *Nat. Rev. Immunol.* **15**, 87–103 (2015).
30. Ivashkiv, L. B. & Donlin, L. T. Regulation of type I interferon responses. *Nat. Rev. Immunol.* **14**, 36–49 (2013).

31. Kovarik, P., Castiglia, V., Ivin, M. & Ebner, F. Type I interferons in bacterial infections: A balancing act. *Front. Immunol.* **7**, 1–8 (2016).

32. Boxx, G. M. & Cheng, G. The Roles of Type i Interferon in Bacterial Infection. *Cell Host Microbe* **19**, 760–769 (2016).

33. Luzina, I. G. *et al.* Regulation of inflammation by interleukin-4: a review of "alternatives". *J. Leukoc. Biol.* **92**, 753–64 (2012).

34. Couper, K. N., Blount, D. G. & Riley, E. M. IL-10: the master regulator of immunity to infection. *J. Immunol.* **180**, 5771–7 (2008).

35. Sara K. B. Cassidy and Mary X. D. O'Riordan. More Than a Pore: The Cellular Response to Cholesterol-Dependent Cytolysins. 618–636 (2013). doi:10.3390/toxins5040618

36. Chakrabarti, R. S. *et al.* Variability of cholesterol accessibility in human red blood cells measured using a bacterial cholesterol-binding toxin. *Elife* **6**, 1–27 (2017).

37. Infante, R. E. & Radhakrishnan, A. Continuous transport of a small fraction of plasma membrane cholesterol to endoplasmic reticulum regulates total cellular cholesterol. *Elife* **6**, 1–23 (2017).

38. Endapally, S., Infante, R. E. & Radhakrishnan, A. Monitoring and modulating intracellular cholesterol trafficking using ALOD4, a cholesterol-binding protein. in *Methods in Molecular Biology* **1949**, 153–163 (Humana Press, New York, NY, 2019).

39. Gay, A., Rye, D. & Radhakrishnan, A. Switch-like responses of two cholesterol sensors do not require protein oligomerization in membranes. *Biophys. J.* **108**, 1459–1469 (2015).

40. He, C. *et al.* Macrophages release plasma membrane-derived particles rich in accessible cholesterol. *Proc. Natl. Acad. Sci.* **115**, E8499–E8508 (2018).

41. He, C. *et al.* High-resolution imaging and quantification of plasma membrane cholesterol by NanoSIMS. *Proc. Natl. Acad. Sci.* **114**, 2000–2005 (2017).

42. Maxfield, F. R. & Wüstner, D. Analysis of cholesterol trafficking with fluorescent probes. *Methods Cell Biol.* **108**, 367–93 (2012).

43. Das, A., Goldstein, J. L., Anderson, D. D., Brown, M. S. & Radhakrishnan, A. Use of mutant 125I-Perfringolysin O to probe transport and organization of cholesterol in membranes of animal cells. *Proc. Natl. Acad. Sci.* **110**, 10580–10585 (2013).

44. Fessler, M. B. & Parks, J. S. Inflammatory Cell Signaling Microdomains as Organizing Principles in Intracellular Lipid Flux and Membrane. doi:10.4049/jimmunol.1100253

45. Dykstra, M., Cherukuri, A., Sohn, H. W., Tzeng, S.-J. & Pierce, S. K. L OCATION IS E VERYTHING : Lipid Rafts and Immune Cell Signaling. *Annu. Rev. Immunol.* **21**, 457–481 (2003).

46. Lingwood, D. & Simons, K. Lipid rafts as a membrane-organizing principle. *Science* **327**, 46–50 (2010).

47. Muro, E., Atilla-Gokcumen, G. E. & Eggert, U. S. Lipids in cell biology: how can we understand them better? *Mol. Biol. Cell* **25**, 1819–23 (2014).

48. Simons, K. & Toomre, D. Lipid rafts and signal transduction. *Nat. Rev. Mol. Cell Biol.* **1**, 31–39 (2000).

49. Anderson, H. A. & Roche, P. A. MHC Class II Association with Lipid Rafts on the Antigen Presenting Cell Surface. *Biochim. Biophys. Acta* **1853**, 775 (2015).

50. Anderson, H. A., Hiltbold, E. M. & Roche, P. A. Concentration of MHC class II molecules in lipid rafts facilitates antigen presentation. *Nat. Immunol.* **1**, 156–162 (2000).

51. Poloso, N. J., Muntasell, A. & Roche, P. A. MHC class II molecules traffic into lipid rafts during intracellular transport. *J. Immunol.* **173**, 4539–46 (2004).

52. Eckert, G. P., Igbavboa, U., Müller, W. E. & Wood, W. G. Lipid rafts of purified mouse brain synaptosomes prepared with or without detergent reveal different lipid and protein domains. *Brain Res.* **962**, 144–50 (2003).

53. Hering, H., Lin, C.-C. & Sheng, M. Lipid rafts in the maintenance of synapses, dendritic spines, and surface AMPA receptor stability. *J. Neurosci.* **23**, 3262–71 (2003).

54. Chamberlain, L. H., Burgoyne, R. D. & Gould, G. W. SNARE proteins are highly enriched in lipid rafts in PC12 cells: Implications for the spatial control of exocytosis. *Proc. Natl. Acad. Sci.* **98**, 5619–5624 (2001).

55. Horton, J. D. J. J. D. *et al.* SREBPs: activators of the complete program of cholesterol and fatty acid synthesis in the liver. *J. Clin. Invest.* **109**, 1125–31 (2002).

56. Matsuda, M. *et al.* SREBP cleavage-activating protein (SCAP) is required for increased lipid synthesis in liver induced by cholesterol deprivation and insulin elevation. *Genes Dev.* **15**, 1206–16 (2001).

57. Krycer, J. R., Sharpe, L. J., Luu, W. & Brown, A. J. The Akt-SREBP nexus: Cell signaling meets lipid metabolism. *Trends Endocrinol. Metab.* **21**, 268–276 (2010).

58. Lev, S. Nonvesicular lipid transfer from the endoplasmic reticulum. *Cold Spring*

Harb. Perspect. Biol. **4**, a013300 (2012).

59. Hölttä-Vuori, M. & Ikonen, E. Endosomal cholesterol traffic: vesicular and non-vesicular mechanisms meet. *Biochem. Soc. Trans.* **34**, 392–394 (2006).

60. Prinz, W. A. Non-vesicular sterol transport in cells. *Prog. Lipid Res.* **46**, 297–314 (2007).

61. Hao, M. *et al.* Vesicular and non-vesicular sterol transport in living cells. The endocytic recycling compartment is a major sterol storage organelle. *J. Biol. Chem.* **277**, 609–17 (2002).

62. Subramanian, K. & Balch, W. E. NPC1/NPC2 function as a tag team duo to mobilize cholesterol. *Proc. Natl. Acad. Sci.* **105**, 15223–15224 (2008).

63. Sandhu, J. *et al.* Aster Proteins Facilitate Nonvesicular Plasma Membrane to ER Cholesterol Transport in Mammalian Cells. *Cell* **175**, 514-529.e20 (2018).

64. Chang, T.-Y., Chang, C. C. Y., Ohgami, N. & Yamauchi, Y. Cholesterol sensing, trafficking, and esterification. *Annu. Rev. Cell Dev. Biol.* **22**, 129–157 (2006).

65. Andreyev, A. Y. *et al.* Application of proteomic marker ensembles to subcellular organelle identification. *Mol. Cell. Proteomics* **9**, 388–402 (2010).

66. Andreyev, A. Y. *et al.* Subcellular organelle lipidomics in TLR-4-activated macrophages. *J. Lipid Res.* **51**, 2785–2797 (2010).

67. Liu, S. Y. *et al.* Interferon-Inducible Cholesterol-25-Hydroxylase Broadly Inhibits Viral Entry by Production of 25-Hydroxycholesterol. *Immunity* **38**, 92–105 (2013).

68. Sokolov, A. & Radhakrishnan, A. Accessibility of cholesterol in endoplasmic reticulum membranes and activation of SREBP-2 switch abruptly at a common cholesterol threshold. *J. Biol. Chem.* **285**, 29480–29490 (2010).

69. Bielska, A. A. *et al.* Side-chain oxysterols modulate cholesterol accessibility through membrane remodeling. *Biochemistry* **53**, 3042–3051 (2014).

70. Gold, E. S. *et al.* 25-Hydroxycholesterol acts as an amplifier of inflammatory signaling. *Proc. Natl. Acad. Sci. U. S. A.* 1–6 (2014). doi:10.1073/pnas.1404271111

71. Gratz, N. *et al.* Type I Interferon Production Induced By Streptococcus Pyogenes-Derived Nucleic Acids is Required for Host Protection. *PLoS Pathog.* **7**, e1001345 (2011).

72. Du, X., Pham, Y. H. & Brown, A. J. Effects of 25-Hydroxycholesterol on Cholesterol Esterification and Sterol Regulatory Element-binding Protein Processing Are Dissociable. *J. Biol. Chem.* **279**, 47010–47016 (2004).

73. Lange, Y., Ye, J. & Strebel, F. Movement of 25-hyd h rol from the plasma membr e to the rough endopl reticulum in cu ma cells. *J. Lipid Res.* **36**, 1092–1097 (1995).

74. Hozoji, M. *et al.* Direct interaction of nuclear liver X receptor-beta with ABCA1 modulates cholesterol efflux. *J. Biol. Chem.* **283**, 30057–63 (2008).

75. Lai, L. *et al.* MicroRNA-33 Regulates the Innate Immune Response via ATP Binding Cassette Transporter-mediated Remodeling of Membrane Microdomains. *J. Biol. Chem.* **291**, 19651–60 (2016).

76. Trasino, S. E., Kim, Y. S. & Wang, T. T. Y. Ligand, receptor, and cell type-dependent regulation of ABCA1 and ABCG1 mRNA in prostate cancer epithelial cells. *Mol. Cancer Ther.* **8**, 1934–1945 (2009).

77. Beyea, M. M. *et al.* Selective Up-regulation of LXR-regulated Genes *ABCA1* ,

ABCG1 , and *APOE* in Macrophages through Increased Endogenous Synthesis of 24(*S*),25-Epoxycholesterol. *J. Biol. Chem.* **282**, 5207–5216 (2007).

78. Gaillard, J. L., Berche, P., Mounier, J., Richard, S. & Sansonetti, P. In vitro model of penetration and intracellular growth of Listeria monocytogenes in the human enterocyte-like cell line Caco-2. *Infect. Immun.* **55**, 2822–9 (1987).

79. Kayal, S. & Charbit, A. Listeriolysin O: a key protein of *Listeria monocytogenes* with multiple functions. *FEMS Microbiol. Rev.* **30**, 514–529 (2006).

80. Bielecki, J., Youngman, P., Connelly, P. & Portnoy, D. A. Bacillus subtilis expressing a haemolysin gene from Listeria monocytogenes can grow in mammalian cells. *Nature* **345**, 175–176 (1990).

81. Lu, F. *et al.* Identification of NPC1 as the target of U18666A, an inhibitor of lysosomal cholesterol export and Ebola infection. *Elife* **4**, 14850–14856 (2015).

82. Gellings, P. S. & McGee, D. J. Arcanobacterium haemolyticum Phospholipase D Enzymatic Activity Promotes the Hemolytic Activity of the Cholesterol-Dependent Cytolysin Arcanolysin. *Toxins (Basel).* **10**, (2018).

83. Ouyang, X. *et al.* Cooperation between MyD88 and TRIF pathways in TLR synergy via IRF5 activation. *Biochem. Biophys. Res. Commun.* **354**, 1045–1051 (2007).

84. Adelaja, A. & Hoffmann, A. Signaling crosstalk mechanisms that may fine-tune pathogen-responsive NFκB. *Front. Immunol.* **10**, 433 (2019).

85. Cheng, Q. *et al.* Sequential conditioning-stimulation reveals distinct gene- and stimulus-specific effects of Type I and II IFN on human macrophage functions. *Sci. Rep.* **9**, 1–14 (2019).

86. Castiglia, V. *et al.* Type i Interferon Signaling Prevents IL-1β-Driven Lethal Systemic Hyperinflammation during Invasive Bacterial Infection of Soft Tissue. *Cell Host Microbe* **19**, 375–387 (2016).

87. Escajadillo, T., Olson, J., Luk, B. T., Zhang, L. & Nizet, V. A Red Blood Cell Membrane-Camouflaged Nanoparticle Counteracts Streptolysin O-Mediated Virulence Phenotypes of Invasive Group A Streptococcus. *Front. Pharmacol.* **8**, 477 (2017).

88. Li, C. *et al.* 25-Hydroxycholesterol Protects Host against Zika Virus Infection and Its Associated Microcephaly in a Mouse Model. *Immunity* **46**, 446–456 (2017).

89. Divakaruni, A. S. *et al.* Thiazolidinediones are acute, specific inhibitors of the mitochondrial pyruvate carrier. *Proc. Natl. Acad. Sci.* **110**, 5422–5427 (2013).

90. Blich, E. G. & Dyer, W. J. Canadian Journal of Biochemistry and Physiology. *Can. J. Biochem. Physiol.* **37**, 911–917 (1959).

91. Williams, K. J. *et al.* An essential requirement for the SCAP/SREBP signaling axis to protect cancer cells from lipotoxicity. *Cancer Res.* **73**, 2850–2862 (2013).

92. Argus, J. P. *et al.* Development and Application of FASA, a Model for Quantifying Fatty Acid Metabolism Using Stable Isotope Labeling. *Cell Rep.* **25**, 2919-2934.e8 (2018).

93. Wickham, H., Chang, W., Henry, L. & Pedersen, T. L. ggplot2: Elegant Graphics for Data Analysis. in (Springer-Verlag New York, 2016).

94. He, C., Fong, L. G., Young, S. G. & Jiang, H. NanoSIMS imaging: An approach for visualizing and quantifying lipids in cells and tissues. *Journal of Investigative Medicine* **65**, 669–672 (2017).

95. Kim, D., Langmead, B. & Salzberg, S. L. HISAT: a fast spliced aligner with low memory requirements. *Nat. Methods* **12**, 357–360 (2015).

96. Metsalu, T. & Vilo, J. ClustVis: A web tool for visualizing clustering of multivariate data using Principal Component Analysis and heatmap. *Nucleic Acids Res.* **43**, W566–W570 (2015).

CHAPTER 3:

Investigating the mechanism underlying how cholesterol regulates STING activity

Introduction

The previous chapter focused on how Type I IFN reprograms cellular lipid metabolism. Here we'll focus on the other direction of the crosstalk: how does perturbation in lipid metabolism regulate Type I IFN response?

Many groups including ours have observed decreased cholesterol synthesis in macrophages in response to Type I IFN stimulation. Different models have been proposed to explain the biological impact of this particular metabolic reprogramming[1–5]. Cyster and colleagues showed decreased cholesterol synthesis has an impact on AIM2-mediated inflammation via regulation of mitochondrial membrane integrity[2]. Ghazal's group proposed that inhibiting the multi-step cholesterol synthesis pathway involves inhibition of the mevalonate-isoprenoid branch[3], where isoprenoids are required by viruses for protein prenylation[6]. Suarez group showed that inhibiting cholesterol synthesis result in accumulation of an intermediate metabolite lanosterol, which can suppress IFN mediated inflammation and as well as increasing macrophage phagocytic activity[5]. In addition to these models above, our group showed the decreased cholesterol synthesis by Type I IFN establishes an unexpected feed-forward circuit, where limiting cholesterol synthesis can turn on spontaneous IFN production via an upstream adaptor protein Stimulator of interferon genes (STING)[1]. Perturbation of cholesterol synthetic flux can alter STING function, although the biochemical mechanism remains unclear. We hypothesize that cholesterol metabolism might regulate STING directly or indirectly. In

this chapter, we'll investigate the possible mechanisms underlying how cholesterol regulates STING, with a focus on the direct regulation hypothesis.

STING, also known as MITA, MPYS, and ERIS, was first characterized as an critical immune sensor back in 2008[7–10]. Later studies showed that the cGAS-STING-TBK1 signaling pathway is the predominant pathway to trigger IFNβ signaling in response to cytosolic DNA, which may come from microbial infection or aberrant cellular DNA[11–14]. Upon sensing cytosolic DNA, the enzyme cGAS synthesizes 2'3'-cGAMP[15–17], a cyclic dinucleotide (CDN), which activates STING. In addition to the endogenous ligand 2'3-cGAMP, bacterial CDNs such as c-di-GMP and c-di-AMP can also bind to and activate STING[17,18], although with lower affinity. Upon activation, STING changes its conformation[19–21] and translocalizes from the ER to an ER-Golgi intermediate compartment (ERGIC) as well as the Golgi apparatus[10,22–24]. Next, STING recruits the protein kinase TBK1 to phosphorylate itself, STING, and downstream transcription factor Interferon Regulatory Factor 3 (IRF3). IRF3 monomers then dimerize, enter the nucleus and turn on Ifnb1 expression[11,25]. The cGAS-STING pathway plays pivotal roles in anti-pathogen immunity, autoimmune disorder pathogenesis and cancer immune therapy[11,26]. Therefore, it is of great interest and significance to understand how STING activity could be regulated at different levels and how the pathway could be therapeutically targeted. A growing list of proteins can regulate STING function, involving post-translational modifications, protein trafficking, stability and crosstalk with other immune signaling pathways[11,27,28]. In addition, palmitoylation of STING at the Golgi has been shown to be

critical[23], and Ablasser's group have developed irreversible palmitoylation inhibitor to block STING function in STING associated autoimmune disease models[29].

How could perturbation of cholesterol metabolism alter STING function? Given the various ways by which cholesterol could regulate membrane protein function, here we propose several possible models: 1) Cholesterol might directly bind to and regulate the function of STING; 2) Cholesterol could alter the membrane physical feature such as lipid packing and fluidity[30,31], which might change STING clustering in the membrane. There is indeed evidence showing clustering is important for STING function[23]; 3) Cholesterol can be sensed by known cholesterol sensors to affect STING indirectly[32,33]; 4) Downstream metabolites of cholesterol, such as an oxysterol, might interact with STING.

Gain of function mutations of STING are sufficient to cause autoimmune disorder. Six mutations so far have been identified in patients with STING-associated vasculopathy with onset in infancy (SAVI): the better characterized V147L, N154S and V155M[34,35], and the more recently identified C206Y, R281Q, R284S[36,37]. For the first 3 mutants, *in vitro* assays showed these substitutions lead to constitutive TBK1/IRF3 activation and uncontrolled interferon response, and further studies showed spontaneous translocation of these mutants to Golgi[24]. These three mutations localize close to transmembrane domain 4. Therefore, it's been proposed that these residues, or this region in general may play an important role in retaining STING in the ER in unstimulated cells, although the mechanism remains elusive[24]. Strikingly, our *in silico* analysis identified a putative cholesterol recognition amino acid consensus (CRAC) motif also close to transmembrane

domain 4 of STING. We therefore hypothesize that cholesterol regulates STING via direct binding in the ER membrane.

CARC-CRAC domain regulates STING activity

The CRAC motif[38–41] is the best characterized cholesterol binding motif in proteins and can regulate a growing list of membrane protein function such as SLC38A9, STIM1 and Orai1[32,42,43]. We found the consensus CRAC sequence (L/V)-X_{1-5}-Y-X_{1-5}-(K/R) close to transmembrane domain 4 of STING. In addition, this CRAC motif is closely followed by a similar but inverted motif (K/R)- X_{1-5}-(Y/F)- X_{1-5}-(L/V) known as CARC (Fig 1A). Both CRAC and CARC have been described in cholesterol regulated proteins. We ask whether this CARC-CRAC motif identified in STING is important for STING function.

To assess this, we mutated 7 key residues, K150, F153, V155, L159, Y163, Y164 and R169, to either isoleucine or alanine, and assessed STING activity based on 3 different downstream signaling events of STING activation: 1) phosphorylation of TBK1, 2) IRF3 transcription activity indicated by luciferase assay with *Ifnb1* promoter and 3) relative RNA expression of ISG15, an interferon stimulated gene. Three SAVI mutations have gain of function shown by luciferase assay under the *Ifnb1* promoter, and the artificial mutation V155R used in previous papers as a negative control abolished STING activity, consistent with previous findings[34,35] (Fig 1B). Interestingly, F153 mutation to isoleucine and alanine both led to gain of function, and the level matches that of SAVI mutations (Fig 1B). Four other residues, L159, Y163, Y164 and R169, turned out to be critical as well, as mutations

of these residues to alanine or isoleucine totally abolished STING function (Fig 1C), whereas mutation of K150 showed no difference in *Ifnb1*-luciferase intensity (Fig 1D).

We then focused on F153I, since it has the same phenotype as SAVI mutations. We engineered cell lines stably expressing STING mutants using the 293FRT system, where each cell integrates only one copy of exogenous STING DNA sequence at the same genomic location. We assessed activation of STING with p-TBK1 after cGAMP stimulation. While WT STING gradually upregulates p-TBK1 level after stimulation (Fig 1E), SAVI mutant V155M has higher basal level p-TBK1, which can be further enhanced by cGAMP. The F153I mutant has a very high basal level of p-TBK1 which is no longer enhanced by cGAMP (Fig 1E), but F153I can still upregulate ISG15 expression level after stimulation (Fig 1F).

To conclude, we identified a putative cholesterol-recognition region in STING known as CARC-CRAC motif, and most of the key residues play important roles in STING function as mutations of them can fundamentally change STING activity. Particularly, F153 mutations phenocopy SAVI mutations and led to STING gain of function.

The CARC-CRAC motif is critical for STING's response to cholesterol alterations

Next, we asked whether the CARC-CRAC motif can mediate how cholesterol regulates STING. Previously we observed genetic deletion of SCAP, an essential protein controlling cholesterol synthesis, results in higher IFNβ production at the basal level as well as in

response to one of its ligand di-c-GMP[1]. Here we found that even WT BMDMs' response to STING endogenous ligand 2'3'-cGAMP can be significantly blunted by cholesterol addition (Fig 2A). TLR3 activation with double-strand RNA mimetic Poly(I:C) can also lead to IFNβ production via another adaptor TRIF, a cytosolic protein[44]. Cholesterol addition doesn't affect WT BMDMs *Ifnb1* and *Mx1* expression level in response to Poly(I:C) (Fig 2B), indicating that *Ifnb1* induction by cholesterol is a STING specific phenotype. To further investigate whether the putative CARC-CRAC motif can alter STING response to cholesterol regulation, we took 293FRT cells stably expressing different STING mutants, and measured p-TBK1 after altering cholesterol metabolism. If the CARC-CRAC motif is critical for STING to bind cholesterol, then disruption of this motif in STING should lead to different response to cholesterol metabolism perturbation. In cells expressing WT STING, p-TBK1 signal was increased by cholesterol depletion with MβCD, and decreased by exogenous cholesterol addition (Fig 2C). However, MβCD depletion resulted in an opposite response in both F153I and V155M mutations, and cholesterol addition didn't inhibit p-TBK1 in F153I mutant anymore (Fig 2C). This data indicated that the CARC-CRAC motif plays a key role in STING's response to cholesterol perturbation.

STING directly binds to cholesterol mimetic probes mediated by CARC-CRAC motif

Next, we asked whether STING can bind to cholesterol directly. To test this, we used two photo-reactive probes *trans-sterol*[45] and LKM38[43]. These probes have 3 features: 1) they structurally resemble cholesterol, 2) they have an azide group that can be covalently linked to adjacent protein under UV exposure, and 3) their alkyne group can be efficiently

conjugated with other azide-containing moieties compatible with downstream analysis, such as Rhodamine-azide or biotin-azide. Labeling of the probe can be easily done via a high yield copper catalyzed reaction called “Click” chemistry[46].

To test whether these cholesterol mimetic probes can bind to STING, we overexpressed WT STING-FLAG in HEK293T cells, and incubated cells with *trans-sterol* or LKM38 for an hour followed by UV exposure to crosslink probes with binding proteins in cells. We then conjugated a fluorescent Rhodamine group to the probes within the lysate, where the Rhodamine signal can be visualized on an SDS-PAGE gel (Fig 3A and B; Fig S3B). After probing with either *LKM38* or *trans-sterol, a* strong band around the size of STING (37 kDa) can be seen in cells with STING-FLAG overexpression, but not in parental 293T cells which don’t express endogenous STING. This band overlaps with anti-FLAG Western Blot band (Fig 3B). Furthermore, the signal of *trans-sterol*-Rhodamine signal is attenuated when excess cholesterol was present during probe incubation, indicating cholesterol competition of the probe (Fig 3B), although the competition of cholesterol is less obvious with LKM38 probing.

To further validate that STING *per se* is binding to the probes, we did proteomics analysis on probe-enriched proteins using mass spectrometry, and detected peptide sequences that can be mapped to STING with a coverage of 44.6% of full length STING (Fig 3C). STING peptides were significantly enriched in HEK293T cells transfected with STING over parental cells or no probe controls (Fig 3D). Consistent with in-gel Rhodamine results, the peptide signal is lower in the presence of excess cholesterol during probe incubation.

Next, we asked whether the CARC-CRAC motif plays a role in direct binding to cholesterol mimetic probes. We overexpressed STING mutants in HEK293T cells and assessed their ability to be labeled by *trans-sterol* probe. Interestingly, preliminary data showed that both SAVI mutants tested here as well as F153I have lower Rhodamine signal compared to WT STING-FLAG (Figure 3E and F). This data further indicates that the putative CARC-CRAC motif in STING plays a critical role in its interaction with cholesterol.

Discussion

In this study, we investigate the underlying mechanism of how cholesterol, a lipid, can regulate STING activity. We first identified a tandem cholesterol binding motif CARC-CRAC close to the last transmembrane domain of STING, which turned out to be important for proper STING activity as well as response to cholesterol metabolism perturbation. Then we used photo-reactive cholesterol mimetics *trans-sterol* and LKM38 as probes to covalently label adjacent binding proteins, and found both can directly bind to STING. Furthermore, we found that binding between *trans*-sterol and STING can be inhibited by competition with excess cholesterol. Finally, the binding between the probe and STING is mediated by the CARC-CRAC motif in STING.

Here we propose a model of how cholesterol directly regulates STING function in a cell (Fig 4). At quiescent state, a cell synthesizes a certain amount of cholesterol in the ER, which could bind STING via the CARC-CRAC motif and retian STING in the ER; upon activation by cGAMP, STING changes confirmation, polymerizes in the ER membrane

and can no longer bind to cholesterol. Then, STING translocalizes to the ERGIC and Golgi to trigger TBK1, IRF3 and result in Type IFN production. However, under altered metabolic conditions such as low cholesterol synthesis or cholesterol depletion, there is not enough cholesterol to retain STING in the ER, which could lead to STING hyperactivity, even in the absence of its ligand cGAMP. Furthermore, disrupting the CARC-CRAC motif by mutating the key residues, namely F153 and V155M, can also disrupt the interaction between STING and cholesterol.

According to the classic definition of CARC-CRAC motif, the sequence should be within or at least close to the transmembrane domain. The tandem CARC-CRAC motif has been shown to span the lipid bilayers with K/R residues pointing outward to the cytosolic side and Y/F interacting with 4 rings of cholesterol molecule as well as the more hydrophobic acyl tails of the membrane lipids. Interestingly, the CARC-CRAC sequence of STING were predicted to be the 5th transmembrane region in early studies[9,10], but later studies found that amino acids 139-379 are soluble, indicating this region is in cytosol[19]. However, given the hydrophobicity of α-helixes in aa 150-170 and that it contains two cholesterol binding motifs, it's likely that this region could directly interact with cholesterol either on or close to the ER lipid bilayer or without spanning the whole membrane.

Dimerization of STING is considered critical in STING activation[9,19]. The full length structure of chicken STING protein before and after cGAMP ligand binding has just recently been revealed[21], and it was shown that upon cGAMP binding to the c-terminus pocket formed by the apo-STING dimer, the “connector” between transmembrane domain

4 and the C-terminus rotates 180˚, which enables polymerization of STING as well as exposes phosphorylation sites for TBK1. The same group also observed hyperactivity of STING mutant F153A, and their explanation is that this residue F153 falls into the "connector loop" of STING dimer, which might be critical for the unstimulated STING dimer to maintain the "unrotated" or autoinhibitory dimer orientation, as mutating F153 to a less structural amino acid alanine can increase the flexibility of the connector and lead to spontaneous C-terminus rotation and oligomerization. With all these recently gained knowledge of STING structure, we think it's possible that CARC-CRAC, which largely overlaps with STING dimer interface and the "connector loop" can interact with cholesterol, and this interaction is possibly in favor of STING in a more inhibitory conformation. We have to point out that the current full-length structure is solved in liposome membrane without cholesterol, and co-crystallization of STING and cholesterol will be highly informative to understand cholesterol and STING interaction.

Apart from the CARC-CRAC motif proposed here, we also found a single CRAC motif between transmembrane domain 2 and 3 in STING as a "TM2-TM3 linker"[21] at the cytosolic side of ER membrane, with residues K76, Y81 and V85 lining up to fit the CRAC motif criteria. Y81A and V85A mutants didn't change STING activity, while K76A totally abolished STING activity as assessed by *Ifnb1*-luciferase assay (data not shown). Therefore, it is possible that cholesterol can interact with STING at multiple regions. So far we have only confirmed that LKM38 and *trans-sterol* as cholesterol mimetic probes can covalently label STING, but more mass-spec based assays will need to be performed to figure out the sites-of-labeling in STING protein. Again, co-crystallization of STING and

cholesterol will be the ultimate assay to confirm binding to eliminate the artifacts brought by the two cholesterol mimetic probes.

In this study we focused our hypothesis on cholesterol-STING interaction in the ER. However STING can be regulated at multiple levels along its trafficking route ERGIC-Golgi-lysosome, and all these membranous organelles have higher nmol % of cholesterol compared to the ER[30]. A previous paper showed that palmitoylation of STING is required for STING clustering in the Golgi, and the underlying mechanism possibly involves better anchoring of STING to the "lipid raft" in Golgi[23]. Cholesterol plays a critical role in lipid packing in lipids rafts[47–49]. Thus if cholesterol in the Golgi is required for STING clustering, then cholesterol depletion should abolish STING function. However this is unlikely since we observed the opposite phenomenon (Fig 2C). Despite this, it remains unclear where exactly cholesterol-STING interaction is happening, and we cannot rule out other subcellular organelles at this point.

Besides the direct binding and regulation hypothesis, it is also possible that cholesterol can regulate STING via other cholesterol sensors. For example, STIM1 was originally known as a calcium sensor in the ER, and a recent study has shown that STIM1 also acts as an ER-retention factor anchoring STING in the ER[50]. Interestingly, other papers have shown that cholesterol could regulate STIM1 activity via a CRAC motif[32]. Therefore it is possible that cholesterol can regulate STING via STIM1. In addition to STIM1, INSIG1 has long been understood as a critical cholesterol sensing protein in the ER that regulates cholesterol synthesis[51,52]. An earlier paper has shown that AMFR, an E3 ubiquitin ligase,

can complex with INSIG1, and polyubiquitinate STING to maximize recruitment of TBK1[33], although how cholesterol perturbation can alter STING activity via INSIG1-AMFR is largely unexplored. The direct binding and indirect regulation of STING may not be mutually exclusive. All these pieces of evidence suggest that cholesterol may regulate STING activity at multiple levels, which further emphasizes the importance of understanding cholesterol and STING interaction.

Researchers are developing compounds targeting the cGAS-STING pathway signaling in multiple settings. These compounds include modified CDNs that can be administrated intratumorally[53], as well as small molecule inhibitors that agonize STING in a totally different manner and could be administrated systematically[54]. Recently, a compound, C178, has been developed to covalently target STING palmitoylation[29]. Understanding how cholesterol regulates STING will provide more therapeutic potential.

Experimental Procedures for Chapter 3:

Mouse cells: Bone marrow was differentiated into macrophages in DMEM containing 10% v/v FBS (HyClone, GE SH3007103), 5% v/v M-CSF conditioned media, 1% v/v pen/strep, 1% v/v glutamine (Invitrogen) 0.5% v/v sodium pyruvate (Invitrogen) for 7-9 days prior to experimental use. Cells were changed to media with 5% FBS at the time of stimulation.

Plasmids and Stable cell lines: For luciferase assay, pcDNA3.1-STING-HA was a kind gift from Cheng Lab (UCLA). The WT STING in this chapter is R232.

293FRT expressing STING-HA: The Flp-In™ Complete System (Invitrogen) were used to generate 293FRT cells stably expressing WT STING-HA and mutants according to the manufacturer protocol. Briefly, cells were transfected with pcDNA5-STING-HA and pOG44 using Lipofectamine 3000 followed by selection in Hygromycin B Gold (Invivogen #ant-hg-1). pcDNA5 and pOG44 plasmids are kind gifts from Wohlschlegel lab (UCLA). Empty pcDNA5 vector were used as a control.

HEK293T expressing STING-FLAG: pHAGE-CMV plasmid was a kind gift from Sun lab (UCLA), gibson assembly (NEB # E5520S) was used to generate pHAGE-CMV-STING-FLAG from pHAGE vector, STING ORF from pcDNA3.1-STING-HA, and synthesized FLAG sequence (IDT). HEK293T expressing STING-FLAG were generated using second generation of lentiviral system. Where lentiviral particles were made by co-transfection of PAX2, VSVG and pHAGE vector or WT STING or mutants into 293FT cells with Fugene 6 Transfection Reagent (Fisher Cat# PR-E2691). All mutations were generated using QuikChange II XL Site-Directed Mutagenesis Kit (Agilent #200521)

Reagents: BMDMs were stimulated with Poly(I:C) (Invivogen tlrl-pic (HMW)) or 2'3'-cGAMP (Invivogen tlrl-nacga23-1) complexed with lipofectamine 2000 with 1 µg : 1 µL ratio. The following antibodies were used for Western Blots: STING (Cell Signaling 3337S), TBK1 (Cell Signaling 3013), phopho-TBK1 (Cell Signaling 5483), and anti-FLAG M2 antibody (Sigma F3165).

Gene expression analysis: RNA was extracted from cells with Trizol (ThermoFisher, 15596-018) using manufacturer's protocols. cDNA was synthesized with high-capacity cDNA reverse transcription kit (Applied Biosystems, 4368814) as per manufacturer's instructions (700 ng/µL RNA per cDNA synthesis reaction). Quantitative PCR (qPCR) was conducted on the Roche LightCycler 480 using SYBR Green Master Mix (Kapa Biosciences) or PowerUp™ SYBR™ Green Master Mix (Thermofisher, A25778) and 0.5 µmol/L primers. Relative expression values are normalized to control gene (36b4) and expressed in terms of linear relative mRNA values.

IFN-b Luciferase Reporter Assay: HEK293T cells were co-transfected with firefly luciferase under Ifnb1 promoter, renilla luciferase reporter plasmids, empty pcDNA3.1 vector or pcDNA3.1-hSTING-HA WT or mutations for 24 hr. Then firefly and renilla luciferase activities were determined by a Dual Luciferase Assay System (Promega) and a platereader (Berthold).

Immunoblotting: Cells were lysed in RIPA buffer containing protease inhibitors (Thermo 87786) and phosphatase inhibitor cocktail (Sigma P5726), followed by incubation at 95˚C

for 15 min with laemmli buffer (BioRad161-0737) and separation by SDS-PAGE gel (Invitrogen NP0336BOX) and blotted with indicated antibodies.

Protein labeling with cholesterol alkyne probes: Proteins were labeled with *trans-sterol* (Sigma 804657) or LKM38 (a kind gift from Covey lab at Washington University), similar to previously described[43,45].

Probe preparation*:* LKM38, *trans-sterol* and cholesterol were complexed to MβCD before delivery to cells. A desired amount of probe or cholesterol in ethanol stock was added to a glass vial and dried under argon flow. Then 38mM MβCD solution was added to the same glass vial followed by vigorous vortex, and sonication for 1 h. then the vial was shaked overnight at 37˚C to complete complexing. The MβCD conjugated probe is then added to the desired media and filtered with 0.22 μm filter.

Cell culture and probe incubation: On Day 0, 293T cells stably over-expressing STING-FLAG, or empty vector were plated in 10%FBS for o/n, next day, media were replaced with blank DMEM for 3 h to maximize probe uptake. Then media was aspirated and incubated with DMEM +/- 10uM MβCD-probe +/- 100uM MβCD-chol 1 h at 37˚C. Then cells washed with ice-cold PBS and subject to +/- UV crosslinking for 5min. Then cells were scraped, pelleted, resuspended with cold PBS, and lysed by probe sonication at 4 ˚C. Protein content was quantified by BCA kit and diluted to 1 mg/ml. Then Click-chemistry were performed for 1 h at room temperature as described below, followed by incubation at 65˚C for 30 min with laemmli buffer (BioRad161-0737) and separation by SDS-PAGE gel (Invitrogen NP0336BOX) and blotted with indicated antibodies.

Click chemistry: Click chemistry was performed to conjugate Rhodamine-azide or biotin-azide group to probe labeled proteins. 50 µg of protein lysate in PBS was mixed with 20 µM rhodamine-azide, 1 mM Tris(2-carboxyethyl)phosphine (TCEP, Sigma-Aldrich), 100 µM Tris[(1-benzyl-1H-1,2,3-triazol-4-yl)methyl]amine (TBTA) (Sigma-Aldrich) and 1 mM CuSO4 in PBS at room temperature.

Rhodamine Signal detection: Cell lysate after clicking to Rhodamine-azide was incubation with laemmli buffer and β-ME at 65˚C for 20 min. Then the denatured lysates were resolved on a 4-12% SDS gel, and Rhodamine signal was detected by Chem-Station with 40 s exposure, and the same gel were transferred to Nitro-cellulose membrane for anti-FLAG detection.

Mass-spec analysis of probe labeled proteomics: Cell lysate after clicking to biotin-azide was incubated with PBS equilibrated streptavidin agarose slurry with agitation for 1.5 – 3 h at 4 ˚C. beads were then pelleted and washed with 0.2% SDS / PBS once, PBS twice and miliQ water 3 times. Then proteins bound to beads were denatured with 6 M urea and 10 mM DTT in PBS at 65 ˚C for 15 min. samples were allowed to cool down to room temp and were shaken at 37 ˚C for 30min with 20 mM IA. Then 20 µg beads pellet were washed with PBS and incubated overnight at 37˚C with trypsin and urea for on bead digestion. Next morning, proteins were eluted to low bind tube through bio-spin column (Biorad Micro Bio-Spin™ Chromatography Columns) followed by zip tip protocol to concentrate and clean up peptides.

Chapter 3: Figure 1

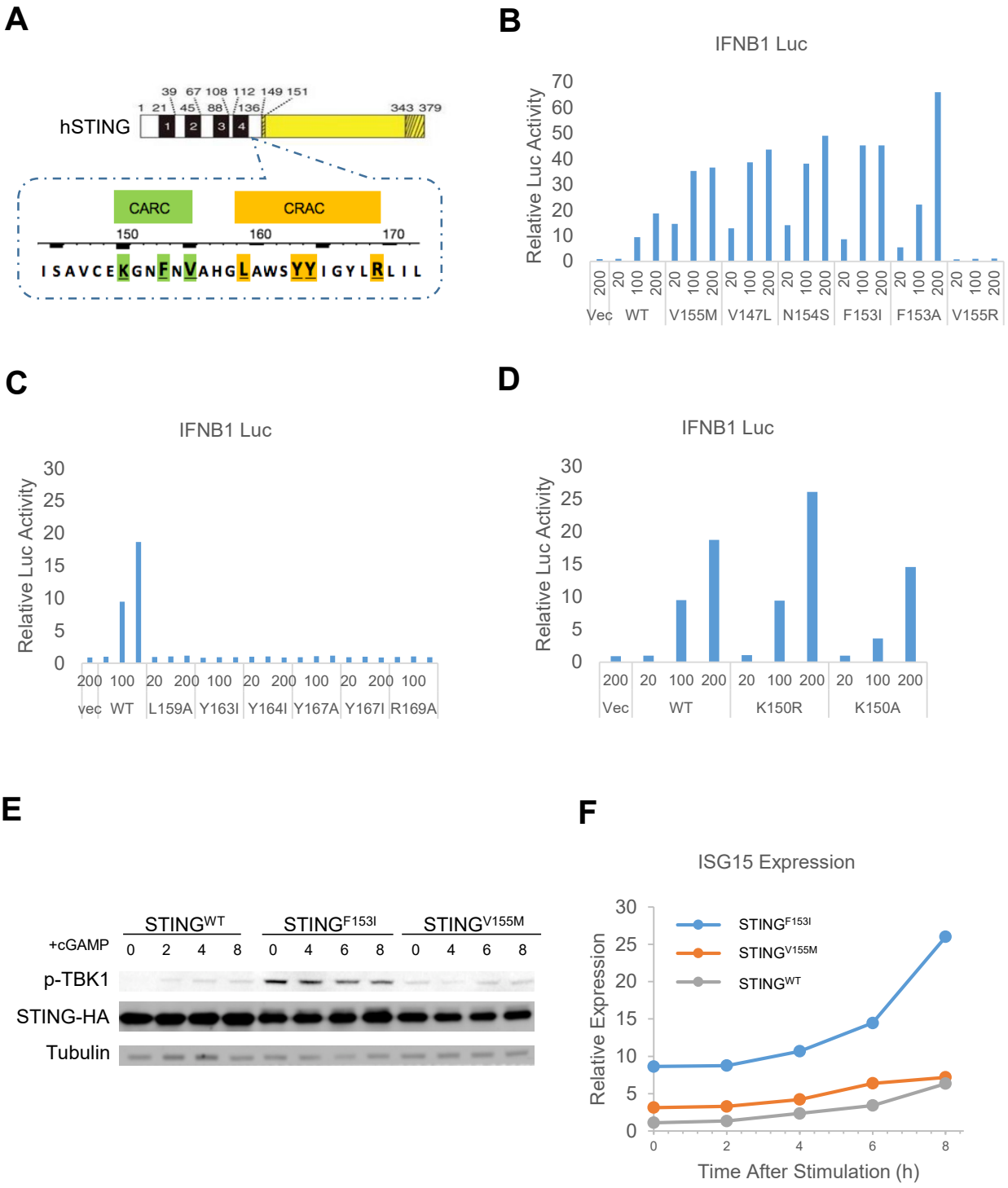

Chapter 3: Figure 1. CARC-CRAC domain regulates STING activity

A. CARC-CRAC motif in STING. AA 150-170 of STING close to transmembrane 4 with the CARC and CRAC motifs are indicated green and yellow bars. The essential amino acids within the CARC and CRAC motif are highlighted in green and yellow respectively.

B. Luciferase induction in HEK293T cells. Cells were transfected with various amount (20, 100 and 200 ng) of empty vector (Vec), WT STING and 6 different mutants, in combination with a luciferase plasmid under the control of the IFNB promoter.

C. Same as B with indicated STING mutations.

D. Same as B with indicated STING mutations.

E. Immunoblot of phosphor-TBK1 expression in 293FRT cells expressing HA-tagged WT STING, SAVI mutation V155M and CARC mutation F153I. Cells were stimulated with synthetic 2′3′-cGAMP (cGAMP, 4 μg/ml) complexed to lipofectamine 2000 for different time points 2, 4, 6 and 8 h.

F. qPCR analysis of ISG15 in 293FRT cells expressing HA-tagged WT STING, SAVI mutation V155M and CARC mutation F153I. Cells were stimulated with synthetic 2′3′-cGAMP (cGAMP, 4 μg/ml) complexed to lipofectamine 2000 for 2, 4, 6 and 8 h as E.

Chapter 3: Figure 2

A

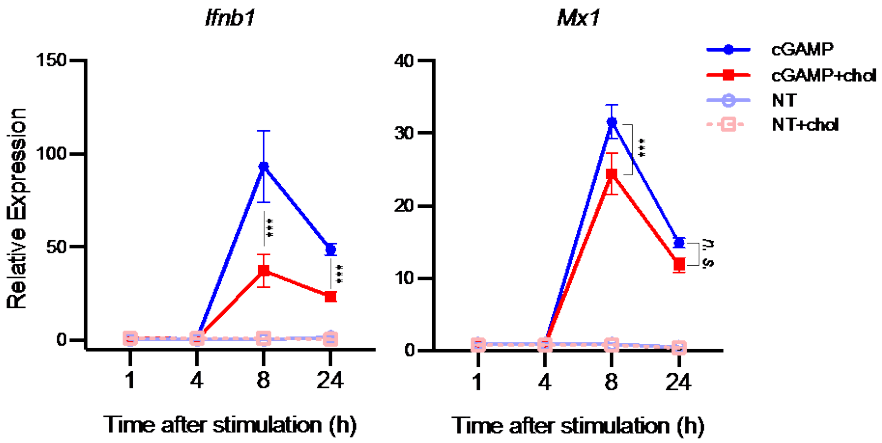

B

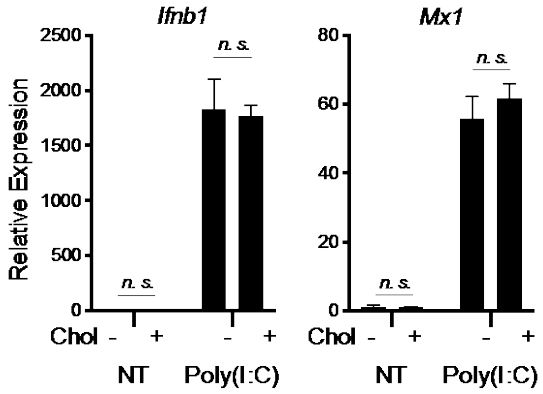

C

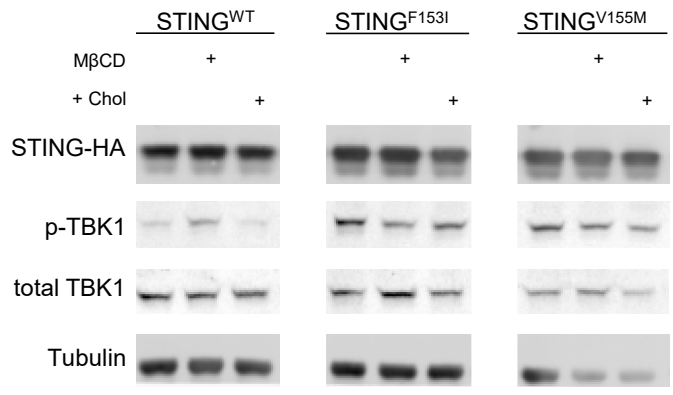

D

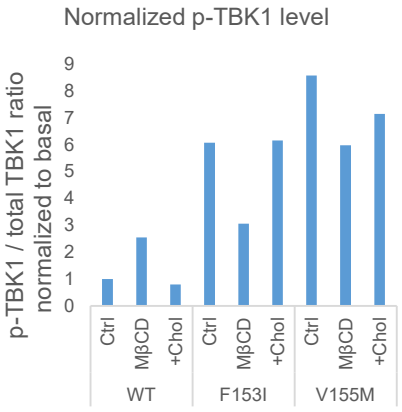

Chapter 3: Figure 2. CARC-CRAC motif is critical for STING's response to cholesterol alterations

D. qPCR analysis of *Ifnb1* and *Mx1* in mouse bone marrow derived macrophages (mBMDMs). Cells were incubated with media containing water-soluble cholesterol (4 μM) for 48 h, followed by stimulation with 2'3'cGAMP (4 μg/ml) for 1, 4, 8 and 24 h.

E. qPCR analysis of *Ifnb1* and *Mx1* in mBMDMs. Cells were incubated with media containing water-soluble cholesterol (4 μM) for 48 h, followed by stimulation with TLR3 agonist (Poly(I:C), 1 μg/ml) 12 h.

F. Immunoblot of phospho-TBK1 (pTBK1) expression in 293FRT cells expressing HA-tagged WT STING, SAVI mutation V155M and CARC mutation F153I. Cells were cultured in full media, then switched to media with 0.5% lipo-protein depleted serum (LPDS) with MβCD or water-soluble cholesterol for 2 h.

G. Quantification of pTBK1 signal normalized to total TBK1.

Chapter 3: Figure 3

A

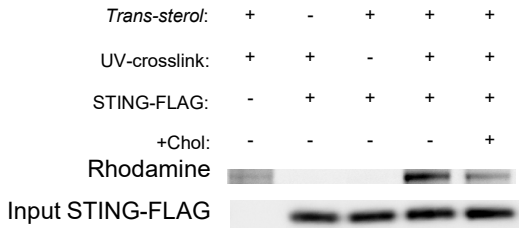

B

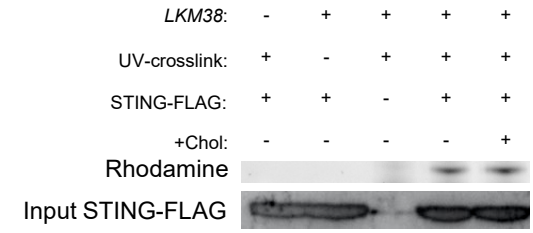

C

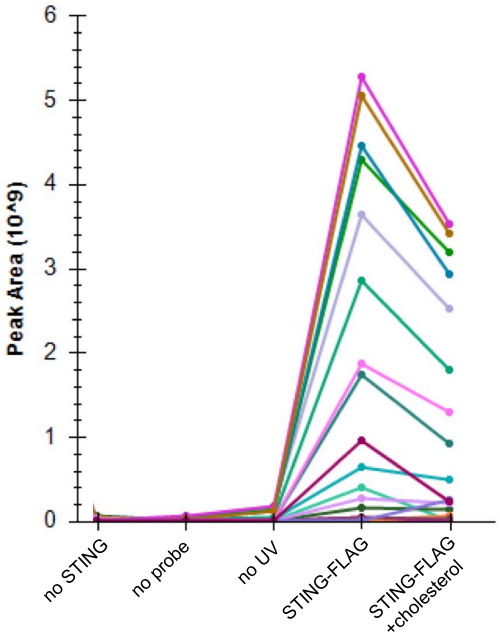

D

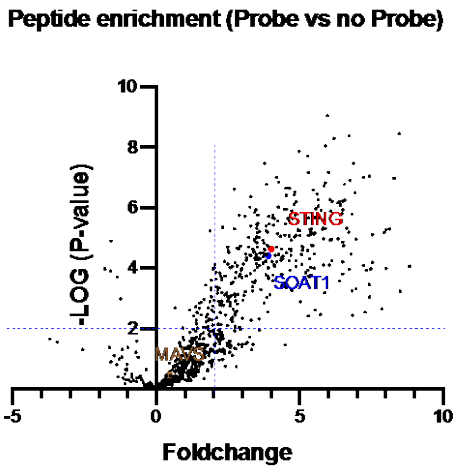

E

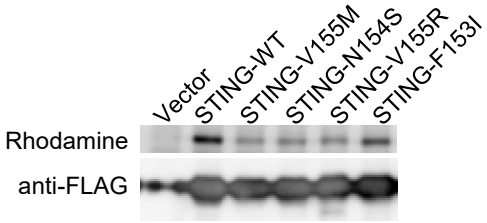

preliminary data

F

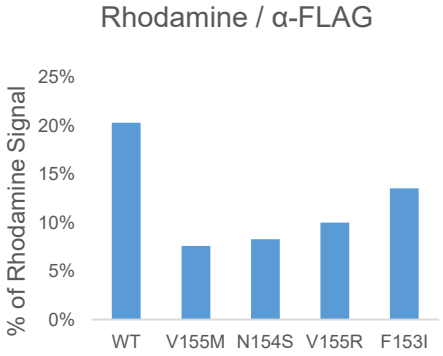

preliminary data

Chapter 3: Figure 3. STING directly binds to cholesterol

J. Crosslinking of *Trans*-sterol (10 μM) to STING-FLAG. HEK293T cells expressing FLAG-tagged wild-type STING are incubated with either *Trans*-sterol or LKM38 in the presence of excess competing cholesterol for 1 h followed by UV-crosslinking and clicking to rhodamine-azide. The FLAG blot shows the input signal of STING.

K. Crosslinking of LKM38 (10 μM) to STING-FLAG as described in (A)

L. Mass-spec quantification of *trans-sterol* enriched STING peptides. HEK293T cells expressing FLAG-tagged wild-type STING are incubated with either *Trans*-sterol in the presence of excess competing cholesterol for 1 h followed by UV-crosslinking and clicking to biotin-azide. Then proteins labeled with biotin are enriched by streptavidin beads followed by trypsin digestion and mass-spec analysis.

M. Volcano plot of STING peptides in sample with *trans-sterol* (Probe) compared to no *trans-sterol* (no Probe). The foldchange and -log (P value) is shown, with STING highlighted in red, SOAT1 highlighted in blue and MAVS highlighted in brown, respectively.

N. Crosslinking of LKM38 (10 μM) to FLAG tagged wild-type STING-FLAG as well as SAVI and CARC mutants, as described in (A).

O. Quantification of fraction labeled from (E).

Chapter 3: Figure 4

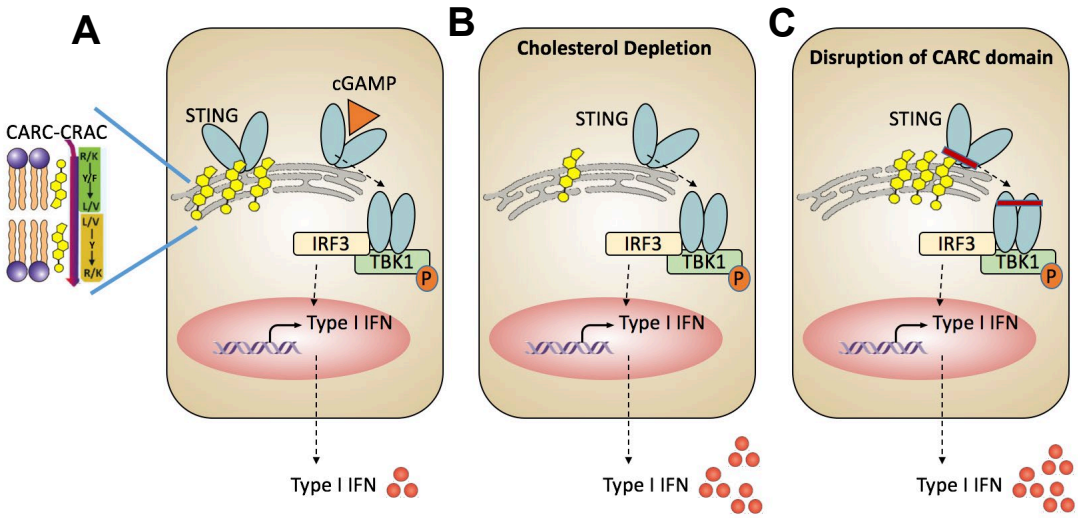

Chapter 3: Figure 4. Proposed model of cholesterol STING interaction

A. Cholesterol in the ER bind to STING, likely via the CARC-CRAC motif, which retains STING protein in the ER. Upon activation by its ligand 2'3-cGAMP, STING changes confirmation and translocalize to ERGIC and signal through TBK1 and IRF3.
B. When cholesterol is limited by depletion or synthesis inhibition, STING is hyperactive, possibly due to more trafficking to the ERGIC.
C. When the putative cholesterol recognition motif CARC-CRAC in STING is disrupted, STING can no longer bind to cholesterol, which leads to gain of function of STING despite sufficient cholesterol present.

Chapter 3: Supplemental Figure 3

A

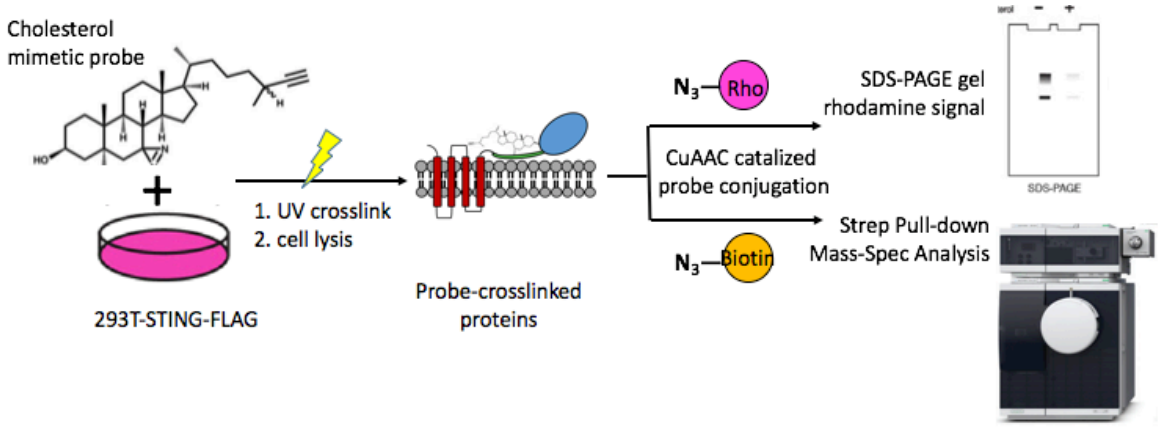

B

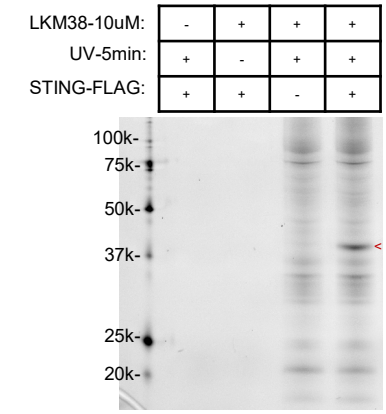

C

```
1+   MPHSSLHPSI PCPRGHGAQK AALVLLSACL VTLWGLGEPP EHTLRYLVLH
51+  LASLQLGLLL NGVCSLAEEL RHIHSRYRGS YWRTVRACLG CPLRRGALLL
101+ LSIYFYYSLP NAVGPPFTWM LALLGLSQAL NILLGLKGLA PAEISAVCEK
151+ GNFNVAHGLA WSYYIGYLRL ILPELQARIR TYNQHYNNLL RGAVSQRLYI
201+ LLPLDCGVPD NLSMADPNIR FLDKLPQQTG DHAGIKDRVY SNSIYELLEN
251+ GQRAGTCVLE YATPLQTLFA MSQYSQAGFS REDRLEQAKL FCRTLEDILA
301+ DAPESQNNCR LIAYQEPADD SSFSLSQEVL RHLRQEEKEE VTVGSLKTSA
351+ VPSTSTMSQE PELLISGMEK PLPLRTDFS
```

Chapter 3: Supplemental Figure 3. STING directly binds to cholesterol

A. Schematic of photo-reactive cholesterol mimetic probing assay. HEK293T cells expressing FLAG-tagged wild-type STING are treated with either *Trans*-sterol or LKM38 for 1 h followed by UV-crosslinking and clicking to rhodamine-azide for gel analysis, or biotin-azide for proteomics analysis.

B. Rhodamine signal on SDS-PAGE with whole cell lysates. HEK293T expressing empty vector of wild-type STING were probed with LKM38, followed by UV-crosslinking and clicking to rhodamine-azide.

C. STING peptides detected by Mass-spec. Mass-spec quantification of *trans-sterol* enriched STING peptides. HEK293T cells expressing FLAG-tagged wild-type STING are incubated with either *Trans*-sterol for 1 h followed by UV-crosslinking and clicking to biotin-azide. Then proteins labeled with biotin are enriched by streptavidin beads followed by trypsin digestion and mass-spec analysis. Peptides detected my Mass-spec were mapped to human proteome, and the peptides mapped to STING are highlighted in yellow, showing ~ 44% coverage.

References for Chapter 3:

1. York, A. G. *et al.* Limiting Cholesterol Biosynthetic Flux Spontaneously Engages Type I IFN Signaling. *Cell* **163**, 1–14 (2015).
2. Dang, E. V., McDonald, J. G., Russell, D. W. & Cyster, J. G. Oxysterol Restraint of Cholesterol Synthesis Prevents AIM2 Inflammasome Activation. *Cell* 1–15 (2017). doi:10.1016/j.cell.2017.09.029
3. Blanc, M. *et al.* The Transcription Factor STAT-1 Couples Macrophage Synthesis of 25-Hydroxycholesterol to the Interferon Antiviral Response. *Immunity* **38**, 106–118 (2013).
4. Reboldi, A. *et al.* Inflammation. 25-Hydroxycholesterol suppresses interleukin-1-driven inflammation downstream of type I interferon. *Science* **345**, 679–84 (2014).
5. Araldi, E. *et al.* Lanosterol Modulates TLR4-Mediated Innate Immune Responses in Macrophages. *Cell Rep.* **19**, 2743–2755 (2017).
6. Einav, S. & Glenn, J. S. Prenylation inhibitors: a novel class of antiviral agents. *J. Antimicrob. Chemother.* **52**, 883–886 (2003).
7. Jin, L. *et al.* MPYS, a novel membrane tetraspanner, is associated with major histocompatibility complex class II and mediates transduction of apoptotic signals. *Mol. Cell. Biol.* **28**, 5014–5026 (2008).
8. Zhong, B. *et al.* The Adaptor Protein MITA Links Virus-Sensing Receptors to IRF3 Transcription Factor Activation. *Immunity* **29**, 538–550 (2008).
9. Sun, W. *et al.* ERIS, an endoplasmic reticulum IFN stimulator, activates innate immune signaling through dimerization. *Proc Natl Acad Sci U S A* **106**, 8653–

8658 (2009).

10. Ishikawa, H. & Barber, G. N. STING is an endoplasmic reticulum adaptor that facilitates innate immune signalling. *Nature* **455**, 674–8 (2008).
11. Li, T. & Chen, Z. J. The cGAS-cGAMP-STI NG pathway connects DNA damage to inflammation, senescence, and cancer. *Journal of Experimental Medicine* **215**, 1287–1299 (2018).
12. Tao, J., Zhou, X. & Jiang, Z. cGAS-cGAMP-STING: The three musketeers of cytosolic DNA sensing and signaling. *IUBMB Life* **68**, 858–870 (2016).
13. Ma, Z. & Damania, B. The cGAS-STING Defense Pathway and Its Counteraction by Viruses. *Cell Host and Microbe* **19**, 150–158 (2016).
14. Cai, X., Chiu, Y. & Chen, Z. J. Review The cGAS-cGAMP-STING Pathway of Cytosolic DNA Sensing and Signaling. *Mol. Cell* **54**, 289–296 (2014).
15. Sun, L., Wu, J., Du, F., Chen, X. & Chen, Z. J. Cyclic GMP-AMP Synthase Is a Cytosolic DNA Sensor That Activates the Type I Interferon Pathway. *Science (80-.).* **339**, 786–791 (2013).
16. Zhang, X. *et al.* Cyclic GMP-AMP containing mixed Phosphodiester linkages is an endogenous high-affinity ligand for STING. *Mol. Cell* **51**, 226–235 (2013).
17. Wu, J. *et al.* Cyclic GMP-AMP is an endogenous second messenger in innate immune signaling by cytosolic DNA. *Science* **339**, 826–30 (2013).
18. Burdette, D. L. *et al.* STING is a direct innate immune sensor of cyclic di-GMP. *Nature* **478**, 515–518 (2011).
19. Ouyang, S. *et al.* Structural Analysis of the STING Adaptor Protein Reveals a Hydrophobic Dimer Interface and Mode of Cyclic di-GMP Binding. *Immunity* **36**,

1073–1086 (2012).

20. Shang, G. *et al.* Crystal structures of STING protein reveal basis for recognition of cyclic di-GMP. *Nat. Struct. Mol. Biol.* **19**, 725–7 (2012).
21. Shang, G., Zhang, C., Chen, Z. J., Bai, X. & Zhang, X. Cryo-EM structures of STING reveal its mechanism of activation by cyclic GMP–AMP. *Nature* **567**, 389–393 (2019).
22. Saitoh, T. *et al.* Atg9a controls dsDNA-driven dynamic translocation of STING and the innate immune response. *Proc. Natl. Acad. Sci. U. S. A.* **106**, 20842–6 (2009).
23. Mukai, K. *et al.* Activation of STING requires palmitoylation at the Golgi. *Nat. Commun.* **7**, 11932 (2016).
24. Dobbs, N. *et al.* STING Activation by Translocation from the ER Is Associated with Infection and Autoinflammatory Disease. *Cell Host Microbe* **18**, 157–168 (2015).
25. Zhang, C. *et al.* Structural basis of STING binding with and phosphorylation by TBK1. *Nature* **567**, 394–398 (2019).
26. Barber, G. N. STING: infection, inflammation and cancer. *Nat. Rev. Immunol.* **15**, 760–770 (2015).
27. Chen, Q., Sun, L. & Chen, Z. J. Regulation and function of the cGAS–STING pathway of cytosolic DNA sensing. *Nat. Immunol.* **17**, 1142–1149 (2016).
28. Surpris, G. & Poltorak, A. The expanding regulatory network of STING-mediated signaling. *Current Opinion in Microbiology* **32**, 144–150 (2016).
29. Haag, S. M. *et al.* Targeting STING with covalent small-molecule inhibitors. *Nature* (2018). doi:10.1038/s41586-018-0287-8

30. Van Meer, G., Voelker, D. R. & Feigenson, G. W. Membrane lipids: Where they are and how they behave. *Nature Reviews Molecular Cell Biology* **9**, 112–124 (2008).

31. Ohvo-Rekilä, H., Ramstedt, B., Leppimäki, P. & Peter Slotte, J. Cholesterol interactions with phospholipids in membranes. *Progress in Lipid Research* **41**, 66–97 (2002).

32. Pacheco, J., Dominguez, L., Bohórquez-Hernández, A., Asanov, A. & Vaca, L. A cholesterol-binding domain in STIM1 modulates STIM1-Orai1 physical and functional interactions. *Sci. Rep.* **6**, 29634 (2016).

33. Wang, Q. *et al.* The E3 Ubiquitin ligase AMFR and INSIG1 bridge the activation of TBK1 kinase by modifying the adaptor STING. *Immunity* **41**, 919–933 (2014).

34. Liu, Y. *et al.* Activated STING in a Vascular and Pulmonary Syndrome. *NEJM* **371**, 507–518 (2014).

35. Jeremiah, N. *et al.* Inherited STING-activating mutation underlies a familial inflammatory syndrome with lupus-like manifestations. *J. Clin. Invest.* **124**, 5516–20 (2014).

36. Melki, I. *et al.* Disease-associated mutations identify a novel region in human STING necessary for the control of type I interferon signaling. *J. Allergy Clin. Immunol.* **140**, 543-552.e5 (2017).

37. Saldanha, R. G. *et al.* A mutation outside the dimerization domain causing atypical STING-associated vasculopathy with onset in infancy. *Front. Immunol.* **9**, 1535 (2018).

38. Fantini, J. & Barrantes, F. J. How cholesterol interacts with membrane proteins:

An exploration of cholesterol-binding sites including CRAC, CARC, and tilted domains. *Frontiers in Physiology* **4 FEB**, 31 (2013).

39. Baier, C. J., Fantini, J. & Barrantes, F. J. Disclosure of cholesterol recognition motifs in transmembrane domains of the human nicotinic acetylcholine receptor. *Sci. Rep.* **1**, 69 (2011).

40. Grouleff, J., Irudayam, S. J., Skeby, K. K. & Schiøtt, B. The influence of cholesterol on membrane protein structure, function, and dynamics studied by molecular dynamics simulations ☆. *BBA - Biomembr.* **1848**, 1783–1795 (2015).

41. Fantini, J. *et al.* A mirror code for protein-cholesterol interactions in the two leaflets of biological membranes. *Sci. Rep.* **6**, 21907 (2016).

42. Derler, I. *et al.* Cholesterol modulates Orai1 channel function. *Sci. Signal.* **9**, ra10 (2016).

43. Castellano, B. M. *et al.* Lysosomal cholesterol activates mTORC1 via an SLC38A9–Niemann-Pick C1 signaling complex. *Science (80-.).* **355**, 1306–1311 (2017).

44. Könner, A. C. & Brüning, J. C. Toll-like receptors: linking inflammation to metabolism. *Trends Endocrinol. Metab.* **22**, 16–23 (2011).

45. Hulce, J. J., Cognetta, A. B., Niphakis, M. J., Tully, S. E. & Cravatt, B. F. Proteome-wide mapping of cholesterol-interacting proteins in mammalian cells. *Nat. Methods* **10**, 259–264 (2013).

46. Kolb, H. C., Finn, M. G. & Sharpless, K. B. Click Chemistry: Diverse Chemical Function from a Few Good Reactions. *Angew. Chem. Int. Ed. Engl.* **40**, 2004–2021 (2001).

47. Simons, K. & Toomre, D. Lipid rafts and signal transduction. *Nat. Rev. Mol. Cell Biol.* **1**, 31–39 (2000).

48. Muro, E., Atilla-Gokcumen, G. E. & Eggert, U. S. Lipids in cell biology: how can we understand them better? *Mol. Biol. Cell* **25**, 1819–23 (2014).

49. Lingwood, D. & Simons, K. Lipid rafts as a membrane-organizing principle. *Science* **327**, 46–50 (2010).

50. Srikanth, S. *et al.* The Ca 2+ sensor STIM1 regulates the type I interferon response by retaining the signaling adaptor STING at the endoplasmic reticulum. *Nat. Immunol.* **20**, 152–162 (2019).

51. Horton, J. D. J. J. D. *et al.* SREBPs: activators of the complete program of cholesterol and fatty acid synthesis in the liver. *J. Clin. Invest.* **109**, 1125–31 (2002).

52. Matsuda, M. *et al.* SREBP cleavage-activating protein (SCAP) is required for increased lipid synthesis in liver induced by cholesterol deprivation and insulin elevation. *Genes Dev.* **15**, 1206–16 (2001).

53. Li, L. *et al.* Hydrolysis of 2'3'-cGAMP by ENPP1 and design of nonhydrolyzable analogs. *Nat. Chem. Biol.* **10**, 1043–8 (2014).

54. Ramanjulu, J. M. *et al.* Design of amidobenzimidazole STING receptor agonists with systemic activity. *Nature* **564**, 439–443 (2018).